nagra.

ARBEITSBERICHT NAB 24-13

Geological long-term evolution: Neotectonics

November 2024

Nagra | National Cooperative for the Disposal of Radioactive Waste
Hardstrasse 73 | 5430 Wettingen | Switzerland
+41 56 437 11 11 | info@nagra.ch | nagra.ch

ARBEITSBERICHT NAB 24-13

Geological long-term evolution: Neotectonics

November 2024

KEYWORDS
Neotectonic activity, Active tectonics, Tectonic geomorphology, Geodesy, Strain rates, Inherited faults, Northern Switzerland, Deckenschotter, Fluvioglacial terraces

Nagra | **National Cooperative for the Disposal of Radioactive Waste**
Hardstrasse 73 | 5430 Wettingen | Switzerland
+41 56 437 11 11 | info@nagra.ch | nagra.ch

Main authors (in alphabetical order): Angela Landgraf, Raphael Schneeberger

Contributions: J Ramón Arrowsmith, M. Schnellmann, W. Schwanghart, F. Maier

Editorial and language support: Petra Blaser, Barbara Habermacher, Rebecca Green, Miryam Unger, Reto Flückiger

This report has benefitted from numerous technical discussions and reviews by various people inside and outside Nagra. We would like to thank these people and all others who have contributed to this report.

Executive summary

In general, neotectonics involves recent or active crustal deformation, the forces that are responsible for the crustal state of stress and its relation to plate tectonic processes. The temporal borders are often set to the Neogene and Quaternary or, generally, since the last plate-tectonic reorganisation. Accordingly, neotectonics considers the deformation that was/is active under the prevailing stress regime.

This report provides a basis for the assessment of effects of seismicity and faulting on the deep-geological repository. It also provides argumentation for scenarios of future deformation.

During SGT Stage 3, the geoscientific database for a better assessment of neotectonic scenarios was improved by a comprehensive scientific field investigation program. For a detailed understanding of the subsurface, ~ 200 km^2 of 3D-seismic reflection data have been acquired in the three siting regions. Within the analysis of the 3D-seismic surveys it was determined that faults with a minimum vertical throw of 5 m were detected. Monitoring using the seismic weak motion network, as well as the Nagra-owned GNSS network was continued. Longer operational phases of such instrumental networks allow a better signal-to-noise ratio and more complete datasets. In addition, new precise levelling measurements around the Bözberg area were integrated. The digital model of the Base Quaternary or Top bedrock surface was updated, including mapping and an uncertainty assessment of the Deckenschotter basis. This allowed a systematic evaluation of potential tectonic offsets across regional fault zones, including determination of a maximum possible rate since Deckenschotter deposition.

Present-day seismicity is sparse within all siting regions, with the exception of the Eglisau cluster of shallow, low-magnitude events. Vertical velocities derived from precise levelling show a decreasing gradient from south to north at the longitude of JO and a slight gradient in NL, but less in ZNO. Within the realm of the siting regions, the majority of vertical velocities are between 0.2 and 0.4 mm/yr with respect to a stable-Europe framework. No evidence of differential horizontal movement across regional fault zones in horizontal velocities from GNSS was observed across Northern Switzerland.

Detailed inspection of the landscape provided few indications of possible Quaternary deformation. If such deformation happened, the inferred deformation rates must be low, and deformation appears to be associated with inherited regional fault zones.

Future deformation rates are expected to be low and comparable to the rates derived from instrumental records and geological rates from the last few million years. Inherited faults act as zones of weakness and thus possible future strain will be preferentially localised along them. The rock volume in between these larger faults may also be strained, as evidenced by the small-scale faults observed in the retrieved core material, but the overall strain will be substantially lower than in the regional fault zones. Accordingly, positioning the long-term safety-relevant repository elements outside regional fault zones will minimise any neotectonic effects.

Table of Contents

Executive summary I

Table of Contents III

List of Tables V

List of Figures V

List of Acronyms VII

1 Introduction 1

2 Geodynamic setting of Northern Switzerland 2
2.1 Northern Switzerland within the European geodynamic framework 2
2.2 Tectonic framework of Northern Switzerland 7
2.3 Effects of glacial isostatic adjustment (GIA) 11

3 Basis to evaluate neotectonic activity 13
3.1 Continuation and densification of weak motion seismic network 14
3.2 3D surface velocity monitored using the Global Navigation Satellite System 19
3.3 Recent vertical surface motion 22
3.4 Seismic reflection datasets 25
3.5 Age dating of faults 25
3.6 Tectonic geomorphology 25
3.6.1 Update of Base Quaternary 27
3.6.2 Stream network analysis 27
3.6.3 Criteria to evaluate potential Quaternary deformation 28

4 Indications for neotectonic activity in Northern Switzerland 32
4.1 Regional tectonic deformation signals 32
4.2 A sharper focus on the siting regions 40
4.2.1 Jura Ost 41
4.2.1.1 Local tectonic inventory 41
4.2.1.2 Tectonic geomorphology and geodesy 41
4.2.2 Nördlich Lägern 52
4.2.2.1 Local tectonic inventory 52
4.2.2.2 Tectonic geomorphology, seismicity and geodesy 56
4.2.3 Zürich Nordost 64
4.2.3.1 Local tectonic inventory 64
4.2.3.2 Tectonic geomorphology, seismicity, and geodesy 68
4.3 Discussion and conclusions with respect to neotectonic activity 75

5 Possible future tectonic evolution ... 78
5.1 Introduction ... 78
5.2 Future deformation rate ... 78
5.2.1 Geological past ... 79
5.2.2 Present-day horizontal movements inferred from GNSS ... 80
5.3 Proposed evolution ... 82
6 Conclusions ... 83
7 References ... 85

List of Tables

Tab. 3-1: Qualitative description of precise levelling measurement data quality ranking 23
Tab. 3-2: Uncertainty classification for the strain marker Base Deckenschotter 27
Tab. 3-3: Quality criteria for geomorphic markers 31
Tab. 4-1: Ranking of geomorphic evidence for tectonic activity in Jura Ost......................... 51
Tab. 4-2: Ranking of geomorphic evidence for tectonic activity in Nördlich Lägern 57
Tab. 4-3: Ranking of geomorphic evidence for tectonic activity in Zürich Nordost 72
Tab. 4-4: Qualitative weighting and summary proxies for neotectonic activity 77
Tab. 5-1: Shortening estimates and partitioning between internal and external domains for the eastern Jura Fold-and-Thrust Belt based on 2D geometric restoration 80

List of Figures

Fig. 2-1: Velocity fields, seismicity, and tectonic stress field in Europe 3
Fig. 2-2: Deformation model of the Alpine region from GNSS velocities with normal and shear strain distribution in the Alpine region and beyond 5
Fig. 2-3: Overview map of historical and instrumentally recorded earthquakes and modelled probability of occurrence for earthquakes with $M_W \geq 6$ 6
Fig. 2-4: Simplified tectonic map between the Upper Rhine Graben and Hegau – Bodensee Graben and containing the siting regions 10
Fig. 3-1: Sketch showing tectonic phenomena, key topics, and instrumentation and involved spatiotemporal scales 13
Fig. 3-2: Earthquake magnitude of completeness for Switzerland and evolution of seismic recordings in Northern Switzerland 16
Fig. 3-3: Earthquake distribution in Northern Switzerland and Southern Germany 18
Fig. 3-4: Map of Northern Switzerland with the horizontal velocity vectors for the permanent GNSS stations for different time periods 20
Fig. 3-5: Present-day horizontal motion of permanent GNSS stations in Northern Switzerland 21
Fig. 3-6: Map of Northern Switzerland showing the vertical surface motion measured by precise levelling measurements 24
Fig. 4-1: Topographic map and normalised steepness index over geology map for Northern Switzerland... 33
Fig. 4-2: Overview of tectonic domains with data and associated swath profiles for regional neotectonic analysis 34
Fig. 4-3: Data swath (WSW-ENE) across all three siting regions 35
Fig. 4-4: Data swath profile across the Jura Ost siting region.. 36
Fig. 4-5: Data swath profile across the Nördlich Lägern siting region 38
Fig. 4-6: Data swath profile across the Zürich Nordost siting region 39

Fig. 4-7: Location of specific data swath and seismic profiles of the siting regions 40

Fig. 4-8: Map compilation of river steepness and sinuosity, tectonic information and precise levelling, and Quaternary morphostratigraphic units – Jura Ost 42

Fig. 4-9: Summary profile along the 2D seismic reflection line 83-NF-15 43

Fig. 4-10: Summary profile along the 2D seismic reflection line 11-NS-06 44

Fig. 4-11: Summary profile along the 2D seismic reflection line 11-NS-10 45

Fig. 4-12: Detailed geological map of the Lower Aare Valley and the potential geomorphic anomaly #1 46

Fig. 4-13: Profile of Lower Aare Valley with focus on Niederterrasse between Rhine and Limmat confluences 48

Fig. 4-14: Detailed topographic map of the Lower Aare Valley around potential geomorphic anomaly #3 49

Fig. 4-15: Parallel profiles in the Lower Aare Valley 50

Fig. 4-16: Map compilation of river steepness and sinuosity, tectonic information and precise levelling, and Quaternary morphostratigraphic units – Nördlich Lägern 53

Fig. 4-17: Summary profile along the 2D seismic reflection line 91-NO-58 54

Fig. 4-18: Summary profile along the 2D seismic reflection line 11-NS-20 55

Fig. 4-19: Detailed topographic map of the area around potential geomorphic anomalies #1 – 3 in the eastern part of Nordlich Lägern 58

Fig. 4-20: Detailed topographic map of the "Egg" area 60

Fig. 4-21: Parallel profiles across the Baden – Irchel – Herdern Lineament at the "Egg" location 61

Fig. 4-22: Apparent fault throw rate at the Baden – Irchel – Herdern Lineament since HDS deposition 63

Fig. 4-23: Map compilation of river steepness and sinuosity, tectonic information and precise levelling, and Quaternary morphostratigraphic units – Zürich Nordost 65

Fig. 4-24: Summary profile along the 2D seismic reflection line 91-NO-68 66

Fig. 4-25: Summary profile along the 2D seismic reflection line 91-NO-77 67

Fig. 4-26: Detailed topographic map of the Cholfirst area 70

Fig. 4-27: Parallel profiles across the Neuhausen Fault at the "Cholfirst" location 71

Fig. 4-28: Apparent fault throw rate of the Neuhausen Fault since TDS deposition (profile 3) 73

Fig. 4-29: Apparent fault throw rate of the Neuhausen Fault since TDS deposition (profile 4) 74

Fig. 4-30: Magnitude and depth distribution of earthquakes presented in the swath profiles 75

Fig. 5-1: Horizontal velocity components deduced from repeated GNSS measurements for NaGNet stations (black) and surrounding permanent stations (grey) 81

List of Acronyms

a	year (date)
AD	Anno Domini
AGNES	Automated GNSS Network for Switzerland
a.s.l.	above sea level
BIH	Baden-Irchel-Herdern Lineament
DEM	Digital Elevation Model
DTM(-AV)	Digital Terrain Model (-Amtlicher Vermessung)
ECRIS	European Cenozoic Rift System
ETRF	European Terrestrial Reference Frame
Fm.	Formation
FMT	Mont Terri rock laboratory
GIA	Glacial isostatic adjustment
GNSS	Global navigation satellite system
HDS	Höhere Deckenschotter
HLW	High-level waste (spent fuel assemblies and high-level waste from reprocessing)
HT	Hochterrasse
ITRF	International Terrestrial Reference Frame
JO	Jura Ost siting region
ka	Thousand years (date, age)
Ksn	Normalised channel steepness
kyr	Thousand years (duration)
LAV	Lower Aare Valley
L/ILW	Low- and intermediate-level waste
LEB	Local erosion base
LGM	Last Glacial Maximum
Ma	Million years (date, age)
Max	Maximum value of distribution
Mean	Mean value of distribution
Min	Minimum value of distribution
M_L	Local magnitude (scale)
Mode	Modal value of distribution

MT	Mandach Thrust
M_W	Moment magnitude (scale)
Myr	Million years (duration)
NAB	Nagra Work Report ('Nagra Arbeitsbericht')
NagNet	Nagra's permanent GNSS Network
NF	Neuhausen fault
NL	Nördlich Lägern siting region
NT	Niederterrasse
NTB	Nagra Technical Report ('Nagra Technischer Bericht')
PDF	Probability density function
PEGASOS	Probabilistic seismic hazard analysis for Swiss nuclear power plant sites
PRP	PEGASOS Refinement Project
R, r	Pearson correlation coefficient
SED	Schweizerischer Erdbebendienst (Swiss Seismological Service)
SFOE	Swiss Federal Office of Energy
SGT	Sectoral Plan for Deep Geological Repositories
S_{Hmax}	Maximum horizontal stress magnitude
S_{hmin}	Minimum horizontal stress magnitude
SI	Channel sinuosity index
SRTM	Shuttle Radar Topographic Mission (of NASA)
STA3	Nagra deep borehole Stadel 3
S_v	Vertical stress magnitude
swissALTI3D	Swiss high-resolution digital elevation model
TDS	Tiefere Deckenschotter
TRU1	Nagra deep borehole Trüllikon 1
TWT	Two-way travel time
WGE	Weiach-Glattfelden-Eglisau Lineament
wrt.	with respect to
yr	year(s)
z	depth
ZNO	Zürich Nordost siting region

1 Introduction

Neotectonic activity involves recent or active crustal deformation and associated seismicity, the forces that are responsible for the crustal state of stress and their relation to plate tectonic processes (e.g. Strecker et al. 2009, Trifonov 1989). The temporal range for "neotectonic activity" is often set to the Neogene and Quaternary or, more generally, since the last plate-tectonic reorganisation in a region. Accordingly, the neotectonic framework considers the crustal movement that has been active under the prevailing stress regime (e.g. Stewart & Hancock 1994). In Northern Switzerland, this dates back to Miocene times (Nagra 2024i). Such a long timeframe might have entailed more processes and uncertainties than seem reasonable to assume for the evaluation of when evaluating the future one next million years – uncertainties may be too high, processes and rates averaged, and evidence largely overprinted. In contrast, the term "active tectonics" is often used and restricted to a shorter timeframe, i.e. Quaternary, late Pleistocene, or even Holocene, depending on the tectonic setting in the area of concern. Wallace (1984) considers "active tectonics" as tectonic activity that is expected to occur in a time span of societal relevance. Consequently, the period under consideration of one million years into the future for high-level nuclear waste defines the minimum period for analysis of the past tectonic evolution. In this report, we focus on the time period after the main thin-skinned phase of folding and thrusting in the Jura i.e. about four million years (Becker 2000, Nagra 2014b, Nagra 2024i). The different temporal and spatial scales involved in neotectonic activity over such long time require different tools to capture short-term and long-term processes and understand the neotectonic system and their interdependencies (Fig. 3-1).

The study of neotectonics may also include the search for "capable faults"; these are faults that have significant potential for displacement at or near the surface (e.g. IAEA 2015) but also "potentially active faults" (that can potentially be active under the present tectonic stress regime; e.g. IAEA 2022, Machette 2000). Along with fault slip, secondary effects of neotectonic activity may cause alteration of a rock volume and result in localised changes to the permeability.

This report provides background information for Section 6.2 (Future tectonic evolution) within the Geosynthesis (Nagra 2024i), as well as reports evaluating the impact of earthquakes on the deep geological repository (Nagra 2024f) and the seismic hazard assessment of the surface facilities of the repository and the encapsulation plant (Nagra 2024e, 2024d).

We start with an integrated summary of the geodynamic setting of Northern Switzerland over different spatial and temporal scales, starting with the European geodynamic framework. Because large-scale geodynamic processes define the regional tectonic regime of Northern Switzerland, plate tectonic processes are linked to observed tectonic domains and regional fault zones (Chapter 2). Because Northern Switzerland is strongly influenced by glacial/interglacial cycles with repeated growth of an Alpine ice cap and advancing glaciers far into the foreland, this chapter also provides a brief review of effects of glacial isostatic adjustment (GIA).

Tectonic deformation rates in Northern Switzerland are low within a European context. Chapter 3 reviews the evidence for this claim. This is based on a brief characterisation of regional faults and the rock volume in between them, a comprehensive summary on existing seismicity data and geodetic surface velocities, as well as a systematic analysis of the landscape and Quaternary landforms for indications of neotectonic activity. These observations are interpreted and summarised on a regional to local (i.e. siting region) scale in Chapter 1.

The available evidence from the tectonic evolution and present state of tectonism provides the basis for a conceptual tectonic model and future scenario for the next million years (Chapter 5).

Finally, the main conclusions that can be drawn from the presented analyses are summarised in Chapter 6.

2 Geodynamic setting of Northern Switzerland

This chapter presents the geodynamic context of the siting regions identified in Northern Switzerland. The review starts with a geodynamic framework of Europe to highlight the (intra)plate-tectonic setting and its low tectonic rates (Section 2.1). This review is followed by further detail on the fault systems that are associated with regional tectonic elements of Northern Switzerland, and which border the siting regions (Section 2.2). These fault systems may be active under neotectonic conditions and play a central role in the interpretative basis for the conceptualisation provided by Chapter 5.

2.1 Northern Switzerland within the European geodynamic framework

Northern Switzerland is part of Central Europe. It is located within a rigid domain bounded by the tectonic zones of Iberia, Eastern Europe, and the northern Mediterranean realm to the south (Nocquet & Calais 2004). Most deformation is accommodated along diffuse block boundaries. Generally, these regions exhibit slow intracontinental deformation expressed by low geodetic velocities hardly exceeding the measurement uncertainties (see Fig. 2-1 b) and low strain rates paired with diffuse seismicity (Fig. 2-1c, e.g. Piña-Valdés et al. 2022). The most pronounced seismicity rates of the European continent are observed in Italy and the Hellenic subduction zone (Piña-Valdés et al. 2022).

The geodynamic setting of Central Europe is influenced by tectonic convergence between the African and Eurasian Plates. The largest geodetic velocities and up-to-a-magnitude-higher strain rates, however, are measured in the eastern part of the Africa-Eurasia plate boundary zone in Greece and Turkey (e.g. DeMets et al. 1990, Serpelloni et al. 2022). Velocities decrease significantly towards the western plate boundary zones, closer to the Alps. Here, active deformation is influenced by independent microplate motion, such as the counterclockwise rotation of the Adriatic plate as well as Tyrrhenian and Aegean back-arc extension (e.g. Nocquet & Calais 2004, Piña-Valdés et al. 2022), see Fig. 2-1d for the maximum horizontal compressive stress (S_{Hmax}) orientations. The highest velocities within the western plate boundary zone are located along diffuse areas, such as the Apennines, the Dinarides, and the Betic Cordillera (Fig. 2-1a). Correlations between seismicity and the horizontal strain rate on one hand or gradients of vertical displacement on the other, indicate that the Betic Cordillera, similar to the high strain areas of the Corinth Rift in Greece or the North Anatolian Fault in Turkey, are mainly controlled by lithospheric processes. The Apennines, however, might show a combined result of tectonic shortening and mantle-driven deformation (Piña-Valdés et al. 2022) and superposed, widespread extensional deformation in the core of the mountain belt (Cavinato & Celles 1999).

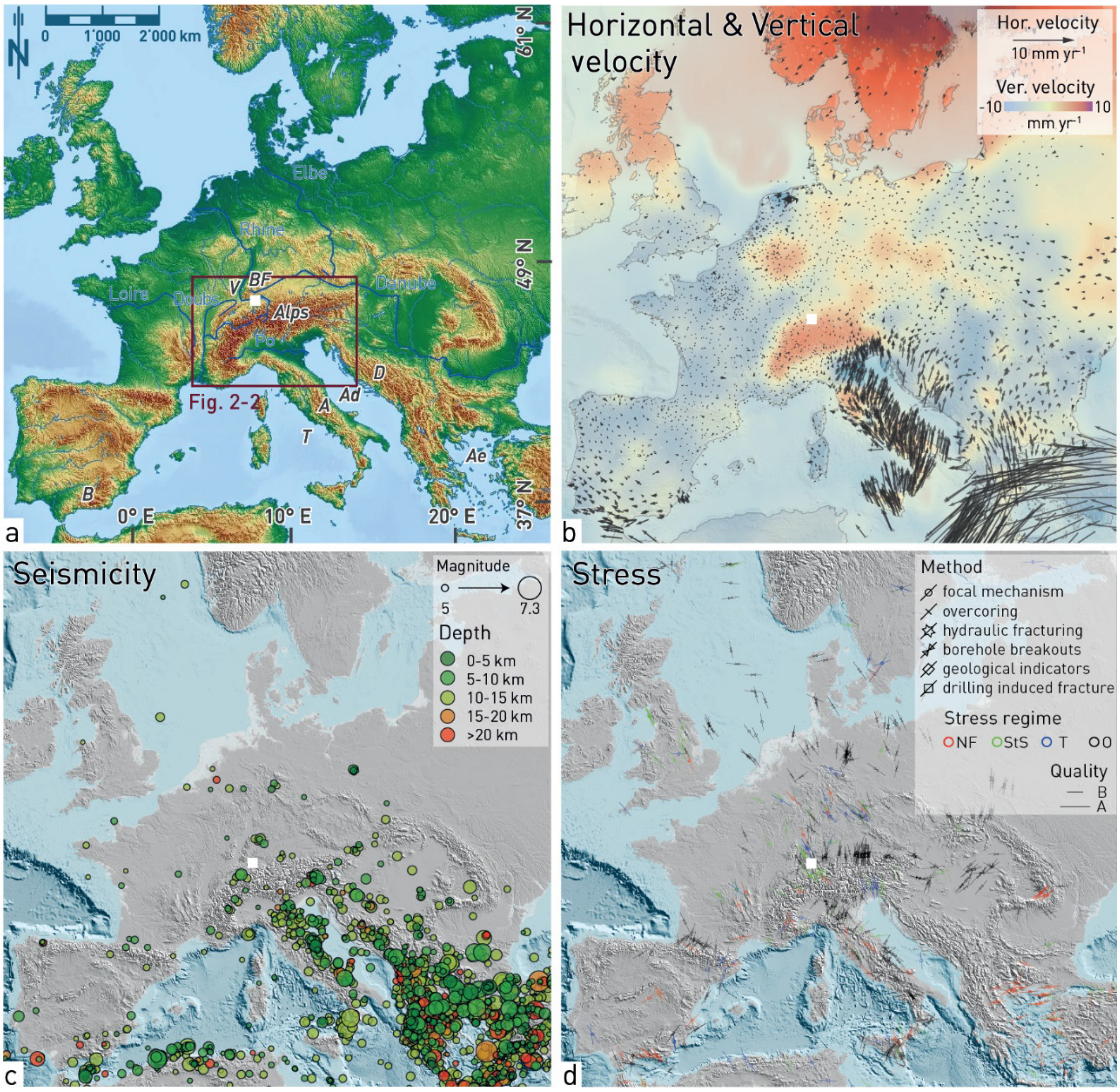

Fig. 2-1: Velocity fields, seismicity, and tectonic stress field in Europe

Hillshade and digital elevation map (a) of Europe. The box highlights the boundary of subsequent figure. Labels of geographic features discussed in Section 2.1. V: Vosges, BF: Black Forest, A: Apennines, B: Betic Cordillera, D: Dinarides, Ad: Adriatic Sea, T: Tyrrhenian Sea, Ae: Aegean. (b) Smoothed and harmonised 3D geodetic velocity field across Europe and within a Stable-Europe framework (Piña-Valdés et al. 2022) (c) Earthquakes with magnitudes equal to and larger than 5 between 1900 AD and July 2023 (https://earthquake.usgs.gov/earthquakes/search/; retrieved July 10th 2023), scaled by magnitude and colour-coded by depth. High seismicity regions in Europe (e.g. Greece and Italy) are associated with subduction processes and coincide with regions of large horizontal tectonic velocities. (d) Axes of maximum horizontal compressive stress (S_{Hmax}). The database for S_{Hmax}-measurements was derived from the World Stress Map project (CASMO); stress indicators are colour-coded by their respective faulting regime (Heidbach et al. 2018). The small white square in all figures represents the approximate position of Zürich. NF: Normal faulting, StS: Strike-slip faulting, TF: Thrust faulting, O: Oblique faulting.

The tectonic drivers of ongoing Alpine uplift are thought to include significant buoyancy-driven processes (Fig. 2-2; e.g. Sternai et al. 2019, Piña-Valdés et al. 2022). Isostatically driven processes, such as postglacial or erosional rebound/unloading, dynamic topography (upper mantle processes) and horizontal gradients of gravitational potential energy vary across Switzerland. The vertical velocity field of the Alps based on GNSS measurements is ~ 2 mm/yr along the Alpine arc (Fig. 2-2), increasing from west to the central Alps with a positive correlation with respect to topography (Sánchez et al. 2018, Piña-Valdés et al. 2022, Serpelloni et al. 2022, Pintori et al. 2022). The total uplift rates are generally higher in the areas that are undergoing less horizontal shortening, i.e. they are higher in the western and central Alps compared to the eastern part (Sternai et al. 2019).

Towards the Alpine forelands north and south, vertical velocities decrease to positive sub-millimetre and even to stable zero mm/yr rates (Sánchez et al. 2018, Henrion et al. 2020, Pintori et al. 2022; see Fig. 2-2a). Low uplift rates are observed in the Jura Mountains and the Molasse Basin. A weak subsidence signal continues into the shoulder areas of the Upper Rhine Graben and the Black Forest and Vosges Mountains. This is probably associated with subsidence in the Southern Upper Rhine Graben north of Basel and west of the Southern Upper Rhine Graben towards the Bresse Graben (Sánchez et al. 2018, Henrion et al. 2020, Pintori et al. 2022). Even farther north, uplift of the Rhenish Massif and specifically the Eifel region is observed at a rate of ~ 0.5 – 1 mm/yr (Fig. 2-1b; Henrion et al. 2020, Piña-Valdés et al. 2022). This is beyond the scope of this section, but it is relevant for the assessments concerning regional baselevels and erosion related to the river Rhine and this topic is therefore addressed in Nagra (2024h).

In the Alpine region, horizontal geodetic velocities are influenced by microplate deformation, but the rates are lower than in above mentioned zones, despite considerable topographic relief and vertical motion (Fig. 2-1a and b, Fig. 2-2). In the Eastern and eastern part of the Southern Alps, ~ 2 mm/yr of plate motion are accommodated between the Adriatic Plate and Stable Europe (Sánchez et al. 2018, Sternai et al. 2019, Serpelloni et al. 2022, Piña-Valdés et al. 2022). These areas exhibit higher strain rates than most areas in the Swiss Alps, where strain rates are very low (Fig. 2-2c and d). Rabin et al. (2018) characterised the Northern Swiss Foreland between Lucelle in the west and Zürich in the east as a zone with consistent low eastward to northeast-directed motion, despite being located partly within the Molasse Basin and the eastern Internal Jura. The general trend of low shortening rates seems to be controlled by the distance from the Alps.

Switzerland has a well-documented historical record of seismicity, which dates back several hundreds of years in terms of felt seismicity. Fig. 2-3 shows a map of Switzerland with the historically documented and instrumentally measured seismicity and modelled occurrence rates of large earthquakes (swissnuclear 2013). The distribution of seismicity in Switzerland generally coincides with large tectonic domains (Fig. 2-3). A recent study by Lanza et al. (2022) provided evidence for active deformation in the Internal Jura, with shallow thrusting in the area of St. Ursanne, in the central Jura Fold-and-Thrust Belt. The area around Basel has a relatively increased seismicity rate, probably related to recent tectonic activity in the Upper Rhine Graben. The canton of Valais and the eastern part of the country show increased levels of seismicity and are located within the Alps. The Hegau – Bodensee Graben extending from the Bodensee to the NW is also characterised by frequent present-day seismicity (Diehl et al. 2023). The area of the siting regions is located between the Upper Rhine Graben and the Hegau – Bodensee Graben. Here, seismicity is generally low. Small earthquakes have, however, also occurred close to the siting regions (Fig. 2-3 and Fig. 3-3).

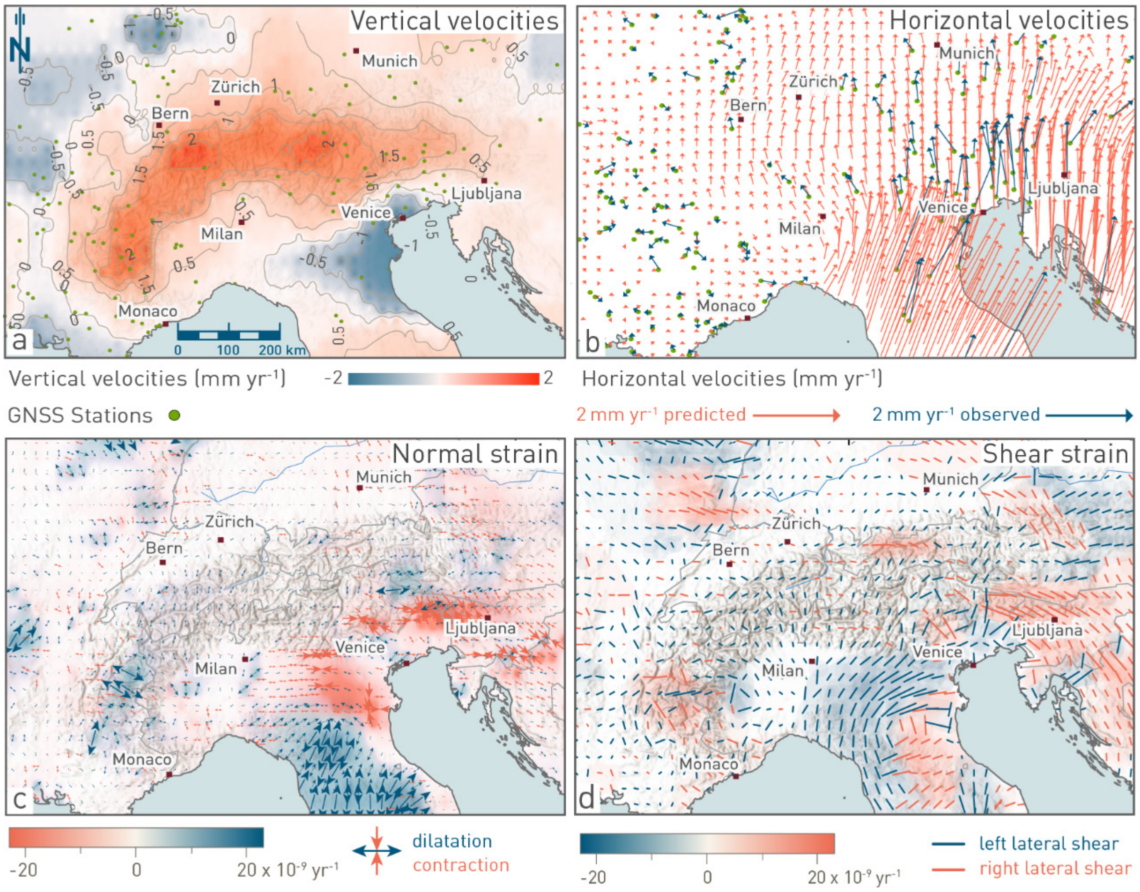

Fig. 2-2: Deformation model of the Alpine region from GNSS velocities with normal and shear strain distribution in the Alpine region and beyond

(a) Observed and modelled vertical velocities (red positive, blue negative) and (b) horizontal velocities (redrawn from Sánchez et al. 2018). Northern Switzerland is located within an area of low deformation rates, low uplift rates and generally northward-decreasing horizontal motions (see Zürich for approximate location). (c) The map outlines areas that undergo shortening (red) or extensional deformation (blue) (d) Map shows areas undergoing left-lateral (blue) versus right-lateral (red) shearing (redrawn from Sánchez et al. 2018). Strain rates are low within the Alpine Foreland and hardly resolvable in the model at the location of the siting regions (see Zürich for approximate location). For strain rates in (c) and (d) refer to the colour spectrum.

In summary, the neotectonic setting of Northern Switzerland is influenced by the Alpine orogeny in the south, low-rate deformation within the Upper Rhine Graben, the Hegau-Bodensee Graben, and modest tectonic activity in the Jura Fold-and-Thrust Belt. Tectonic deformation rates and seismicity in Northern Switzerland are very low. The low observed uplift rates and some seismicity might be related to buoyancy forces applied to the Alps with decreasing influence towards the foreland. Northern Switzerland is a low-strain area with ongoing tectonic deformation.

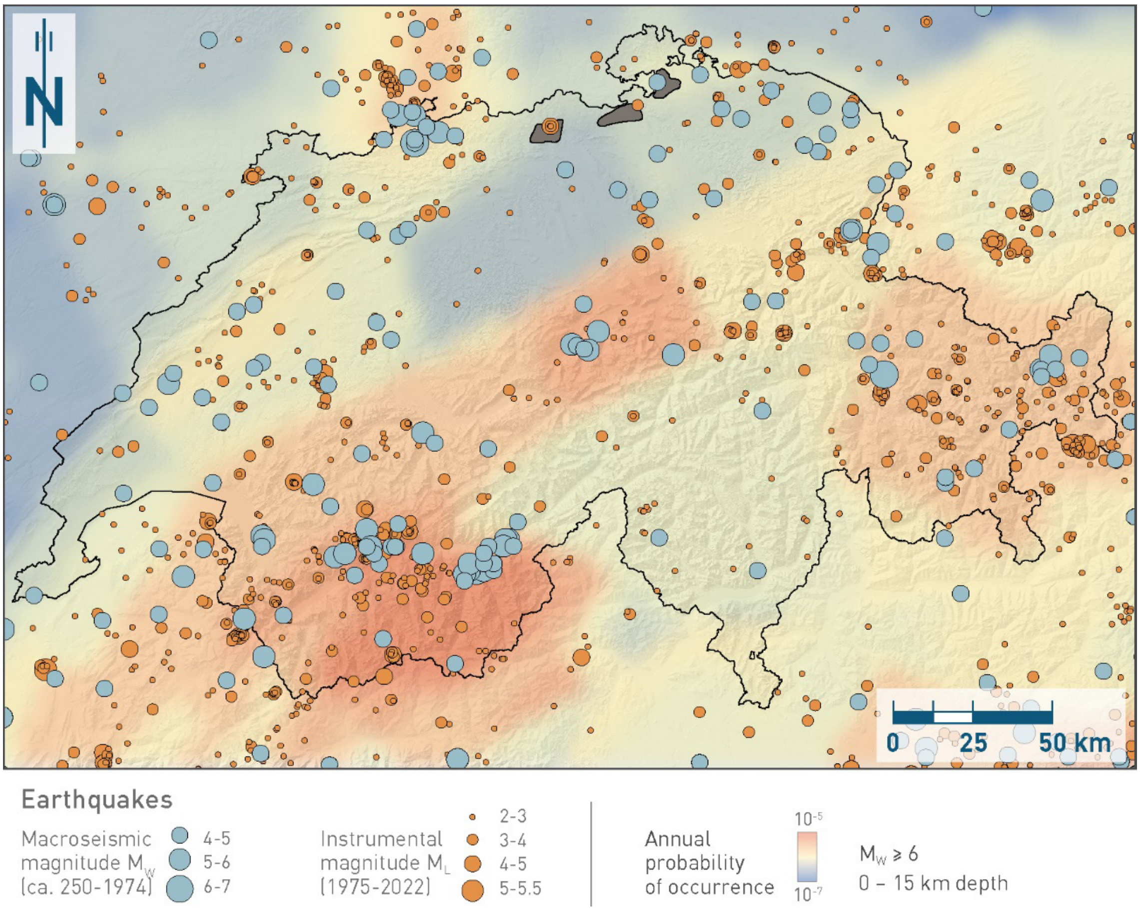

Fig. 2-3: Overview map of historical and instrumentally recorded earthquakes and modelled probability of occurrence for earthquakes with $M_W \geq 6$

Historical earthquakes (blue) and instrumentally recorded events (red; both in same magnitude symbol scaling) show higher concentration in the areas around Basel, the Valais, and Eastern Switzerland. The background colour indicates the smoothed estimated annual probability of occurrence for earthquakes with $M_W \geq 6$ for hypocentral depths < 15 km, determined in the framework of the PRP project (swissnuclear 2013). Siting regions are marked in dark grey.

2.2 Tectonic framework of Northern Switzerland

Multiple tectonic domains and processes have influenced the evolution of Northern Switzerland and have resulted in the present-day structural setting (Nagra 2024i). These include the formation of the Konstanz – Frick Trough, the Alps, the Upper Rhine Graben, the Hegau – Bodensee Graben as well as the folding and thrusting of the Jura Fold-and-Thrust Belt (Nagra 2024i). In this section, the main structural elements and their relative influence on the configuration and state of the three siting regions Jura Ost (JO), Nördlich Lägern (NL) and Zürich Nordost (ZNO) are briefly introduced (Fig. 2-4). A detailed description of the tectonic elements, the overall tectonic setting and the tectonic evolution of Northern Switzerland is given in Nagra (2024i).

Konstanz – Frick Trough

The buried Konstanz – Frick Trough constitutes a graben system trending ENE-WSW across central Northern Switzerland. Its depth is estimated as up to 5 km for the eastern segment, i.e. underneath JO. To the west, the Konstanz – Frick Trough is inferred to link with the Burgundy Trough system (Madritsch et al. 2018 and references therein). Field observations and paleostress reconstructions reported in Madritsch et al. (2018) from the Black Forest Massif, where the Paleozoic basement is exposed, indicate that a Late Paleozoic phase of dextral strike-slip deformation (NW-SE S_{Hmax}) was superseded by approximately NE-SW-directed extension. The ENE-WSW trending southern and northern margins of the trough are partially offset by WNW-ESE striking conjugate faults (Müller et al. 2002, Marchant et al. 2005). The Paleozoic fault pattern provides zones of mechanical weakness within the less deformed rock volume. This localised Mesozoic and Cenozoic deformation (Nagra 2024i).

Alpine orogeny and forebulge migration

The Alpine orogeny resulted in a significant build-up of topography south of Northern Switzerland. The resulting topographic load resulted in lithospheric flexure forming the Molasse Basin in the Cenozoic, which was filled with erosion products derived from the Alps. The lithospheric flexure produced a forebulge marking an area of uplift and erosion (e.g. Schlunegger & Mosar 2011). An increase in lithospheric flexure due to Alpine topographic loading eventually resulted in northward migration of the forebulge, which in turn caused normal faulting during the Paleogene in Northern Switzerland and southward tilting of the Mesozoic strata (Laubscher 1985).

Upper Rhine Graben

Late Cenozoic extensional deformation in Europe was driven by the closure of Apulia with the southern European block and included important extensional and strike-slip reactivation of inherited structures (European Continental Rift System; ECRIS). The structural framework of the Upper Rhine Graben as well as that of the Hegau – Bodensee Graben are strongly influenced by the occurrence of inherited Palaeozoic faults (Egli et al. 2017, Giamboni et al. 2004, Rotstein & Schaming 2011). According to Rotstein & Schaming (2011), the evolution of the Upper Rhine Graben can be subdivided into two phases with an early rifting stage (Eocene – Oligocene) and a later transtension – transpression stage (Early Miocene – Pliocene). The rifting phase was characterised by a normal faulting stress regime with E-W trending S_{hmin}, whereas the subsequent strike-slip dominated stage has been characterised by a NNW-SSE trending orientation of S_{Hmax} (Fig. 2-4). Rift shoulder uplift was accompanied by normal faulting in the Black Forest Massif and surroundings (i.e. Northern Switzerland) as well as additional tilting of the Mesozoic strata.

Hegau – Bodensee Graben

The main tectonic activity in the Hegau – Bodensee Graben occurred during the Upper Miocene to Pliocene (Schreiner 1992). Early stages of deformation were accompanied by volcanic activity and the deposition of the Obere Süsswassermolasse (OSM, Wittmann 1937, Schreiner 1992). Tectonic activity in the graben increased syn-and post-tectonic sedimentation of the Obere Meeresmolasse (OMM, Ibele 2015). The Randen Fault (NE of Zürich Nordost) experienced a total of 170 m down-dip offset since Mid-Miocene (Schreiner 1992). Field data indicate that at least since the Middle Miocene large-scale strike-slip tectonics was the main deformation mechanism in the Freiburg – Bonndorf – Bodensee Fault Zone, which encompasses the Hegau – Bodensee Graben (Egli et al. 2017). The deformation resulted in predominantly NE-SW directed extension. The graben structures are considered as a local kinematic response to the crustal-scale strike-slip motion with extension accommodated along suitably oriented inherited faults (Egli et al. 2017). The regional Neuhausen Fault delimiting the siting region Zürich Nordost to the northeast is related to the Hegau – Bodensee Graben system.

Jura Fold-and-Thrust Belt

The Jura Fold-and-Thrust Belt is often conceptualised as a frontal accretion of the mechanical Alpine wedge related to the NW propagation of the Alpine contractional deformation front in response to exhumation of the External Crystalline Massifs (e.g. Mosar 1999, Bonnet et al. 2007, Willett & Schlunegger 2010, Schlunegger & Mosar 2011). It is subdivided into the Internal Jura, representing the more deformed part and the less deformed External Jura (Sommaruga 1997). Internal Jura is often also referred to as High Jura or Folded Jura. The External Jura was referred to as "deformed Tabular Jura" or "Vorfaltenzone". The deformation propagation occurred along Triassic evaporites acting as décollement horizon (Buxtorf 1916, Laubscher 1961, Jordan & Nüesch 1989, Jordan 1992). The formation of the Jura Fold-and-Thrust Belt initiated at the latest at ~ 14.3 Ma as documented by décollement-related deformation (i.e. thin-skinned deformation) observed in the Schafisheim borehole (Looser et al. 2021). This first thin-skinned dominated deformation phase was superseded by a thick-skinned dominated deformation phase, as documented by fault segments in the Weiach – Glattfelden – Eglisau Lineament cutting from the Paleozoic basement through the Triassic sequence (Nagra 2024i and references therein).

Focus on siting regions

The influence of the aforementioned tectonic elements on the siting regions is detailed in Nagra (2024i). Importantly, the tectonic evolution of Northern Switzerland suggests that the present-day structural inventory is either guided or overprinted by the occurrence and/or evolution of these tectonic elements.

The influence of the Konstanz – Frick Trough is observed within all siting regions with, however, a subordinate influence in ZNO (Fig. 2-4). Evidence for the NW-migration of the Alpine forebulge and the associated normal faulting is found in all three siting regions. Faults that are probably kinematically linked to the transtensional formation of the Upper Rhine Graben are observed in JO only. High-angle faults associated with the formation of the Hegau – Bodensee Graben are observed predominantly in ZNO. The Jura Fold-and-Thrust Belt, both in the early thin-skinned dominated deformation phase and in the later thick-skinned dominated deformation phase, overprint JO, NL and the southwestern corner of ZNO.

In the framework of SGT Stage 1 (SFOE 2008), so-called "regional fault zones" were defined based on outcrop mapping as well as 2D seismic reflection lines. Within SGT Stage 2 and especially Stage 3, these regional fault zones were grouped into corridors (fault polygons in map view) that encompass multiple fault segments. In Northern Switzerland, regional fault zones encompass the Mandach Thrust, the Jura Main Thrust, the Lägern Anticline, the Baden – Irchel – Herdern Lineament, the Weiach – Glattfelden – Eglisau Lineament, the Siglistorf Anticline and the Neuhausen Fault (Fig. 2-4). A complete terminology, comprising all brittle structures and a description of the fault inventory in the siting regions NL, JO and ZNO, is provided in the Geosynthesis (Nagra 2024i).

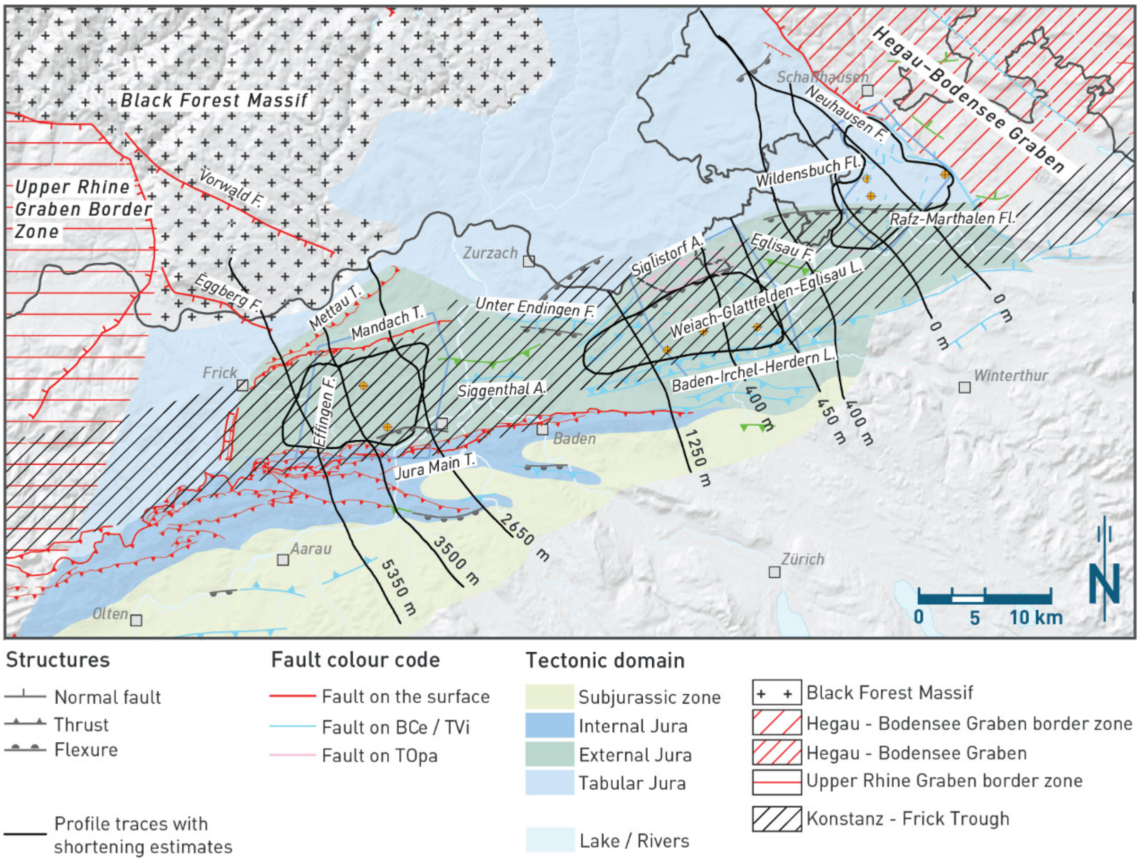

Fig. 2-4: Simplified tectonic map between the Upper Rhine Graben and Hegau – Bodensee Graben and containing the siting regions

The colour code for the faults refers to the highest stratigraphic level upon which the fault trace is observed. Surface refers to the Earth's surface, BTe to Base Cenozoic (i.e. Top Malm Group), TOPa refers to Top Opalinus Clay, TSta refers to Top Lias Group, TMk refers to Top Muschelkalk Group, BMz refers to Base Mesozoic unconformity. Note that only a selection of the structures from 3D seismic interpretation is shown to highlight the structural trends of regional importance. These were projected from Top Villigen Formation to Base Cenozoic.

The shortening estimates are based on geometric restoration of 2D geological profiles along 2D seismic reflection lines (Jordan et al. 2015; see also Tab. 5-1). The Jura Fold-and-Thrust Belt encompasses the Internal and External Jura. Internal Jura is often also referred to as High Jura or Folded Jura. The External Jura was referred to as "deformed Tabular Jura" or "Vorfaltenzone". The Subjurassic zone is part of the Molasse Basin but is probably more deformed than the typical Molasse. A.: Anticline, F.: Fault, Fl.: Flexure, L.: Lineament, T.: Thrust. Black polygons indicate siting regions and black lines country borders.

2.3 Effects of glacial isostatic adjustment (GIA)

During the Pleistocene, orbitally driven glacial-interglacial cycles caused the growth and decay of ice caps in the Alps; consequently, the regions of Northern Switzerland were subjected repeatedly to extensive foreland glaciations (Nagra 2024g). Consequently, the region is expected to be subjected to future glacial cycles as well and undergo glacial isostatic adjustment (GIA) with spatiotemporal modulation of the deformation.

On a global scale, most observations and studies regarding glacial isostatic adjustments have been made in areas previously located below large continental ice sheets, as below the Fennoscandian or the Laurentide ice sheets, for instance. In the core regions of these formerly glaciated areas, ice thicknesses reached heights of several kilometres (e.g. Craig et al. 2016) and post-glacial rebound is measured today (e.g. Johansson et al. 2002, Lambert et al. 2001, Piña-Valdés et al. 2022). GIA is assumed to be the main reason for elevated uplift rates, strain distribution, and even increased seismicity in these areas (e.g. Piña-Valdés et al. 2022, Grollimund et al. 2001, Steffen et al. 2012, 2014, Craig et al. 2016, 2023).

In their recent evaluation of the present-day European velocity field based on GNSS data, Piña-Valdés et al. (2022) reveal that in Scandinavia, GIA-related vertical uplift locally exceeds 10 mm/yr. Strong postglacial uplift is focused on central Scandinavia. Uplift extends towards the southern shore of the Baltic Sea, into Denmark, Scotland, and Ireland, although at lower rates (see Fig. 2-1b). The proportion of present-day body force changes due to glacial (un)loading processes in the Alps is currently debated, with authors attributing GIA-only (e.g. Mey et al. 2016) and others including effects of erosion (Champagnac et al. 2009) or delamination (see Sternai et al. 2019 and Mazzotti et al. 2020 for a summary). GIA and erosional unloading may contribute to ~ 50% of the observed vertical motion in the western and central Alps (Sternai et al. 2019). GIA effects might be still detectable in the Alpine foreland, although at lower levels due to lower ice thickness and duration of glacial loading. The presently observed higher vertical motion measured by GNSS or precise levelling with respect to long-term vertical motion derived from river incision or exhumation data (Nagra 2024h), accordingly, might be the effect of GIA.

From GIA modelling and observational data (e.g. uplifted shorelines) it is known that GIA effects are rapid shortly after deglaciation followed by an apparent exponential decrease in uplift rates and crustal strain (see for instance Turcotte & Schubert 2014, Grosset et al. 2023). Accordingly, the highest rates of deformation, earthquake occurrence, and surface process changes are expected immediately after ice retreat.

Glacial isostatic adjustment also influences the horizontal velocity field (e.g. Craig et al. 2016). Such transient changes are observed in the immediate vicinity of the glacial load but also in the far-field, up to several hundred kilometres away (e.g. Grollimund et al. 2001, Brandes et al. 2015). The temporal coincidence between deglaciation-related isostatic adjustment and an increase in seismicity, partly associated with large-magnitude earthquakes and long fault ruptures in areas otherwise characterised by low tectonic deformation rates, has opened the field of glacio-seismotectonics (Stewart et al. 2000 and references therein). Grollimund et al. (2001) argue that the sequence of large magnitude earthquakes in the New Madrid seismic zone in North America between AD 1811 – 1812, can still be associated with increased seismic strain rates caused by the deglaciation of the Laurentide ice sheet, although the ice-sheet front was located several hundred kilometres away. For this reason, phases of increased fault activity need to be considered in combination with future glacial cycles, especially for a prolonged phase immediately after deglaciation. Fault motion might be suppressed during ice occupation times (Johnston 1987, Craig et al. 2016).

Data on earthquakes or uplift time series in low-strain areas that can document such postglacial-related behaviour unambiguously are rare – this is similar for the Alps or Alpine foreland. Often, postglacial fault scarps are clearly detected, but deformation is difficult to date or may coincide or correlate with deep-seated gravitational slope motion (e.g. Ustaszewski & Schmid 2007, Ustaszewski & Pfiffner 2008), hampering a differentiation between tectonic and non-tectonic origin. Studies compiling palaeoearthquake data from postglacial lake records (Strasser et al. 2013, Chapron et al. 2016, Kremer et al. 2017) show that events occur throughout the Holocene, but the records are less complete with increasing age. These authors generally attribute mass transport – or sedimentary event deposits – to postglacial isostatic adjustment increasing the ambiguity. The evidence is indirect: increased sediment delivery by flooding or glacial advances causes slope instabilities (thus increasing likeliness of failure during an earthquake).

Interestingly, comparison of measured horizontal strain rates (e.g. NW-SE extension in Scandinavia) and observed post-glacial fault motion (e.g. thrusting) shows an inconsistency between the strain rate and stress (Muir-Wood 2000, Craig et al. 2016, 2023, Grosset et al. 2023). While the GIA is able to perturb the overall stress field and either inhibit or trigger faulting (e.g. Hetzel & Hampel 2005, Craig et al. 2016, 2023), the associated faults must be pre-stressed from the long-term tectonic elastic strain accumulation in the lithosphere. For areas with low tectonic deformation rates (i.e. including Northern Switzerland), seismicity rates may vary with non-tectonic fault suppression or triggering modulating steady tectonic loading (Craig et al. 2016).

In a recent modelling study, Craig et al. (2023) compared time-variable GIA-related stress and strain rates in the European continental interiors, caused by transience from (de)glaciation of the Fennoscandian and Laurentide ice sheets. They also include the Alpine ice cap in their model. While minor with respect to the ice sheets, GIA nevertheless has an effect on the strain pattern in central Europe. The shorter wavelength signal is, however, predominantly supported elastically, thus produces a fast and localised crustal response (Craig et al. 2023). These authors furthermore show that magnitude and orientation of the principal horizontal strain axes reveal complex temporal rotations and reversals around the periphery of the major ice sheets and the areas of the forebulge. This in turn has consequences for the failure of favourably oriented faults, which might undergo different phases of failure and suppression of slip. For the area of Northern Switzerland, for instance, their models revealed predominantly NNE-directed horizontal shortening with WNW extension between 25 and 24 ka, a reversal to NNE-directed extension and minor WNW shortening 19 – 18 ka, nearly N-S extension between 13 and 12 ka, changing to NW-SE extension 7 – 6 ka and finally, NNE-directed shortening with similar magnitude of WNW-directed extension between 1 ka and today (Craig et al. 2023). The highest strain rates simulated in the study occurred about 19 – 18 ka.

We conclude that in Northern Switzerland, the rate of seismicity is modulated by transient non-tectonic stress perturbations (e.g. GIA-related), while the overall mechanism of strain release follows the long-term tectonic elastic strain stored in the lithosphere. The low tectonic strain accumulation and non-tectonic modulation of strain release result in a complex temporal and spatial pattern of seismicity (e.g. Stein et al. 2017). This seismicity is expected to be released along the inherited (regional) faults, because the lower magnitudes of GIA-related stress and strain (with respect to tectonic loading) alone are not expected to bring faults to failure (or even create new faults), without them being pre-stressed.

3 Basis to evaluate neotectonic activity

In the previous chapters, we have provided the framework for the assessment of neotectonic activity and timescales that are relevant to deep-geological repositories in Northern Switzerland. The basis for such an assessment is a good understanding of geodynamic processes, the spatial distribution of the main tectonic domains that constitute the structural grain of the region including the present-day character of ongoing deformation and its relationship with pre-existing faults. In addition, we considered the dynamics of glacial isostatic adjustment (GIA) as one of the main non-tectonic modulators of deformation and vertical motion that needs to be accounted for in an overall evaluation of neotectonic processes at different timescales.

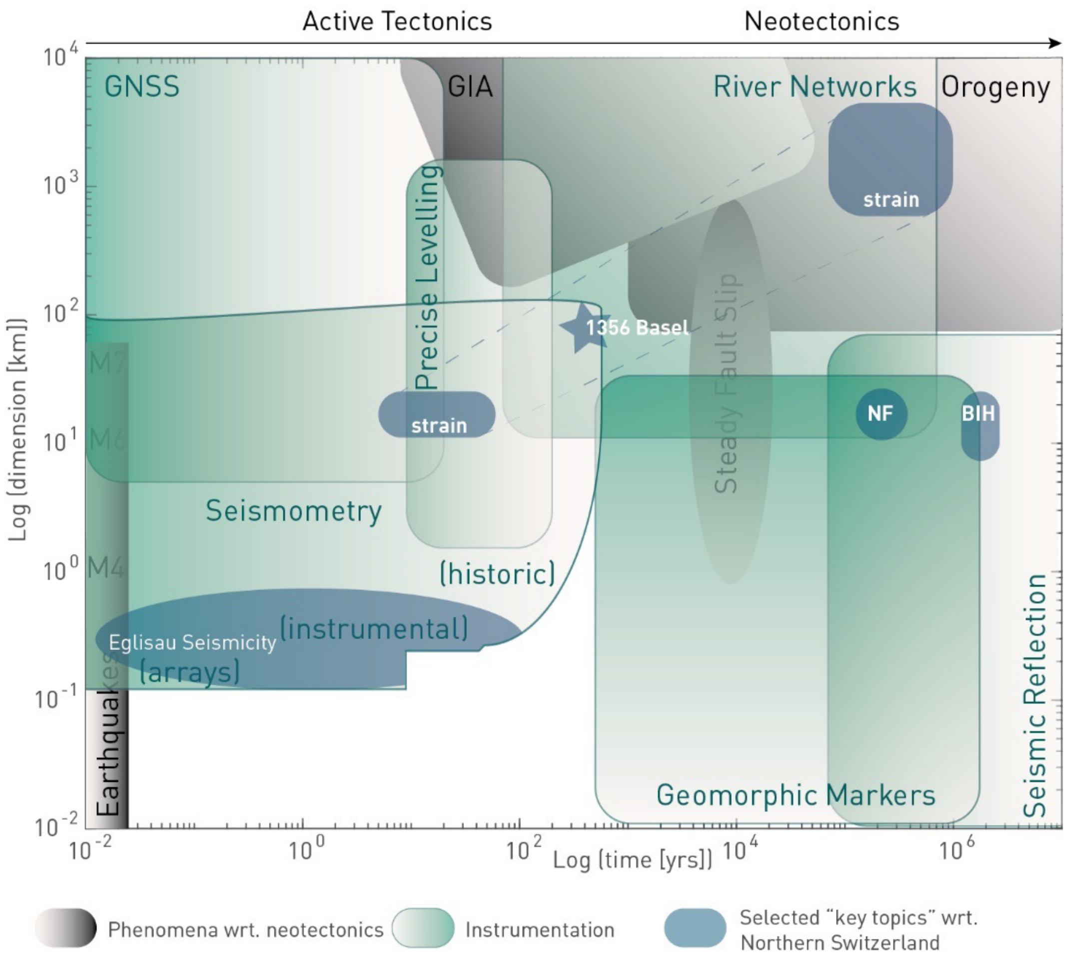

Fig. 3-1: Sketch showing tectonic phenomena, key topics, and instrumentation and involved spatiotemporal scales

This sketch combines the different spatial and temporal dimensions of tectonic and mass loading (GIA) phenomena (grey) and available tools to measure them (green, inspired by McCalpin 2009 and Burbank & Anderson 2001). Focus is the low strain area of Northern Switzerland, thus associated key topics are highlighted in blue. The sketch underscores the need of different tools to capture short-term and long-term processes and understand the neotectonic system and their interdependencies. Note that the activity of the Baden – Irchel – Herdern Lineament (BIH) and the Neuhausen Fault (NF) refer to the potential neotectonic activity and not to their initial formation during folding and thrusting of the Jura. GNSS: Global navigation satellite system, GIA: Glacial isostatic adjustment. wrt.: with respect to.

A number of proxies can be used to evaluate neotectonic activity (Fig. 3-1). These reach from short-term, but spatially available instrumental records such as seismicity or satellite geodesy to longer-term, geomorphic markers of a tectonically active landscape. Below, these proxies are introduced with respect to Northern Switzerland and with a brief review on progress during SGT Stage 3.

The spatio- and temporal ranges of proxies and measurement tools with respect to the observed processes are highlighted in Fig. 3-1. As illustrative examples, we anticipate a few “key topics” that are later introduced in the report.

The Eglisau seismicity (Sections 3.1 and 4.2.2.1) with its shallow and mainly low-magnitude earthquakes was known from a few felt earthquake events documented in historical seismic catalogues. Instrumental seismicity has increased the amount of data and recently installed arrays show continuous seismicity of very low magnitudes that were otherwise not be detectable. Such arrays help to better understand mechanisms behind the specific sequence. The AD 1356 Basel earthquake (M_w 6.6) in turn (see Section 3.1) is the largest known earthquake to be occurred in the region around Northern Switzerland based on historical catalogues. This event could have been well recorded but is too old for instrumental seismicity and geodesy. To go further back in time, for instance to understand neotectonic activity of regional faults like Baden – Irchel – Herdern Lineament or Neuhausen Fault, we need to rely on geomorphic strain markers, e.g, fluvial terrace remnants (see Section 3.6.3 and 4.2) and the river network (Section 3.6.2 and 4.1), to understand the longer-term local to regional deformation. These signals, however, are often the cumulative result of tangled tectonic and non-tectonic processes and are more ambiguous than as for instance the Eglisau seismicity. Accordingly, we seek to combine different instrumentation tools and proxies to capture the tectonic phenomena in Northern Switzerland and discuss them in a holistic way (Fig. 3-1).

3.1 Continuation and densification of weak motion seismic network

In 2013, the Swiss Seismological Survey (SED) in cooperation with Nagra completed the construction of stations that locally densify the seismic network across northeastern Switzerland to monitor the seismicity down to magnitude M_L 1.0 (Plenkers 2014). In addition, to improve the understanding of seismotectonic processes in the vicinity of proposed sites for deep geological repositories and zones of nearby increased seismicity, the existing network in Northern Switzerland and Southern Germany has been significantly densified with seven surface stations and three short-period borehole stations at depths of 120 – 150 m (see Fig. 3-2 for general evolution of seismic recordings in Northern Switzerland). A mobile pool of eight additional stations was approved by Nagra in 2018. In 2019, three of these stations replaced the hardware of semi-permanent stations installed in the region of Eglisau since 2016 to better understand the seismic behaviour of the shallow microseismicity cluster there (Fig. 3-2c, see also Section 4.2.2).

Three additional stations have been installed 2019 to improve the earthquake monitoring of the Neuhausen Fault. Two more stations were temporarily installed in the vicinity of the Nagra exploration drillsites in Bülach, Trüllikon, Marthalen, Bözberg, Stadel, Rheinau and Bachs to monitor and document possible seismicity induced by drilling operations. After the completion of Nagra's drilling campaign in 2022, the two available mobile stations were installed in the Eglisau region to further improve the local monitoring network. Furthermore, the exploration borehole in Bülach was equipped with a seismic sensor at the depth of the Opalinus Clay (about 940 m below the surface) in 2022. The complete set of 24 Nagra stations are fully integrated in the Swiss National Seismic Network operated by the Swiss Seismological Service (SED). Data of all weak and strong-motion stations acquired by the SED are used for nationwide real-time event detection. Combined, the network geometry reaches a magnitude of completeness below M_L 1 for most of Northern Switzerland with improved hypocentre locations (Diehl et al. 2021b, 2023). Since October 2012, the Swiss National Seismic Network uses the SeisComP monitoring software for automatic event detection and characterisation as well as manual review (see (Diehl et al. 2023)). Seismicity detected within the Nagra network is manually analysed (phase-picking, relocation, magnitude determination) during routine earthquake analysis at the SED and in a second step significant events are carefully reviewed. Finally, a local magnitude is estimated for each reviewed event.

In 2021, new 3D crustal V_p and V_s models for Northern Switzerland (Diehl et al. 2021a), developed in the framework of this project, have been implemented for routine analysis. Since June 2022, they provide the standard velocity model for routine analysis in the SED.

To further lower the detection thresholds, improve location accuracy, and to improve the completeness of the Eglisau catalogue, a waveform cross-correlation-based (CC) template-matching (TM) method was applied to the continuous data of station FLACH and complemented by a visual screening procedure using the "sonogram approach" to find additional (previously unknown) earthquake-like signals. To homogenise the absolute locations and corresponding hypocentre uncertainties, the entire instrumental seismicity in the Eglisau region between 1984 and 2022 was relocated with the procedure described in Diehl et al. (2021b). The corresponding formal horizontal uncertainty is 0.7 km. On average, the uncertainty in depth is ± 0.5 km.

Recent efforts of the Swiss Seismological Service resulted in a magnitude of completeness nearly below 1.5 for Switzerland (see Fig. 3-2a) and below 0.75 in the area comprising the siting regions in Northern Switzerland (see box in Fig. 3-2a). Fig. 3-2b and c show the temporal evolution of earthquake detection for Northern Switzerland, including the significant local improvements around the Eglisau seismic cluster.

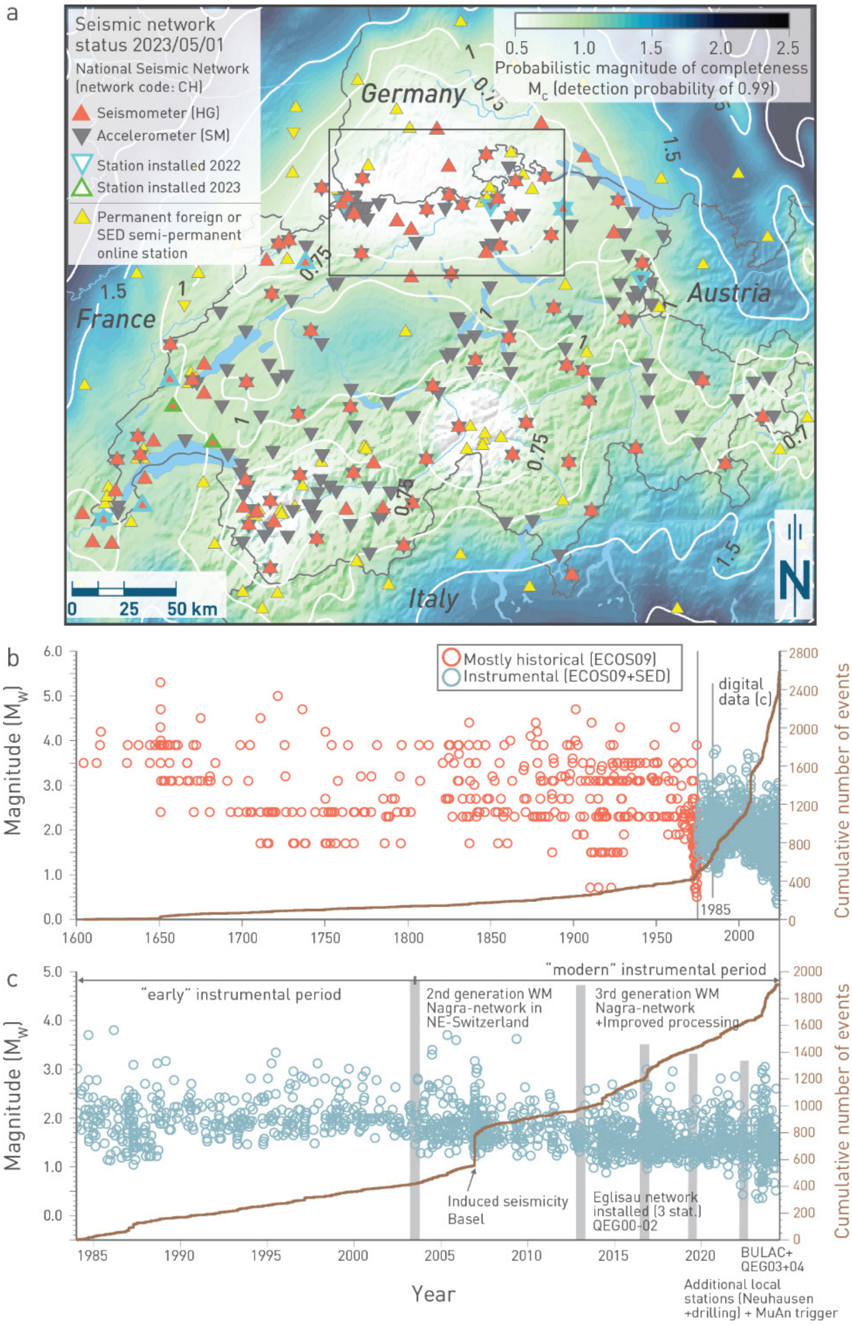

Fig. 3-2: Earthquake magnitude of completeness for Switzerland and evolution of seismic recordings in Northern Switzerland

(a) Seismic stations (triangles) and magnitude of completeness (colour-coded and isolines) for Switzerland (courtesy of T. Diehl, Swiss Seismological Survey). Box depicts the outline for which the evolution of seismic recordings in Northern Switzerland is shown in (b) and (c). Northern Switzerland has a high station density, which is highlighted by the very good magnitude of completeness (0.75); all (micro)-seismic events with magnitude $M_W > 1$ can be detected and reliably located. (b) Evolution of seismic recordings in Northern Switzerland (box in a), their moment magnitudes (local magnitudes were converted to moment magnitudes to allow comparison with historical data) and cumulative numbers of detected events since AD 1600. Number of recordings has significantly increased over the instrumental period. (c) Zoom into the digital data period since AD 1985. Note that the detection limit of magnitudes has improved over time.

Historic earthquake catalogues date as far back as ~ AD 250 (near Basel) with more continuous records since the medieval times (Fäh et al. 2011). The largest reported event is the AD 1356 Basel earthquake with an epicentre located about 10 km south of Basel and a moment magnitude (M_W) of around 6.6 (Fäh et al. 2011). This region has further experienced earthquakes above M_W 5. Seismicity is sparse outside the greater Basel area and magnitudes have not exceeded moment magnitudes of 4.7 (for both the historic and instrumental records, see Fig. 3-6). Earthquakes since 1975 with magnitudes > 4 are related to the Upper Rhine Graben or the Hegau – Bodensee Graben, with the exception of two deep, magnitude 4 and 4.1 events that occurred in 2004 and 2005, respectively, in the NE corner of Jura Ost (see Fig. 3-6, Fig. 4-4, and Fig. 4-8b). An exceptional cluster of seemingly permanent low-magnitude seismicity is recorded for the area around the city of Eglisau, NE of Nördlich Lägern (see Fig. 3-6, Fig. 4-5, and Fig. 4-16b). More information is provided in Section 3.4. Within the polygon outlines of the regional fault zones around the siting regions (see for instance Fig. 4-8c, Fig. 4-16c, and Fig. 4-23c), magnitudes of historical events are reportedly below M_W 3.9 (Fäh et al. 2011) and events since 1975 below M_W 3.2.

Earthquake focal mechanisms were derived for selected events and analysed by Diehl et al. (2023). In general, these focal mechanisms reflect the NNW-oriented S_{Hmax}, which corroborates the present-day stress field inferred from borehole breakout measurements (Nagra 2024j).

Interestingly, within the outlined area of Fig. 3-6, reverse fault mechanisms are lacking, in line with the present-day stress field, showing predominantly larger vertical stress than minimum horizontal stress (Nagra 2024j). Instead, (oblique) normal faulting along approximately N-S or NW-SE striking planes and strike-slip faulting dominate. The main strike-slip mechanisms include right-lateral motion along NW-SE to approximately E-W striking planes, which are the dominant fault strike directions, or left-lateral motion along (subordinate) NE-SW striking planes.

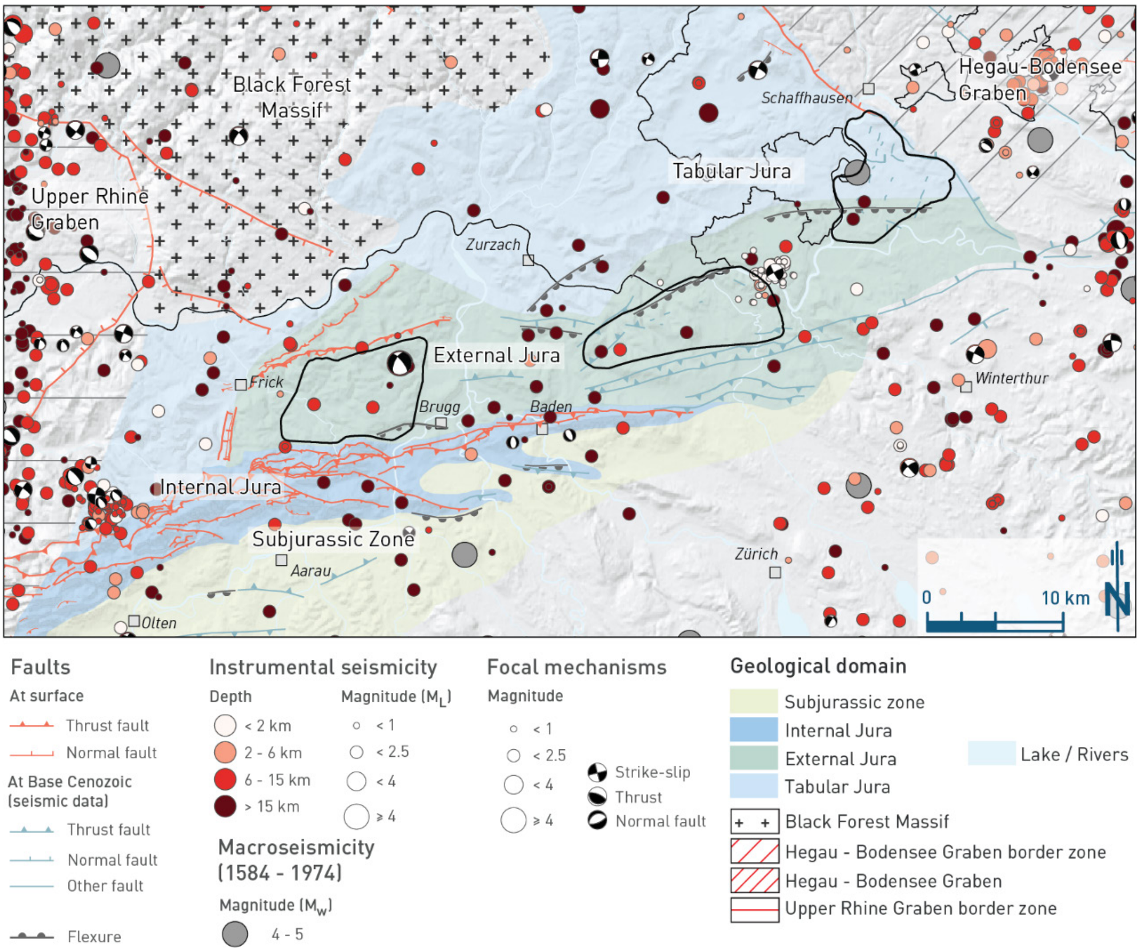

Fig. 3-3: Earthquake distribution in Northern Switzerland and Southern Germany

Seismicity is based on different catalogues: historic data (M_w) prior to 1975 (Fäh et al. 2011) and instrumental data (M_L) between 1975 and 2023 (merged catalogue with data until 2023/10/03, including Swiss Instrumental Network, absolute re-localised events (following Diehl et al. (2021b)) and regional analyses of selected earthquake clusters; courtesy of T. Diehl). Focal mechanisms are shown for selected events of the instrumental catalogue. Seismicity is sparse and distributed, with exception of the clustered seismicity of low-magnitude events near Eglisau, NE of Nördlich Lägern and west of Schaffhausen. Note that only a selection of the structures from 3D seismic interpretation is shown to highlight the structural trends of regional importance. These were projected from Top Villigen Formation to Base Cenozoic.

3.2 3D surface velocity monitored using the Global Navigation Satellite System

Precise positioning measurements using permanently installed stations are commonly used to monitor present-day motion at the earth's surface. Swisstopo operates such a network of permanent stations with about 30 antennas installed since the 1990s (Brockmann et al.).

Between 2010 and 2012 eleven Nagra-owned Global Navigation Satellite System (GNSS) stations (NaGNet) were added to the Automated GNSS Network of Switzerland (AGNES). These stations were optimally placed from a geodynamic viewpoint considering their distribution in the tectonic framework and their connection to the bedrock (Studer & Zanini 2013). Long-term time series of position coordinates measured by permanent stations provide increasing signal to noise ratios with observation time. After more than a decade of measurements with high coordinate repeatability based on weekly GNSS solutions (performed by swisstopo's Permanent Network Analysis Centre (PNAC)), the inferred motions have become increasingly statistically relevant. For most NaGNet stations qualitative errors[1] of ca. 0.05 mm/yr horizontally and ca. 0.2 mm/yr vertically are achieved. This is seen in the error ellipses encompassing the 95% interval that decrease with time (Fig. 3-4). For instance, the ideal case is shown for the station Höhenschwand, Germany (HCHS, Fig. 3-4). The error ellipses decrease with increasing measurement duration but always encompass the velocity vector calculated for previous measurement periods. This is the expected behaviour as the velocity vector is integrated over the entire measurement time. Other stations such as SCHA show behaviours that are more likely to be affected by artefacts. The map in Fig. 3-4 provides a qualitative assessment of the performance of each individual permanent station. The interpretation of the horizontal vector should therefore account for possible artefacts related to the design of the station (e.g. free field station vs. fixation of the antenna on a building or on a high mast) or to near-surface processes (e.g. groundwater level changes).

In conclusion, not all stations are of comparatively good quality. The NaGNet permanent stations (LFNB, HCHS, SLTB, MRGT, HGGL, STDL, BZBG, WLCH, TRKL and BCKL) are considered as reliable stations built in the free field on a solid foundation (stations labelled in red in Fig. 3-4). Some of the other stations FRI3, FRIC, SCHA, ETHZ, ETH2 are considered to be less well designed for monitoring of tectonic movements. The corresponding results of some of these stations are probably less suited for geodynamic interpretations and more prone to artefacts (Fig. 3-4). The stations FRI3 and FRIC are in close vicinity, resulting in two velocity vectors. The same applies for ETHZ and ETH2.

---

[1] The formal error calculated from the daily solution of the coordinate system is known to be too small. Therefore, an empiric factor 20 is multiplied to the formal error.

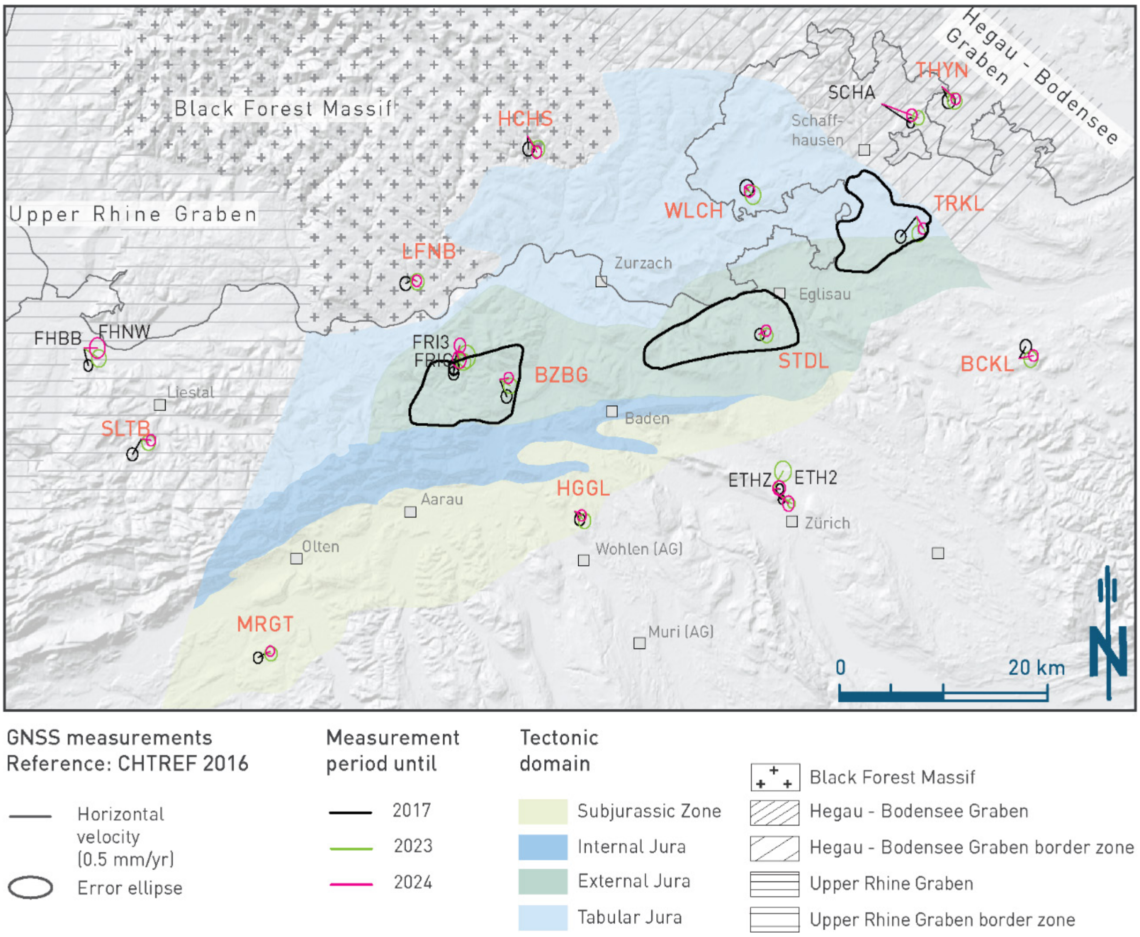

Fig. 3-4: Map of Northern Switzerland with the horizontal velocity vectors for the permanent GNSS stations for different time periods

Red station labels indicate NaGNet stations. Black station labels indicate AGNES stations. Three measurement periods are shown until 2017, 2023 and 2024. All velocity vectors are calculated in the CHTREF16, meaning that after calculation of the solutions in ETRF2014 the velocity vectors are transformed into the Swiss terrestrial reference system with Zimmerwald in the canton of Bern as reference point.

NaGNet and AGNES permanent stations are calculated in IGS' International Terrestrial Reference Frame (ITRF 2014; Altamimi et al. 2016) and then transformed to a European Terrestrial Reference Frame (ETRF 2014; Altamimi 2018) (i.e. assuming a stable-Europe framework). The ETRF2014 was calculated using the following stations mostly over northern Europe: GRAS (Austria), JOZE (Poland), METS (Finland), ONSA (Sweden), POTS (Germany), WTZR (Germany), YEBE (Spain) and ZIMM (Switzerland). Typically, GNSS velocities in Switzerland are further transformed to the Swiss terrestrial reference frame using Zimmerwald as reference point.

The solutions for the permanent stations located in Northern Switzerland in ETRF 2014 (retrieved in February 2024) indicate a general trend in horizontal velocity towards N to NNE. No significant differential movements between stations across tectonic elements such as the Jura Main Thrust are observed (Fig. 3-5).

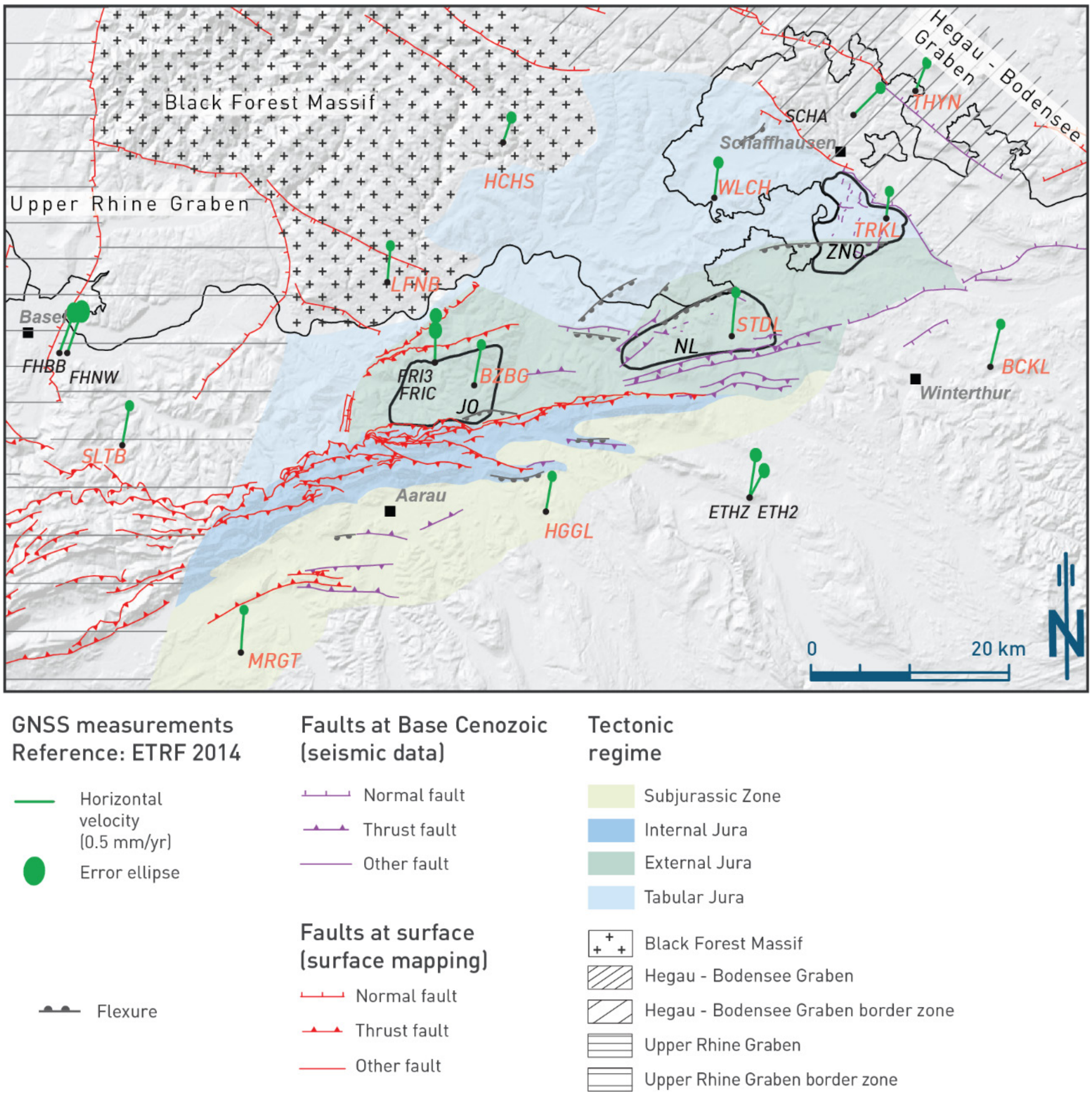

Fig. 3-5: Present-day horizontal motion of permanent GNSS stations in Northern Switzerland

Results are in reference to the ETRF 2014 (i.e. relative to a stable-Europe framework). Red labelled stations are NaGNet stations, whereas black labelled stations are AGNES stations. Stations with two vectors (ETHZ, ETH2, FRI3, FRIC) have two antennas close-by. Fault inventory shows traces of faults mapped at the surface (red) or at Base Cenozoic (violet). Internal and External Jura are part of the Jura Fold-and-Thrust Belt. Note that only a selection of the structures from 3D seismic interpretation is shown to highlight the structural trends of regional importance. These were projected from Top Villigen Formation to Base Cenozoic.

3.3 Recent vertical surface motion

The precise levelling measurements reported in Schlatter (2013) were complemented in 2018 by repeating measurements of the line "Brugg – Frick – Stein AG" (Bözberg line) and integration of the results into the network with the reference point (zero motion) at Laufenburg (crystalline basement, Fig. 3-6). In addition to this Nagra initiative, swisstopo performed repeated measurements along the lines Brugg – Koblenz and Kaiserstuhl – Basel. The Bözberg line was complemented with a perpendicular line towards the Hochrhein (Bözberg – Mönthal – Rheinsulz and Bözen). The kinematic analysis consolidates previous results without significant changes. The mean of the individual mean vertical errors is 0.08 mm/yr.

The kinematic analysis of the complemented precise levelling dataset was carried out by swisstopo. The results presented in Fig. 3-6 show vertical movements of the land surface relative to a reference point in Laufenburg, which is located within the crystalline basement (yellow triangle). The north central Swiss Molasse Basin towards the northern shores of Bodensee shows mainly uplift with respect to Laufenburg (red uplift symbols in Fig. 3-6). In general, uplift rates increase towards the Alps. With exception of few areas within the Internal Jura, the majority of measurements within the Mesozoic rocks are subjected to a subsidence trend with respect to Laufenburg (blue symbols in Fig. 3-6). Differential motion is observed within the Internal Jura with uplift in the eastern parts and subsidence towards Basel. The crystalline basement of the Black Forest regions shows a general subsidence trend relative to Laufenburg (yellow triangle in Fig. 3-6). A significant change of velocities across the faults of the Upper Rhine Graben is not detectable. However, rates decrease from east to west towards the Upper Rhine Graben.

Additional discussion of levelling data along selected regional and local swath profiles around the siting regions is provided in Sections 4.1 and 4.2 and associated figures. In these profiles, the vertical velocities deduced from the precise levelling measurement were raised by the amount of the GNSS-based vertical velocity of the station at Laufenburg (0.28 mm/yr relative to a stable-Europe framework, Section 3.2).

Precise levelling uncertainties generally decrease with repeated measurements. Proper motion cannot be excluded if they were only integrated in two measurement campaigns (Gubler et al. 1984). Particularly conspicuous points were already eliminated during the kinematic analysis. Strong velocity gradients among neighbouring points thus need to be interpreted with caution. Interpretations are most robust, if they are based on a high number of nearby observations.

A first countermeasure to conspicuous points is using a minimum requirement for the quality ranking of the measurement points. In our analyses we only plot measurements with a quality ranking > 8.5. The following qualitative descriptions may help to contextualise this number. (Tab. 3-1):

Tab. 3-1: Qualitative description of precise levelling measurement data quality ranking

Note that additional increments were introduced in the reporting (e.g. 8+, 8-, 9+ etc.). A quality ranking of > 8.5 is better than 8+ and includes 9-.

Quality	Description
7	Bad data point: data are not suitable as fixpoints in precise levelling, because low to strong elevation changes caused by local settlement or object translation are possible.
8	Rather bad data point: points are generally suitable for precise levelling, but elevation changes may also be caused by settlement in unconsolidated sediments or object translations.
9	Rather good data point: suitable points for precise levelling, grounded in bedrock or rather less settling unconsolidated sediments. These points are suited to investigate neotectonic movements. Non-tectonic influences cannot be excluded.
10	Good data point: High probability for tectonic origin of elevation change of associated bedrock. These points are the most suitable for neotectonic investigation.

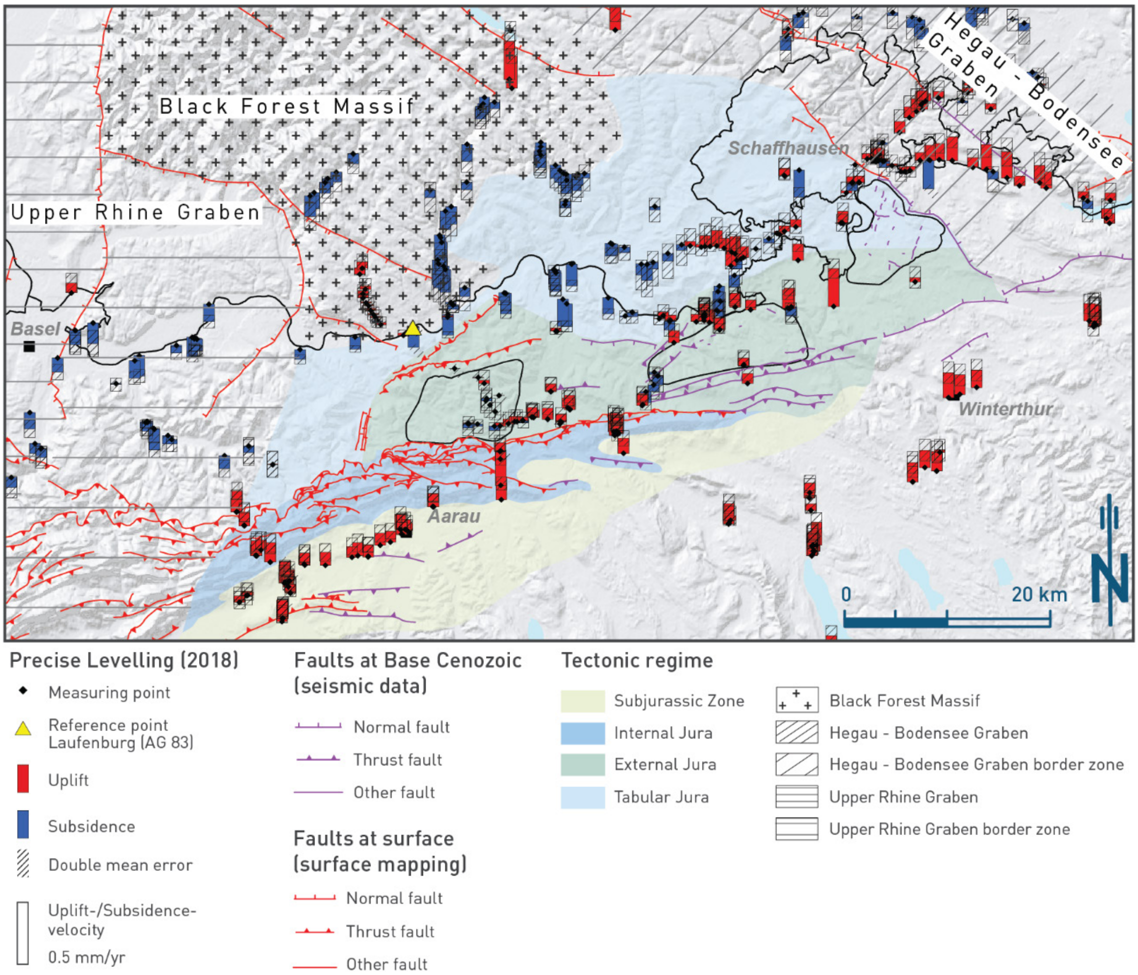

Fig. 3-6: Map of Northern Switzerland showing the vertical surface motion measured by precise levelling measurements

Precise levelling measurements correspond to the 2018 campaign by swisstopo. Only data with a good geologic quality ranking (> 8.5) are shown. Vertical velocities are based on levelling measurements relative to the fixpoint Laufenburg (yellow triangle). These data show a general trend of decreasing rates from the Alps towards the foreland. Note that only a selection of the structures from 3D seismic interpretation is shown to highlight the structural trends of regional importance. These were projected from Top Villigen Formation to Base Cenozoic.

3.4 Seismic reflection datasets

Three types of seismic reflection datasets were acquired. 2D seismic reflection lines of a regional extent were acquired by Nagra over an extended period of time. As part of the SGT Stage 2 new profiles were acquired and the existing ones were reprocessed (Madritsch et al. 2013). 2D geometric balancing was carried out on the geological interpretation of selected 2D seismic reflection lines (Jordan et al. 2015).

As part of the large field investigation programme "Quartäruntersuchungen" (QAU), Nagra acquired a series of high resolution 2D seismic reflection lines in winter 2016/2017 (Nagra 2018b). The bulk of the profiles was dedicated to the study of glacial overdeepenings (Nagra 2024h); however, three areas were covered with 1 to 3 profiles dedicated to the possible detection of post Quaternary tectonic activity. These are the Ruckfeld area (between JO and NL in the Lower Aare Valley), the Schöflisdorf area (NL) and the Cholfirst area (ZNO). The planning, acquisition and processing are reported in Nagra (2018a). The interpretation of faulting is hampered by the near-surface characteristics and possible artefacts. Therefore, no clear conclusion regarding neotectonic activity can be drawn from the high-resolution 2D seismic reflection lines.

Three-dimensional, high-resolution seismic reflection surveys were conducted throughout the three siting regions. This allows arbitrarily oriented cross-sections and three-dimensional views of the underground to be prepared. Consequently, the tectonic structures were mapped in detail in the three siting regions. Fault picking criteria and fault mapping are reported in Nagra (2024a), Nagra (2024b) and Nagra (2024c). Information provided from interpretation of 3D seismic reflection images went into the interpretation of fault systems in Section 4.2.

3.5 Age dating of faults

Recent efforts dedicated to dating regional fault zones surrounding the siting regions are reported in Madritsch et al. (2024), which contains a compilation of U-Pb ages of calcite veins that were mainly sampled within the Malm Group along regional fault zones across the entire area of interest. Based on the newly available age estimates and geometric 2D section balancing, shortening rates across selected regional fault zones were calculated. These results are presented in detail in Section 5.2.1.

In addition to the outcrop-based study (op. cit.), vein material from the recent borehole campaign was sampled and dated using U-Pb age dating. Four samples provided relatively young U-Pb ages that qualified them for further analysis using U-Th age dating for resolution reasons. Three of these samples were disqualified due to contamination of rock matrix into the vein material. The slickenfibre from TRU1-1 (679.02 m MD, core depth) was dated to 0.41 ± 0.01 Ma. This relatively young age, combined with its relatively cold temperature of formation (45 ± 7°C, compared to 31 °C at present-day), provides strong evidence for the dated vein being associated with Quaternary deformation.

3.6 Tectonic geomorphology

As described in Sections 2.1 and 2.2, the tectonic rates in Northern Switzerland are low, and seismicity is sparse and of low magnitude. Although continuous fault systems exist and have been repeatedly active in the past (Nagra 2024i), earthquake recurrence intervals along such faults are expected to be in the order of thousands to tens of thousands of years, considering the presently low strain accumulation (Landgraf et al. 2017). This low level of activity, long recurrence intervals and the scarcity of unambiguous neotectonic manifestations in the landscape of Northern Switzerland does not mean, however, that there is no potential for tectonic activity in this region that could be relevant for future generations (e.g. Wallace 1984). Tectonic geomorphology, the multi-disciplinary approach to decipher indicators of tectonic imprints on landscapes and landforms over a variety of temporal and spatial scales, bridges the gap between instrumentally recorded deformation and those tectonic phenomena that were generated on long, multi-millennial timescales (Fig. 3-1).

An apparent low degree of tectonic activity and highly modified or subtly expressed tectonic landforms characterise the glacially overprinted low-relief cuesta landscape of Northern Switzerland. Wide fluvial channels and extended terrace systems define the postglacial terrain. The main river system is formed by the Aare and Hochrhein streams and tributaries, like the Limmat, Reuss and Thur Rivers (see Fig. 4-1). These rivers have a primarily meandering nature, with locally strong anthropogenic overprint. Although in general the geomorphic process rates are low, large foreland glaciations have repeatedly modified the Quaternary landscape. The ice margin of the last glacial maximum (at 18 – 21 ka) was located northwest of ZNO, within the eastern part of NL, and southeast of JO (Nagra 2024h). Large, associated gravel deposits were formed in front of these glaciers, filling local troughs, and obscuring low-level palaeotopography (e.g. Fig. 4-8d, Fig. 4-16d and Fig. 4-23d). Accordingly, young small-scale landforms of tectonic origin in the vicinity of the siting regions that could provide evidence for recent tectonic activity may have been eradicated by the effects of advancing and retreating glaciers.

Our tectonic geomorphology analysis is focused on cumulative primary evidence for active faulting, potentially created by tectonic deformation (see, for instance, McCalpin 2009). Secondary effects, such as landslides and seismites resulting from seismic shaking, were not considered. However, as clear surface expressions (e.g. fault scarps or offset Quaternary strata) of potential faults are lacking, the analysis has included the search for anomalies in the landscape, such as deformed or tilted landforms that might have been formed by (off-)fault deformation.

The first part of the analysis uses the base of the Quaternary morphostratigraphic units Höhere and Tiefere Deckenschotter (~ 2.5 – 0.7 Ma; see below), which cover the bedrock and provide potential local geomorphic strain markers that help in the identification of offsets across inferred fault traces. Whereas both Höhere and Tiefere Deckenschotter deposits are preserved in the form of isolated relicts, the next younger Hochterrasse and Niederterrasse deposits form an integral part of a fluvial terrace system that follows a continuous and traceable fluvial network. Niederterrasse deposits are still young enough to provide potentially smooth, nearly uneroded surfaces, which can be used as geomorphic marker horizons (see section 3.6.3).

The second part of the analysis addressed the characteristics of the river network. The analysis follows the concept that rivers adjust with respect to transient effects – including tectonic perturbation (e.g. Kirby & Whipple 2012). The river network was analysed using regional steep-ness indicators, complemented with additional morphometric indices of selected streams (e.g. lateral migration, sinuosity) and generally accounting for differences in erodibility of the rock units.

This section summarises the range of tectonic geomorphology analyses performed. At the end of this section a ranking scheme is introduced to evaluate the evidence for Quaternary fault activity. An integrated discussion of tectonic geomorphology of the siting regions is included in Sections 4.1 and 4.2.

3.6.1 Update of Base Quaternary

The digital model of the Quaternary base (or Top bedrock) from 2014 (Pietsch & Jordan 2014) was updated. New datasets regarding the depth of Top bedrock (drilling data, 2D seismic reflection lines) allow improvements to the model, which is one basis on which to evaluate erosion history and neotectonic activity. The basic information for the model update includes data from more than 700 boreholes, 26 high-resolution 2D seismic reflection lines with an emphasis of glacial overdeepening structures (Nagra 2018b, Gegg et al. 2021) and the geologic mapping of areas with Deckenschotter deposits (Thew et al. 2024). For the assessment of Quaternary neotectonic activity, the mapping of Base Deckenschotter and assigning errors based on quality criteria similar to Hammer et al. (2019) is especially relevant (Tab. 3-2). The results are presented in Section 4.2.

Tab. 3-2: Uncertainty classification for the strain marker Base Deckenschotter

With respect to mapping the elevation of the base of the Deckenschotter, the elevation uncertainties were considered based the following classification scheme (Hammer et al. 2019). The uncertainty classes are colour-coded in the outlines of the Deckenschotter bases in Fig. 4-8 c, Fig. 4-16c, and Fig. 4-23c. The asymmetric errors are consistent with greater downslope ambiguity due to colluvial cover.

Class	**Description**	**Suggested uncertainty [m]**
1 (good)	Basis exposed	± 0.5 m
2 (fair)	Basis morphologically mapped in the field	+3 / -7 m
3 (vague)	Basis interpolated	+6 / -14 m
4 (vague)	Basis extrapolated (e.g. below colluvial deposits)	+10 / -20 m

3.6.2 Stream network analysis

Normalised channel steepness analysis ('ksn')

Rock-uplift rate is expected to exert a first-order control on channel steepness that describes the power-law scaling between channel slope and upstream drainage area (e.g. Whipple & Tucker 1999, Wobus et al. 2006). Accordingly, the normalised steepness index 'ksn' might reveal spatial differences in rock-uplift rates when differences in erodibility are accounted for. However, because 'ksn' reflects the ratio between rock uplift and a coefficient of erosion, the concept only works under uniform boundary conditions and results need to be discussed within this context. High 'ksn' values could thus indicate spatially higher rock-uplift rates, but also less erodible rock types that outcrop in the drainage basin.

The 'ksn' values were calculated based on downsampled lidar elevation data (Source: https://sonny.4lima.de/). The DEM has a spatial resolution of 20 m, and we extracted all streams with a minimum upstream area of 80000 m^2. We smoothed river elevations using constrained regularised smoothing (Schwanghart & Scherler 2017) with a smoothing penalty of K = 5. The method is a nonparametric quantile (here, median) regression which ensures that river elevations strictly monotonically decrease in downstream direction. Based on these elevations, we calculated river gradients which, for each river pixel, were then used to calculate 'ksn'. In a second step, we calculated the average 'ksn' for river sections of approximately 1'000 m length, thereby also bootstrapping these averages to obtain estimates of the 5th and 95th percentile of the 'ksn' value in each river segment (Fig. 4-1).

Channels in Northern Switzerland comprise many engineered sections including weirs. We did not directly correct for these, but the averaging method outlined above leads to similar results for a number of mean gradients without weirs and a large gradient at the exact location combined with many small gradients upstream. If calculated river segments were too small, weirs would constitute too high apparent 'ksn' and 'ksn' of dammed sections above them under-estimated.

The delineation of steep and gentle channel sections is marked by knickpoints. It is important to keep in mind that knickpoints in bedrock channels migrate upstream over time (so does the steep section). It is also important to note that a 'ksn' determination is less meaningful in alluviated channels.

Channel sinuosity index (SI)

Alluvial channels respond to changes in boundary conditions by adjusting their slopes. One important local to regional marker is the change of sinuosity along perturbed reaches of a channel (e.g. Burnett & Schumm 1983, Holbrook & Schumm 1999, Ouchi 1985, Timár 2003, Woolderink et al. 2021). Meandering channels tend to increase sinuosity with increased channel slope (Holbrook & Schumm 1999). Changes in sinuosity are expected to differ, depending on the "block uplift" or associated fault motion with respect to river flow direction. For example, a channel crossing an uplifting block may straighten (decrease sinuosity and thus increase channels slope). However, lithological control might additionally influence the channel sinuosity and thus needs to be considered. Channel sinuosity for major meandering channels in the study area (like Aare, Hochrhein, and their main tributaries) was calculated based on the same digital elevation model described above. We obtained the sinuosity in each river segment by calculating the ratio between the flow distance and the Euclidean distance between the first and last point of a river segment. Results are only discussed at a local scale in Section 4.2.

Patterns of aggradation and degradation

A fluvial channel's tendency to restore its profile after a (tectonic) disturbance may also be reflected in spatial patterns of sediment aggradation and degradation (e.g. Holbrook & Schumm 1999). For instance, this can be shown by upstream and downstream aggradation of a potential uplift and degradation at the location or uplift axis, where the channel slope is most pronounced. The response, however, will also depend on the acquired sediment load for aggradation. In this investigation, the spatial distribution of sediment accumulation is only discussed locally and when applicable (see Fraefel 2008).

3.6.3 Criteria to evaluate potential Quaternary deformation

Detection limit for co-seismic fault scarps

The detection probability of neotectonic movements based on examination of high resolution digital topographic images depends on the relationship between the rate of deformation and the rates of surface processes operating over the resulting surface disturbance. This is especially important to keep in mind in a region like Northern Switzerland where the landscape is heavily altered by glacial, fluvial and anthropogenic processes and inherently low vertical offset rates. Considering the natural surface roughness as indicated by lidar topography and uncertainty in the lidar data themselves (lidar DTM-AV), the minimum vertical offset of a neotectonic signal to still be recognisable is considered to lie in the range ± 0.2 m. Assuming a postglacial terrace surface offset produced by an earthquake about 10'000 years ago, that the surface processes are only diffusive and not fluvial or other mass wasting, and a range of reasonable diffusivity values to degrade this topographic step, we estimate that original offsets > 1 – 2 m could still be visible in the landscape if otherwise undisturbed. Such scarps are not observed so far in the siting regions.

Base of Deckenschotter as geomorphic marker

The base of four Quaternary morphostratigraphic units has been interpreted to reflect the stepwise lowering of the regional baselevel (from top to bottom): Höhere Deckenschotter (HDS, "Upper Cover Gravels"), Tiefere Deckenschotter (TDS, "Lower Cover Gravels"), Hochterrasse (HT, "High Terrace") and Niederterrasse (NT, "Low terrace"; Graf & Burkhalter 2016 and references therein). While the respective surfaces of the unconsolidated deposits might be highly altered by erosion, potential offsets of their base (i.e. the bedrock – sediment contact) are expected to be sheltered and preserved. On the other hand, the original bedrock surface prior to filling with Quaternary sediment was an erosional landform and some effect of palaeotopography must be considered. Furthermore, although major efforts were undertaken and supported by Nagra to establish a bedrock model (see Section 3.6.1), uncertainty resulting from interpolation between data points remains (Tab. 3-2).

Finally, each of the Deckenschotter units comprises an internal cut-and fill sequence with considerable time involved. Differential erosion of their base that might be misinterpreted cannot be excluded. This is especially true for the base of the Tiefere Deckenschotter, which comprises considerable relief in places (e.g. Graf 2009, Graf & Burkhalter 2016, Bitterli-Dreher et al. 2007). It is also important to note that information on the Deckenschotter base is even more sparse than the number of surface remnants, as it is mainly derived from intersections with the topography. Boreholes intersecting the Deckenschotter base to be used to update the bedrock model are rare (see for instance Fig. 4-14, Fig. 4-19, Fig. 4-20, and Fig. 4-26). Accordingly, even if an extended body of Deckenschotter is available in an area of interest, the erosional form of their outline can considerably decrease the number of useful data points.

Surface of Niederterrasse as geomorphic marker

Gently inclined fluvial terrace remnants constitute climatic markers in a region of oscillating sediment availability, aggradation and incision (representing for instance sediment dynamics of glacial/interglacial cyclicity), or they represent the response of the fluvial system to baselevel changes (their staircase morphology reflects overall lowering of the baselevel and river adjustment). As such, they are vestiges of once contiguous, gently inclined surfaces and, if affected by vertical motion, may accordingly document deformation that occurred after their abandonment. In this respect, fluvial terraces provide valuable strain markers for an assessment of neotectonic activity.

While the older Deckenschotter surfaces may have experienced prolonged phases of denudation and linear erosion, the youngest gravel surfaces, represented by the Niederterrasse, might still preserve the characteristics of the now abandoned, former fluvial channel. Given the wide distribution of Niederterrasse occurrences in Northern Switzerland this strain marker is very useful to evaluate tectonic overprints during the last ~ 25 kyr (see below).

Age control of Quaternary geomorphic markers

A multitude of dating methods was used to evaluate the ages of the Quaternary fill sediments. For a detailed discussion, see Nagra (2024h). For this investigation, associated ages are used selectively and where applicable. The age determinations, especially for the deposits of the Höhere Deckenschotter (HDS) remain controversial, with biostratigraphy pointing to an age range of 1.8 – 2.2 Ma (Thew et al. 2024); in contrast, radiometric ages based on isochron burial method using cosmogenic nuclides provide a range between 0.95 ± 0.08 and 1.32 ± 0.13 Ma. Tiefere Deckenschotter (TDS) were dated using the isochron burial method to be between 0.68 ± 0.16 and 1.18 ± 0.09 Ma. At two locations, which are discussed in more detail in Section 4.2.2.2 and 4.2.3.2, ages determined at nearby outcrops were used in addition to the full age range. These ages were also based on the isochron burial method: outcrop Feusi (till, HDS): 0.95 ± 0.08 Ma (Section 4.2.2.2) and outcrop Cholfirst (TDS): 0.83 ± 0.15 Ma (Section 4.2.3.2). Niederterrasse was generally dated to be between 30 and 15 ka (Preusser et al. 2021, Kock et al. 2009) and recently in the Lower Aare Valley to 25 – 22 ka (Gaar et al. 2019, Kamleitner et al. 2023, Reber et al. 2014).

Evaluation criteria for potential deformation and associated ranking

The following criteria were addressed and ranked when evaluating potential tectono-geomorphic signals (Tab. 3-3; taking into account ambiguity and caveats presented above). We assume that as more proxies are available for a potential causative fault responsible for deformation, the lower the ambiguity in our interpretation of its activity and the more reasonable is the associated interpretation. However, proxies are not evenly distributed across such potential faults.

We consider a geomorphic strain marker as being good quality if it is associated with a simple initial geography (e.g. a flat base of deposits or surface), and where it is young enough to eliminate substantial erosional bevelling. In contrast, a geomorphic strain marker may show a complex initial form, that might be derived from significant relief with strong lateral changes, or several (crosscutting) levels. Age control is necessary to assign any temporal context to the marker and is thus a prerequisite for a good quality. Furthermore, a potential tectonic signal, which is only observed locally has a lower assigned quality compared to a marker that shows an extended signal. The signal may be interpreted as fault surface offset, if it is not only observed at the fault position itself (where it might be an artifact) but can also be viewed by the far-field slope of the marker horizon. A good marker that shows a signal and that is associated with a causative fault might be reasonably well-suited for a tectonic interpretation. Alternative interpretations can arise from fluvial, glacial, or even anthropogenic overprint of the landform or from projection across differently erodible rock types.

Tab. 3-3: Quality criteria for geomorphic markers

A suitable *good* geomorphic marker is characterised by a simple initial complexity, available age control, and an extended signal. The scale is arbitrary. The relative ranking is defined by the criteria in brackets. Accordingly, a *good* marker comprises 6 points, a *fair* marker comprises 4 – 5 points, and a *vague* marker is associated with 2 – 3 points.

Quality of the geomorphic marker		
Initial geometry		
Simple initial geometry (3)	Limited complexity (2)	Complex initial geometry (1)
Age control		
Available (1)	not available (0)	
Traceability of signal		
extended signal (2)	local signal (1)	

Other important evaluation criteria are association with the potential causative fault (direct, indirect, missing) or the number of associated proxies. In a direct association, a potential signal or anomaly would be spatially associated with a known tectonic feature (e.g. regional fault zone). An indirect association may be a location in the vicinity or inferred up-dip projection of a tectonic feature.

Together, these evaluation criteria are used to guide the interpretation of the geomorphic strain marker with respect to neotectonic activity. The endmembers are a *non-tectonic* interpretation (a tectonic signal is ruled out) and a situation that favours a *tectonic* interpretation. We distinguish two additional interpretations: we call a signal *ambiguous*, if a tectonic influence cannot be excluded, but the signal is similarly easy or even better explained by non-tectonic causes. In contrast, a *mixed* signal is interpretated as a combination of tectonic and non-tectonic causes, although their respective contributions are not defined. A *mixed signal* interpretation might be that the signal could be generated or enhanced by erosional overprint, but erosion might have been guided by previous tectonic deformation. In any case, potential signals are expected to be subtle.

4 Indications for neotectonic activity in Northern Switzerland

In Chapter 3, we reviewed datasets and different methodological approaches used to assess neotectonic activity in Northern Switzerland (Fig. 3-1). In the following sections, we review the available data and their applicability to assess potential tectonic deformation at a regional and site-specific scale.

4.1 Regional tectonic deformation signals

In this section, a regional geomorphic study using the normalised channel steepness index 'ksn' is discussed first (Fig. 4-1). In a second step, selected regional data are shown in swath profiles including the areas of the siting regions (see Fig. 4-2 for location and data distribution) to guide the summary of regional tectonic deformation signals. Results from this section are integrated in the more focused discussions of the siting regions in Section 4.2.

Using a simple classification scheme, the regional analysis reveals low 'ksn' values for most of the channel segments ('ksn' with light blue colours in Fig. 4-1). Slightly higher channel steepness is observed within the terrain of the Mesozoic units of the Internal Jura ('ksn' with dark blue colours), with 'ksn' further increasing towards the west, i.e. the Upper Rhine Graben border zone and beyond ('ksn' with orange and red colours). The Mesozoic units contain more resistant rock types than the Molasse strata, which might explain some of these relationships. However, the increasing 'ksn' values towards west are also in line with increasing uplift/activity of the Jura Fold and Thrust Belt, suggesting that part the signal may be influenced by tectonic processes (e.g. Lanza et al. 2022). High values of normalised steepness index are again observed in parts of the Black Forest, where they correspond to channels that drain the crystalline basement rocks. Although relatively higher rock-uplift of the Black Forest Massif is debated (see Nagra 2024h), an influence of erosion-resistant crystalline rocks is likely (Fig. 4-1).

The long WSW-ENE data swath profile (Fig. 4-3) crosses all siting regions. Its orientation is chosen to be approximately perpendicular to the orientation of S_{Hmax}, and parallel to the Alpine front. Its western part covers the Tabular and External Jura, while the majority of the profile is located within the Molasse Basin and Tabular Jura in its northern part (Fig. 4-2). This difference is reflected very well in the topography (Fig. 4-3c), which generally decreases from the area of the Tabular Jura eastward before it slightly rises again east of ZNO.

Vertical velocities based on precise levelling[2] are relatively stable along this section with rates generally between 0.2 and 0.4 mm/yr, showing mainly an uplift tendency at very low rates with respect to Laufenburg (Fig. 4-3a). Visual inspection of the vertical velocity data shows no significant E-W gradient, but there is more scatter in the central and eastern parts. Slightly higher values (> 0.4 mm/yr) are observed in the eastern half of the profile. Some points, especially in the vicinity of NL, show subsidence with respect to Laufenburg. Two small zones exhibiting lower rates are located between 45 and 60 km from the point of origin in the west. For the Alpine area, a positive correlation of topography and uplift was suggested (Section 2.1). Such a trend is not seen in the area analysed in Fig. 4-3a.

GNSS data are sparse in the eastern part of the section (Fig. 4-3b). Nevertheless, horizontal velocities show generally low rates of up to 0.4 mm/yr and without clear gradient in this direction. The different motion of the two stations in close vicinity to the JO siting region (FRI3 and FRIC) suggests that at least one is less reliable (see Section 3.2 for a general description of uncertainties).

[2] Raised by 0.28 mm/yr (GNSS value at the position of Laufenburg)

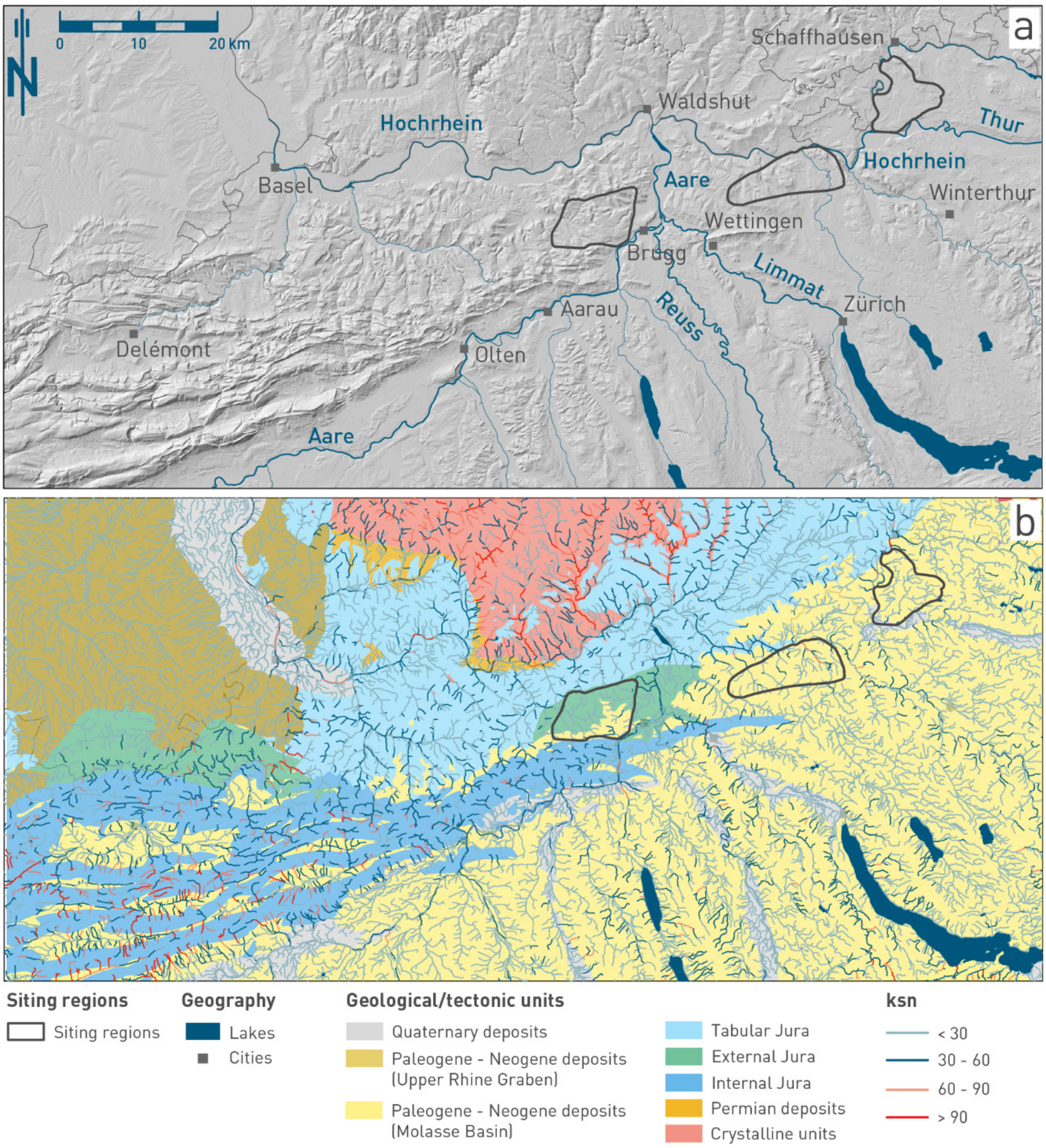

Fig. 4-1: Topographic map and normalised steepness index over geology map for Northern Switzerland

(a) Topography and main geographic elements and labels for orientation. (b) The normalised steepness index ('ksn') was calculated based on a 20-m DEM and is colour-coded. For context, geological units are underlain. The majority of the river profiles exhibit low 'ksn' values (blue colours), although with some exceptions. These are discussed in the main text.

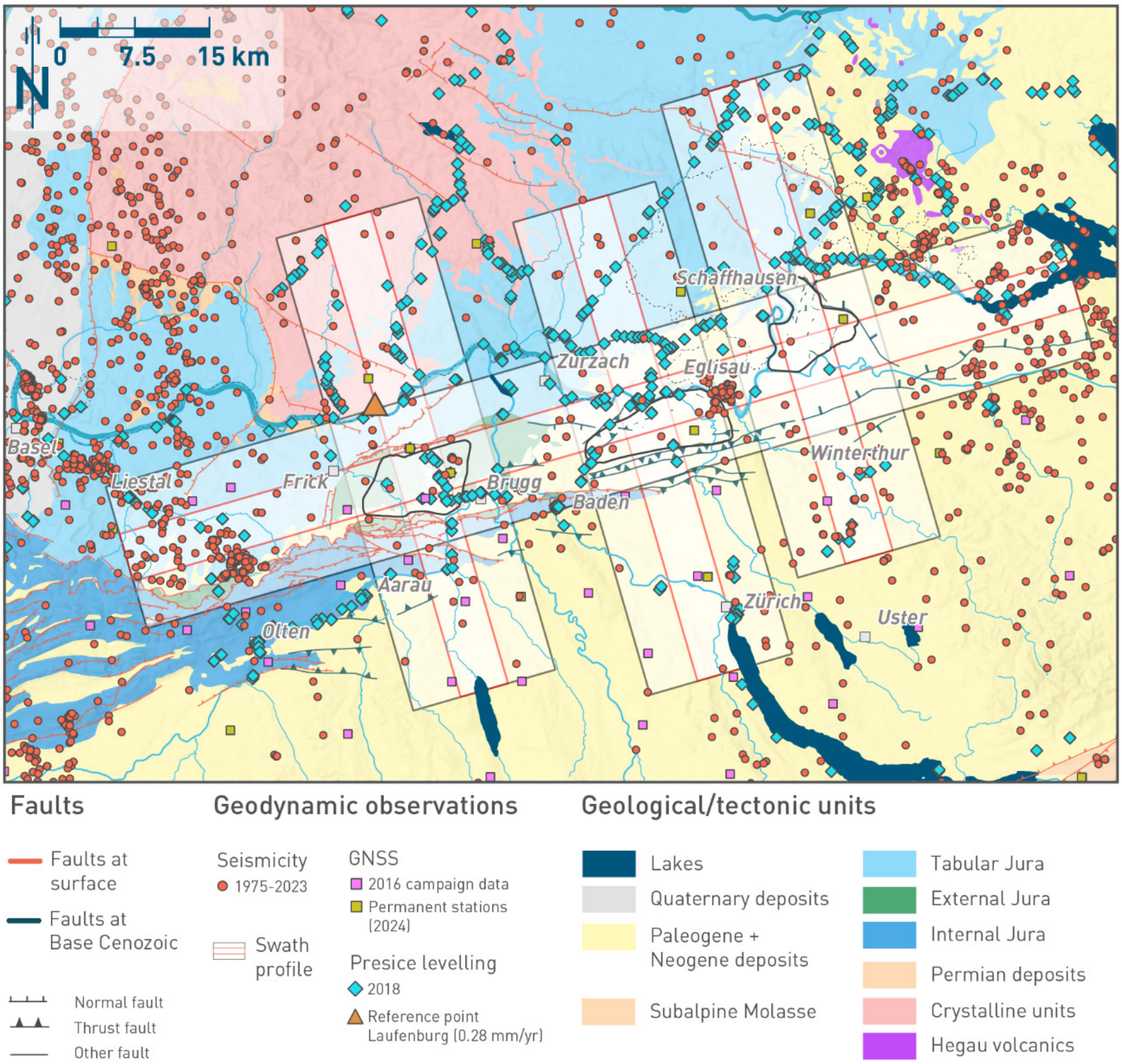

Fig. 4-2: Overview of tectonic domains with data and associated swath profiles for regional neotectonic analysis

Map shows the location and distribution of data used for regional swath profiles and subsequent discussion. The outlines of the swath profiles are shown. Data from within the outlined boxes are integrated and plotted along the box centre line. Topography was calculated for the more narrow, red outlined swaths, respectively, based on a 25-m DEM. The data swaths include a wider range as outlined in black, respectively. Seismicity, precise levelling and GNSS-based velocities were extracted and plotted relative to the box long axis (see description of Fig. 4-3). The spatial distribution of these datasets is shown in the map above for orientation and comparison. The orientation of the NNW-SSE profiles was chosen to be approx. parallel to the direction of S_{Hmax} and perpendicular to the main regional fault systems (see Fig. 4-4, Fig. 4-5, and Fig. 4-6). The WSW-ENE section (Fig. 4-3) is oriented ~ perpendicular to S_{Hmax} and ~ parallel to the Alpine chain, thereby crossing all three siting regions. The regional swath profiles are long enough to cross different tectonic domains.

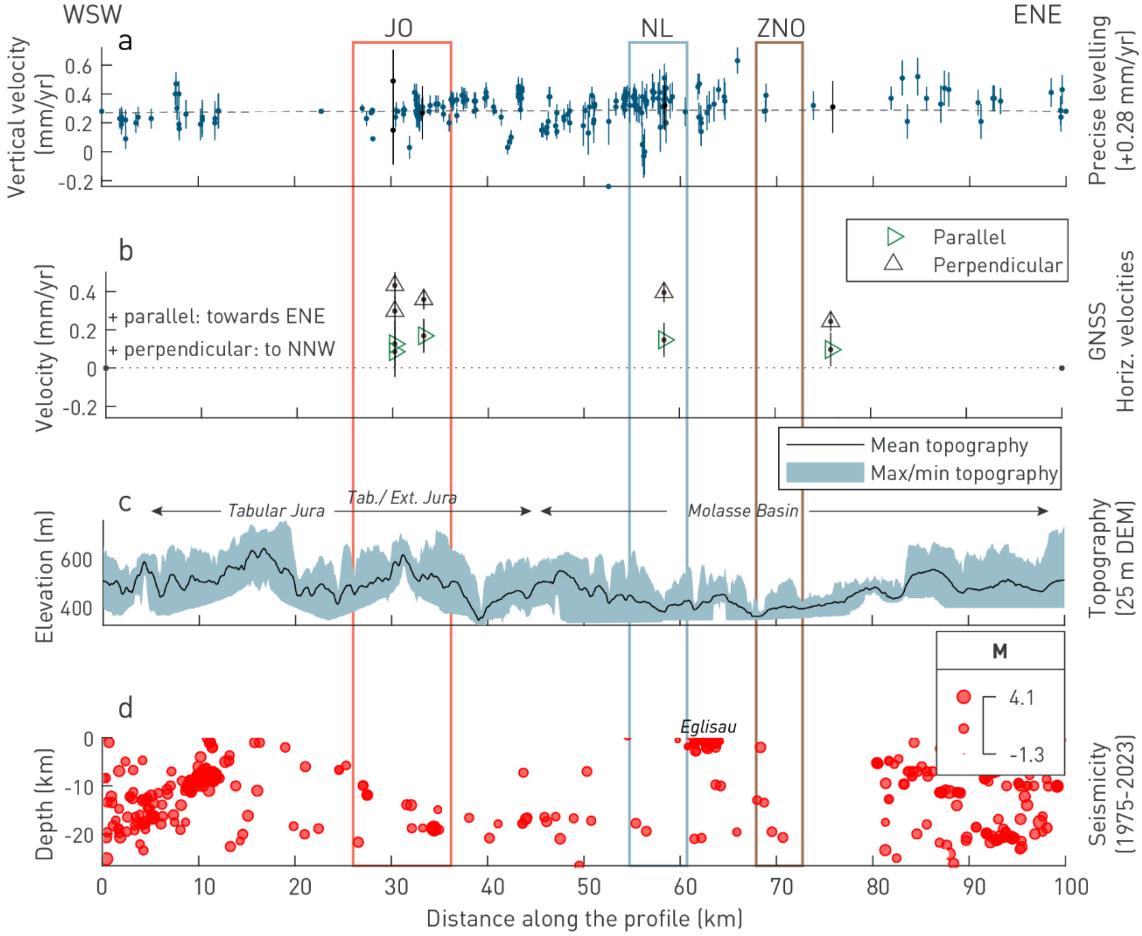

Fig. 4-3: Data swath (WSW-ENE) across all three siting regions

Profile swaths were calculated using a 5 km width for topography and 15 km width for other data (see Fig. 4-2 for location). The areas of the siting regions are highlighted by the coloured frames. (a) Vertical velocities of precise levelling data (blue) and few GNSS-based vertical velocities, calculated w.r.t. Europe (black). Only precise levelling data with a high ranking of geological quality (> 8.5) are shown. Original data were documented with respect to Laufenburg as 'zero-velocity' reference point (see triangle in Fig. 4-2). Here, the GNSS-based uplift (2024) of the Laufenburg station of ~ 0.28 mm/yr was added to each value, respectively (see dashed line), to allow a relative comparison. The GNSS-based vertical velocities blend in with the precise levelling measurements at the scale of this swath profile. (b) GNSS-based horizontal velocities. Green and black symbols are based on permanent stations only and calculated based on a European Terrestrial Reference Frame (ETRF). The velocity vectors are shown as profile-parallel and -perpendicular, respectively. The "±" notation on the y-axis is the result of the swath profile construction and must be seen from the point of origin (here WSW) towards the profile end (here ENE). "+ parallel: towards ENE" means that a vector component in line with the profile direction (i.e. towards ENE) would be positive. Similarly, a positive vector component perpendicular to (across) the profile line points towards NNW ("+ perpendicular: towards NNW"). (c) Swath topography, based on a 25 m DEM. The shaded area highlights the relief between minimum and maximum topography calculated from the 5-km wide swath. (d) Seismicity is based on the instrumental catalogue provided by the Swiss Seismological Service (see Fig. 3-3 and Section 3.1 for a discussion on magnitude of completeness). Tab./Ext.: Tabular/External Jura.

Seismicity is distributed along the length of the entire profile, but the majority of events can be found either west or east of the siting regions, where they cluster across the entire upper crust (Fig. 4-3d). In the central part, the area of the siting regions, seismicity is sparse and mainly located within the lower part of the upper crust, except for the "Eglisau cluster" of shallow, low-magnitude events. Note that the detection limit is significantly higher in the vicinity of Eglisau (Section 3.1 and Fig. 4-3).

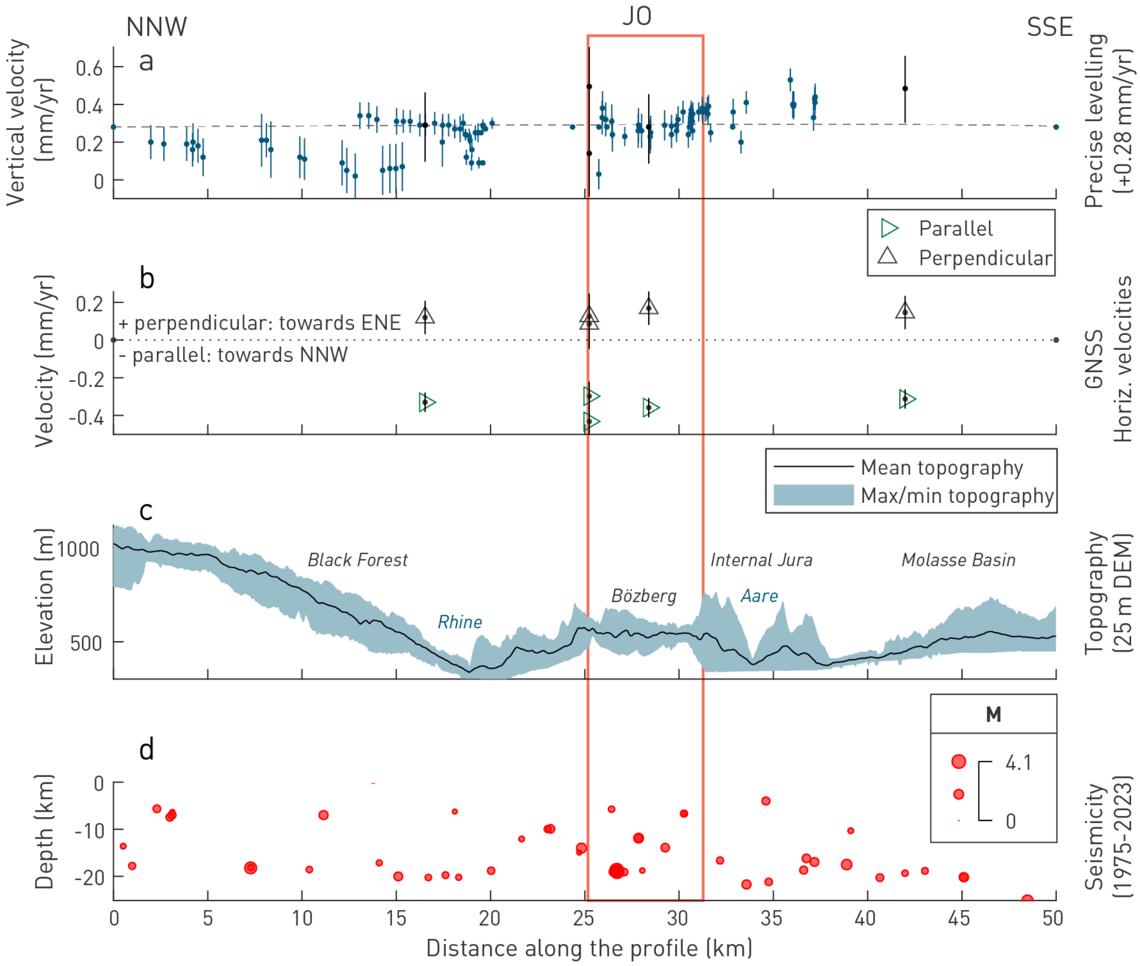

Fig. 4-4: Data swath profile across the Jura Ost siting region

This profile is approximately oriented parallel to the present-day orientation of S_{Hmax} (azimuth 165°). Thus, the parallel component of horizontal GNSS velocities (green right pointing triangles) would reflect shortening, if a gradient was visible. See Fig. 4-2 for location and Fig. 4-3 for general description.

Fig. 4-4 shows a swath profile parallel to the inferred orientation of S_{Hmax} across the Jura Ost siting region. Precise levelling data show a trend of decreasing velocities from the Internal Jura towards the Rhine (Fig. 4-4a). This might reflect the general decrease of uplift with increasing distance from the Alps. The majority of vertical velocities is between 0.2 and 0.4 mm/yr. Points located within the crystalline Black Forest subside with respect to Laufenburg (between 0 and 20 km), although there is some ambiguity between parallel levelling lines that may be related to positions near the river floodplain (see Fig. 4-2 for measurement distribution). Visual inspection of horizontal GNSS velocities suggests no reliable shortening or profile-perpendicular trend along the profile (Fig. 4-4b). The different motion of the two stations in close vicinity to the JO siting region (FRI3 and FRIC) suggests that at least one is less reliable (note that these stations have increased uncertainties as they are mounted on high poles; see Section 3.2 for a general description of uncertainties). Data are sparse north of the Tabular Jura. Seismicity is sparsely distributed across the entire profile, with a larger number of events in the lower part of the upper crust (Fig. 4-4d). The largest event corresponds to a magnitude of 4.1 (see also Section 3.1) and belongs to a sequence of deep events that occurred between 2004 and 2005.

The precise levelling profile across Nördlich Lägern (Fig. 4-5a) suggests a slight gradient of increasing vertical velocities from NNW to SSE, potentially reflecting the decreasing distance to the Alps. Rates are generally between 0.2 and 0.4 mm/yr. The few GNSS-based vertical velocities (black data points) blend in with the levelling data. Between km 20 to 25 from the point of origin in the north, the measurements show slight uplift with respect to Laufenburg, while points, measured immediately NNW of it, subside in comparison. Horizontal velocities (Fig. 4-5b) show no clear trend of profile-parallel motion, the station moves with similar rates of up to 0.4 mm/yr. The profile-perpendicular component exhibits mainly low rates below 0.2 mm/yr. Similar to the other sites, seismicity is distributed and occurs throughout the upper crust. Shallow seismicity is also missing north of NL, before reaching the Black Forest, with the exception of the Eglisau seismic cluster.

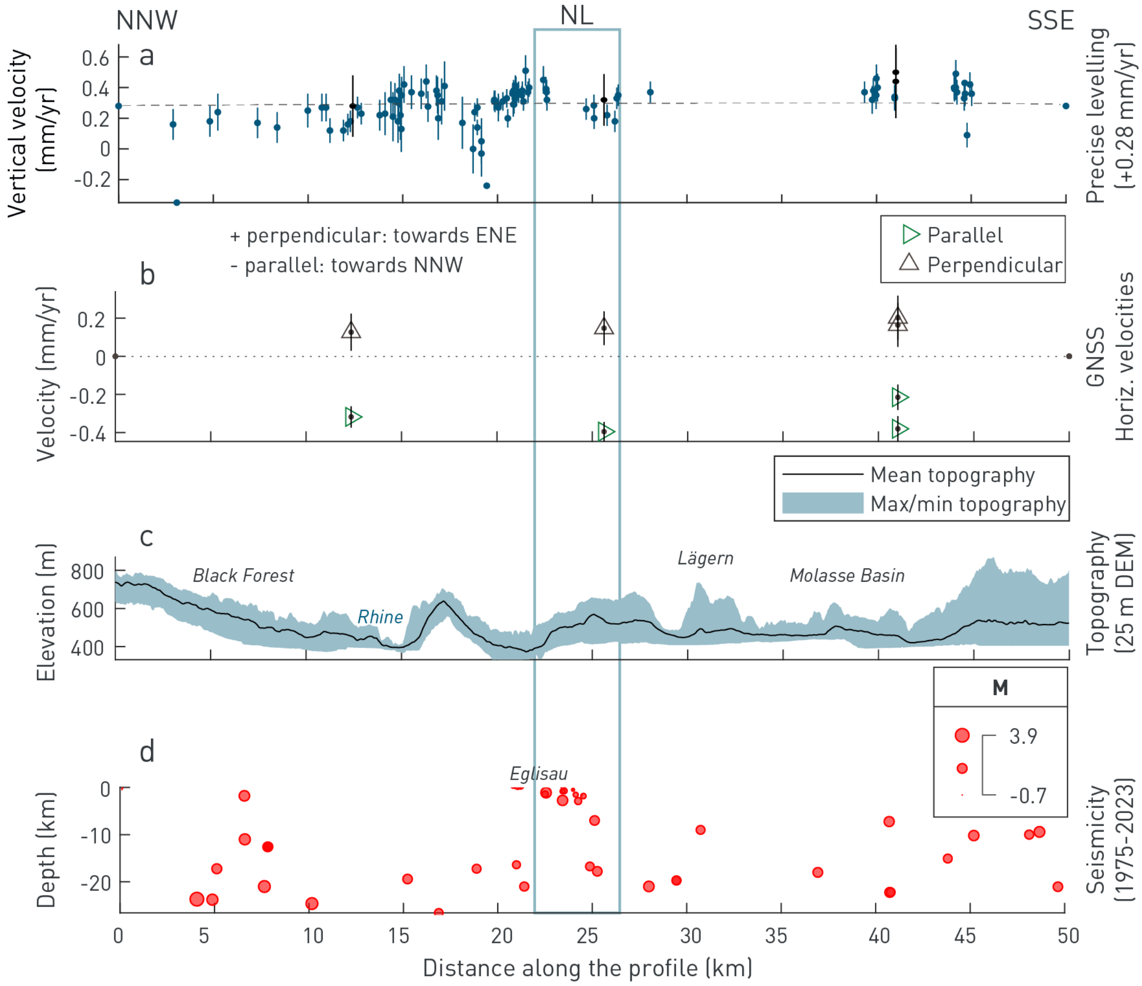

Fig. 4-5: Data swath profile across the Nördlich Lägern siting region

This profile is approximately oriented parallel to the orientation of S_{Hmax}. Thus, the parallel component of horizontal GNSS velocities (green, right pointing triangles) would reflect a 1st order proxy for shortening, if a gradient was visible. See Fig. 4-2 for location and Fig. 4-3 for general description.

For ZNO, the pattern appears to be comparable to Nördlich Lägern with a slight trend of southwardly increasing vertical velocities (Fig. 4-6a). One GNSS-based vertical velocity (black bar and dot near km 15) shows considerably lower rates than the precise levelling data (note that this station has an increased uncertainty as it is mounted on top of a building; see section 3.2 for a general description of uncertainties). The precise levelling data in the area north of ZNO (Schaffhausen, up to Blumberg) record some scatter around the majority of otherwise stable values slightly above the reference point at Laufenburg. GNSS data are sparse along the profile (Fig. 4-6b). Seismicity is sparse with low magnitudes below 2.8 and is distributed across the entire upper crust.

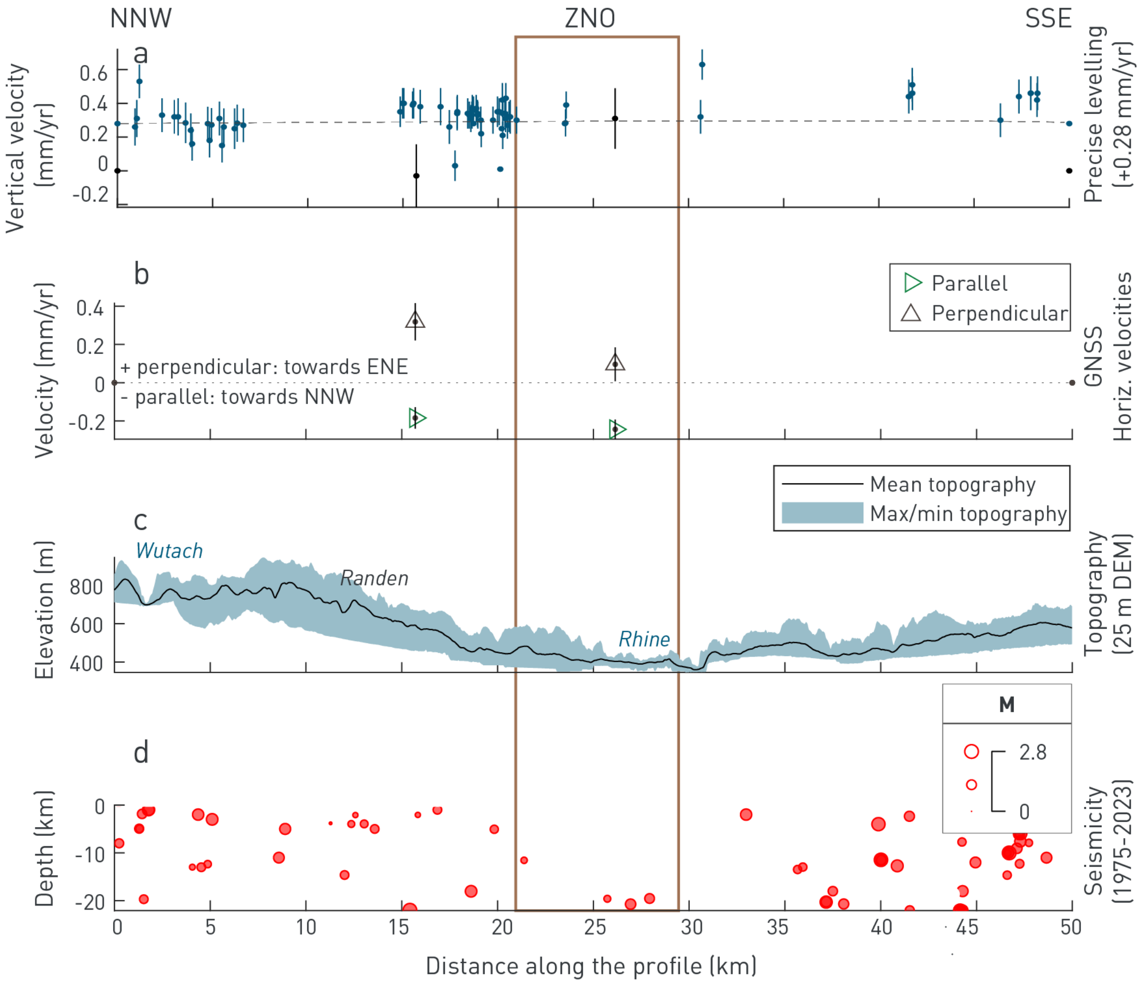

Fig. 4-6: Data swath profile across the Zürich Nordost siting region

This profile is approximately oriented parallel to the orientation of S_{Hmax}. Thus, the parallel component of horizontal GNSS velocities (green, forward pointing triangles) would reflect shortening, if a gradient was visible. See Fig. 4-2 for location and Fig. 4-3 for general description.

4.2 A sharper focus on the siting regions

This section examines available indications of neotectonic activity on a siting region scale. For each site, the present-day situation based on tectonic inventory is reviewed first, followed by a tectono-geomorphological evaluation. The resulting assessment is visualised in maps and interpretative swath and geological profiles (see Fig. 4-7 for location).

Each section provides a short introduction to available structural data and geomorphic strain markers, followed by a description of anomalies possibly related to recent tectonic activity. Ambiguities and/or evidence for absence of their neotectonic origin are discussed. Where possible, the section concludes with maximum tectonic rates considering age information of available strain markers. Further observations available in literature are summarised and contextualised.

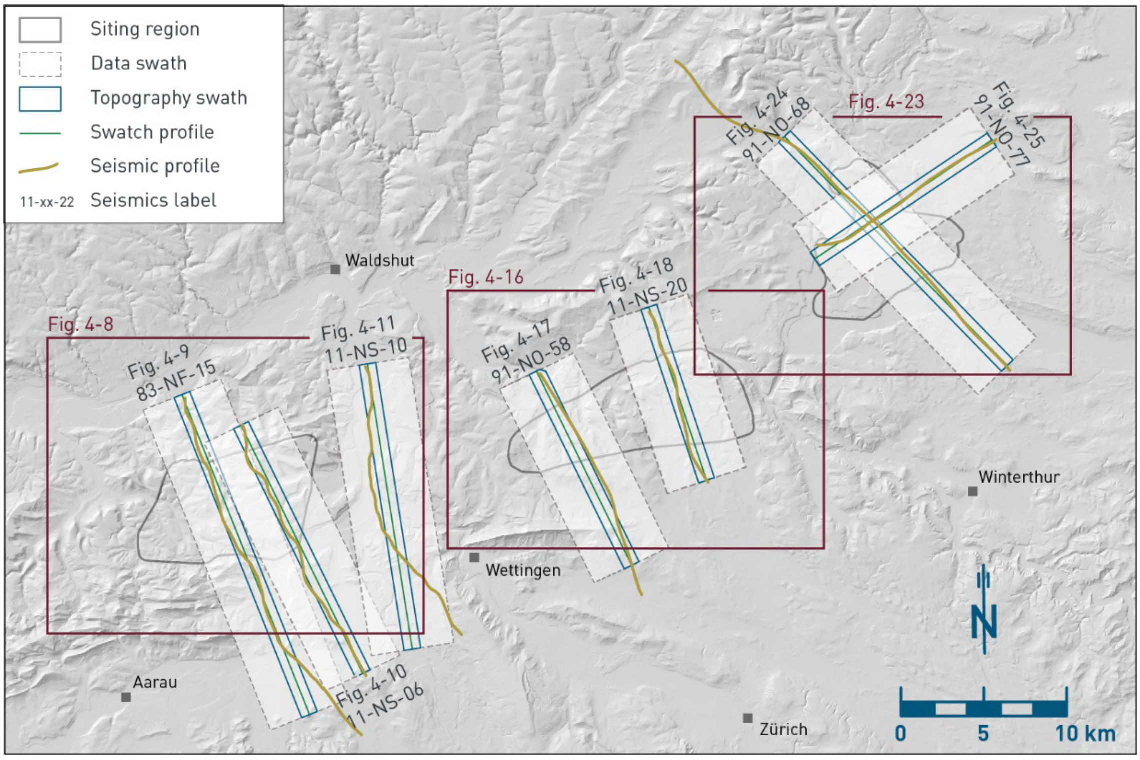

Fig. 4-7: Location of specific data swath and seismic profiles of the siting regions

The traces of 2D seismic reflection lines across the siting regions formed the basis for the structural interpretation. These were accompanied by tectonic proxy data collected in swath profiles approximately following the traces of the seismic lines. Also shown are the outlines of summary maps for each siting regions. These visualisations help to synthesise and assess the regional neotectonic activity relevant to the individual sites.

4.2.1 Jura Ost

4.2.1.1 Local tectonic inventory

The Jura Ost siting region is part of the Herznach – Bözberg Tafel morphotectonic province in the External Jura (Diebold et al. 2006, Nagra 2014a) and located north of the Internal Jura (i.e. the Jura Main Thrust) and south of the Mandach Thrust, which represents a deformed zone within a gently folded but less deformed block; Fig. 2-4, Fig. 4-8 to Fig. 4-11). A detailed overview of the structural inventory and the deformation sequence of JO is provided in Nagra (2024i).

The Jura Main Thrust represents the major fault system in Jura Ost (Fig. 4-8c). It strikes approximately E-W, dips to the south and represents an imbricate fan soling out in the Triassic evaporites (Fig. 4-9c, Fig. 4-10c, Fig. 4-11c). The faults located above the décollement are inferred to accommodate between 2 and 5 km of shortening during Jura-related folding and thrusting as estimated from balanced geological sections. These also show that the shortening decreases towards the east (Fig. 2-4; Jordan et al. 2015). The Jura Main Thrust is located above the southern border fault of the Paleozoic Konstanz – Frick Trough (Diebold et al. 1991, Madritsch et al. 2018). Detailed field and subsequent geochronological investigations provided ages for syn-kinematic calcite slickenfibres in the range between 11.3 ± 0.9 Ma and 4.5 ± 1.5 Ma (Looser et al. 2021, Madritsch et al. 2024). The Internal Jura (a.k.a. Folded Jura) continues to the south with a succession of folds and thrusts, particularly the Chestenberg Anticline or the Gisliflue Anticline (Fig. 4-9).

The Mandach Thrust is known from surface mapping. It is interpreted as a thrust ramp splaying out from the Muschelkalk Group evaporites (e.g. Malz et al. 2020). The location of the thrust ramp is most probably controlled by a step in the pre-Mesozoic basement, linked to the Paleogene normal faulting reactivating the northern border fault of the Paleozoic Konstanz – Frick Trough (Fig. 4-9c, Fig. 4-10c, Fig. 4-11c). The Paleogene normal faulting is related to the northward migration of the flexural Alpine forebulge(Laubscher (1985, Nagra 2024i). The Mettau Thrust located north of the Mandach Thrust is south verging (Fig. 2-4 and Fig. 4-9). It is considered to represent the northern front of the contractional regional overprint related to the Alpine orogeny. It represents also a thrust soling out in the Triassic evaporites (Madritsch et al. 2024). Additional structures imaged on seismic reflection data encompass the Siggenthal Anticline (Fig. 2-4) and the Effingen Fault (Nagra 2024a). The Siggenthal Anticline is a north vergent anticline associated with a thrust ramp rooted in the Triassic evaporites (Fig. 4-11). It has a rather well constrained age range between 8.4 ± 0.38 and 6.6 ± 3.4 Ma (Madritsch et al. 2024). The Effingen Fault is known from seismic reflection images (no surface expression is known; Nagra 2019a). It strikes NNE-SSW and dips towards the E. The Rhenish orientation and fault kinematics suggest a probable association with the Upper Rhine Graben extensional province (Nagra 2024a).

4.2.1.2 Tectonic geomorphology and geodesy

JO is situated between the Aare River in the east and the Hochrhein in the north. Compared to the other sites, JO has considerably more local topographic relief, with the Bözberg-plateau forming the central part. Unlike the other siting regions, JO is less influenced by the erosive and depositional effects of Quaternary glaciations (see Nagra 2024h).

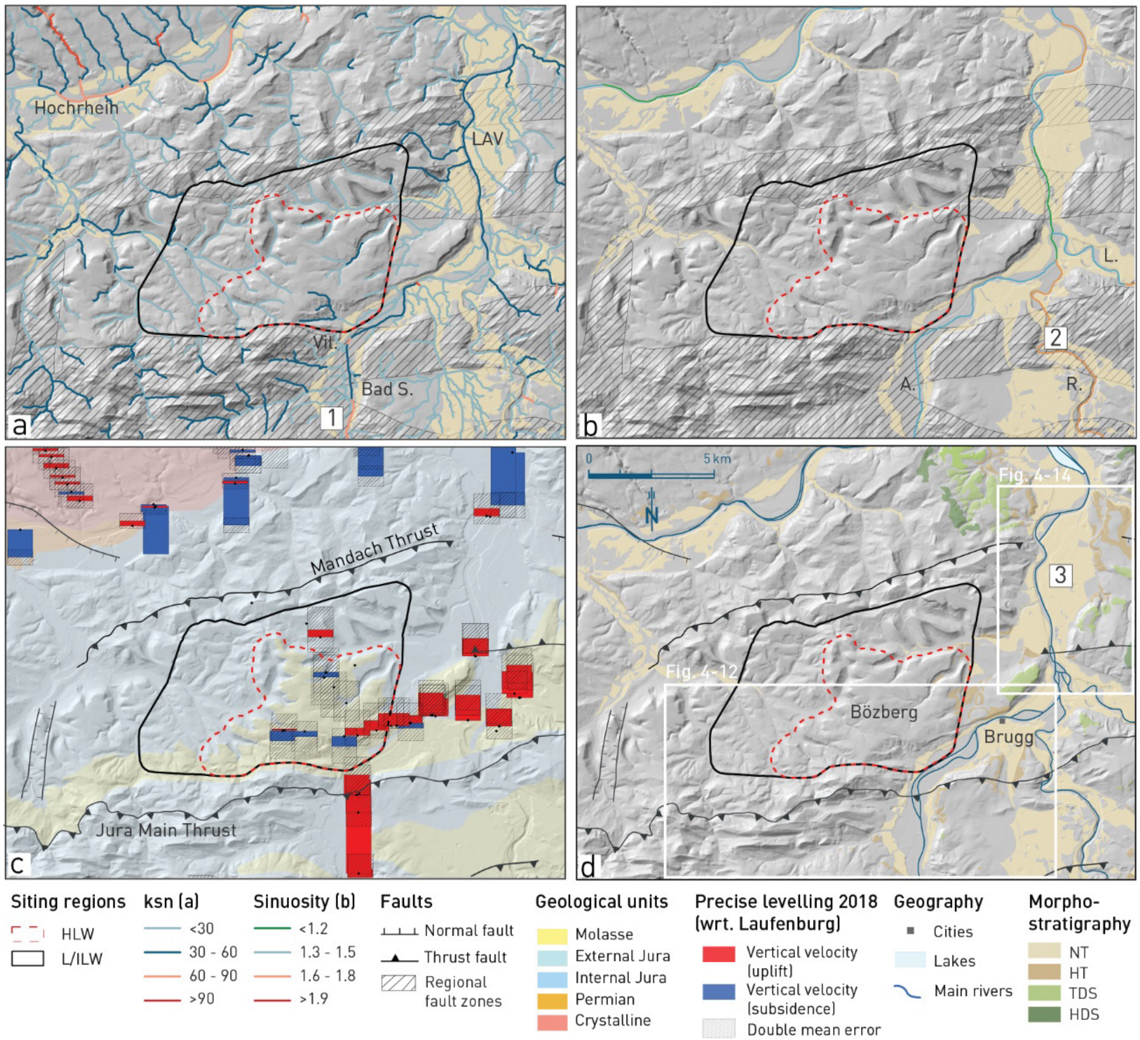

Fig. 4-8: Map compilation of river steepness and sinuosity, tectonic information and precise levelling, and Quaternary morphostratigraphic units – Jura Ost

Compilation of tectonic proxy data (a) Hillshade based on 2-m lidar data overlain by polygons highlighting the regional fault zones. Distribution of NT is shown. The river network is coloured according to the channel steepness ('ksn'). The #1 points to a comparably steep river section. (b) Similar to (a), but river network (main streams only) is colour-coded by sinuosity. # 2 points to the highly sinuous Reuss River section, but the location is also discussed with respect to the morphostratigraphic units TDS and NT. (c) Hillshade and tectonic units with simplified faults, based on Nagra (2014a) and seismic reflection interpretation of Base Cenozoic and Top Villigen Formation (see Fig. 2-4). Vertical velocities are based on precise levelling and measured with respect to Laufenburg (orange triangle on Fig. 4-2). Only data with a good geologic quality ranking (> 8.5) are shown. (d) Quaternary morphostratigraphic units that overlie the incised bedrock and potentially constitute strain markers: Höhere Deckenschotter (HDS), Tiefere Deckenschotter (TDS), Hochterrasse (HT) and Niederterrasse (NT). #3 points to an apparent warping of the Niederterrasse deposits that is analysed in more detail in Fig. 4-11, Fig. 4-14 and Fig. 4-15. The white rectangles outline Fig. 4-12 and Fig. 4-14. Selected geographic elements discussed in text or profiles are labelled. Vil: Villnachern, Bad S: Bad Schinznach, A: Aare River, R: Reuss River, L: Limmat River. #numbers relate to anomalies, listed in Tab. 4-1.

The traces of three 2D seismic reflection lines (83-NF-15, 11-NS-06, and 11-NS-10) formed the basis for geological interpretation and synthesis swath profiles, along which geomorphic disturbances were analysed (Fig. 4-8 to Fig. 4-11). Potential geomorphic anomalies that might indicate Quaternary tectonic activity are labelled with numbers, discussed below and summarised in Tab. 4-1.

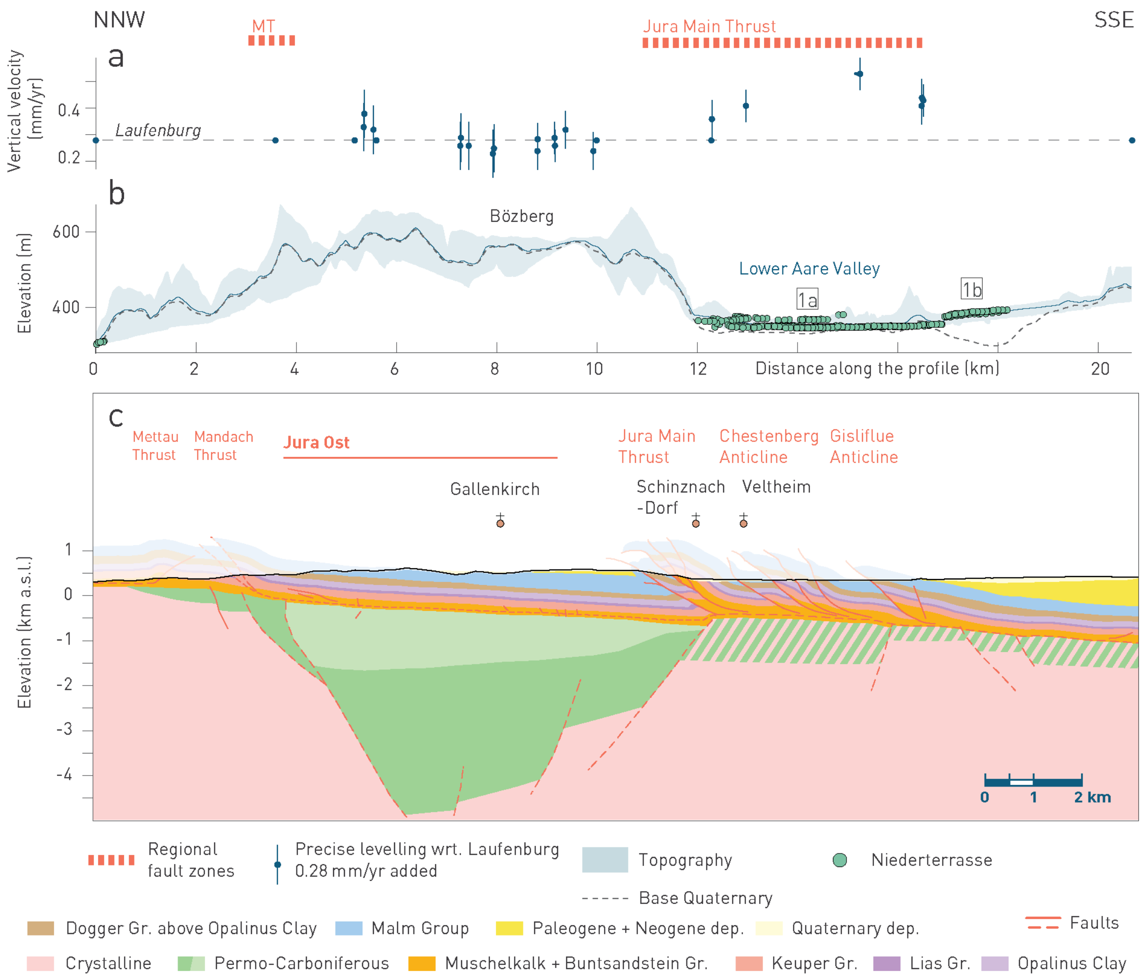

Fig. 4-9: Summary profile along the 2D seismic reflection line 83-NF-15

Synthesis profile through the JO siting region (see Fig. 4-7 for location): (a) Vertical velocity based on precise levelling. Original data were documented with respect to Laufenburg as 'zero-velocity' reference point (see triangle in Fig. 4-2). Here, the GNSS-based uplift (2024) of the Laufenburg station of ~ 0.28 mm/yr was added to each value, respectively (horizontal dashed line), to allow a relative comparison. The relative locations of associated regional fault zones (Fig. 4-8a, b) are highlighted with the dashed red line. MT: Mandach Thrust. (b) Topography (min-max) based on swissALTI3D lidar data resampled to 10 m with Quaternary sediments of Niederterrasse (green circles) and mean Base Quaternary (black dashed line). #1 indicates the location of the steep Aare reach (see high 'ksn' in Fig. 4-8a). (c) Geological profile based on 2D seismic reflection line 83-NF-15. The intersection with the siting region is highlighted. Green hatched zone denotes basement that could be Permo-Carboniferous deposits or crystalline basement. wrt.: with respect to.

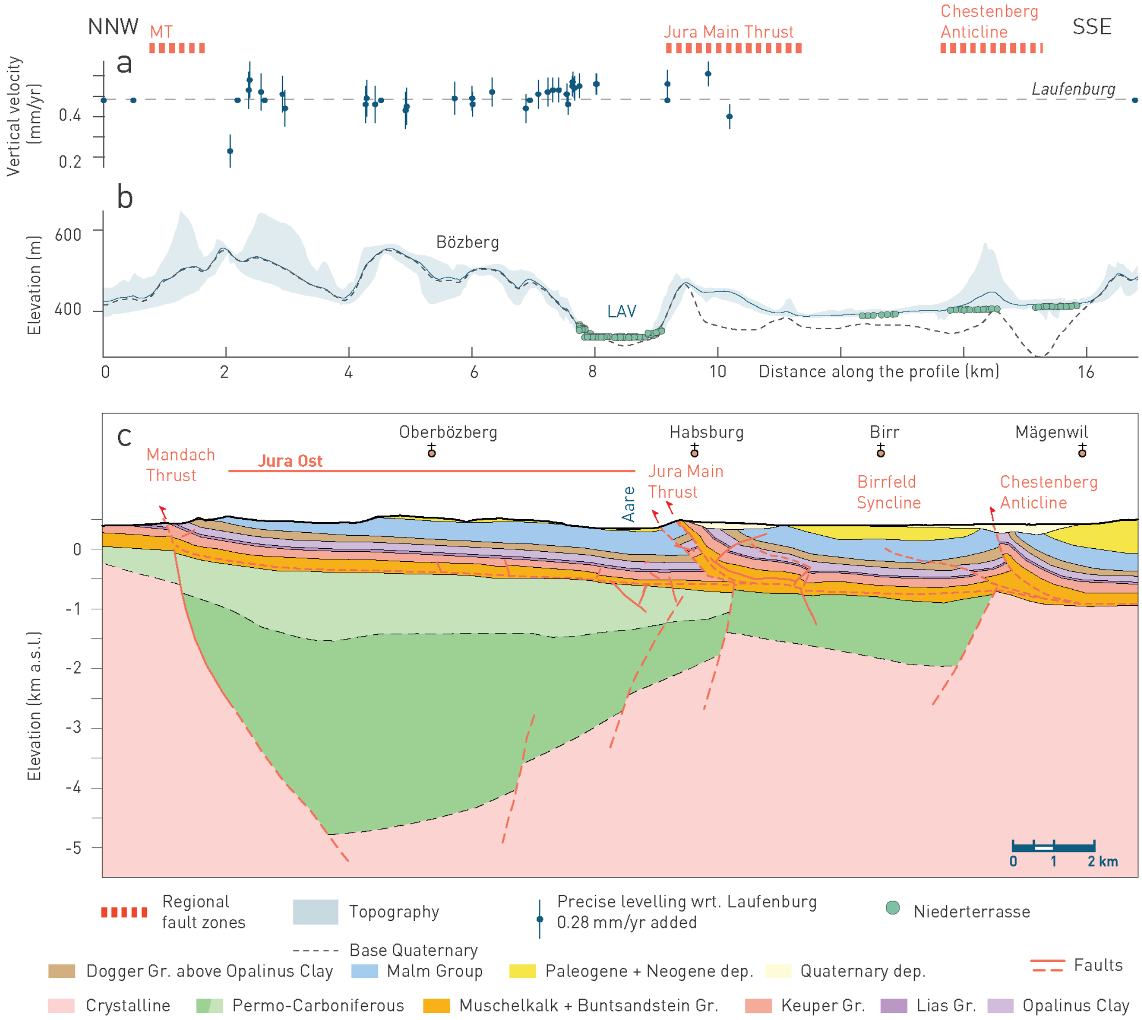

Fig. 4-10: Summary profile along the 2D seismic reflection line 11-NS-06

Synthesis profile through the eastern JO siting region (see Fig. 4-7 for location and Fig. 4-9 for general description). LAV: Lower Aare Valley, wrt.: with respect to.

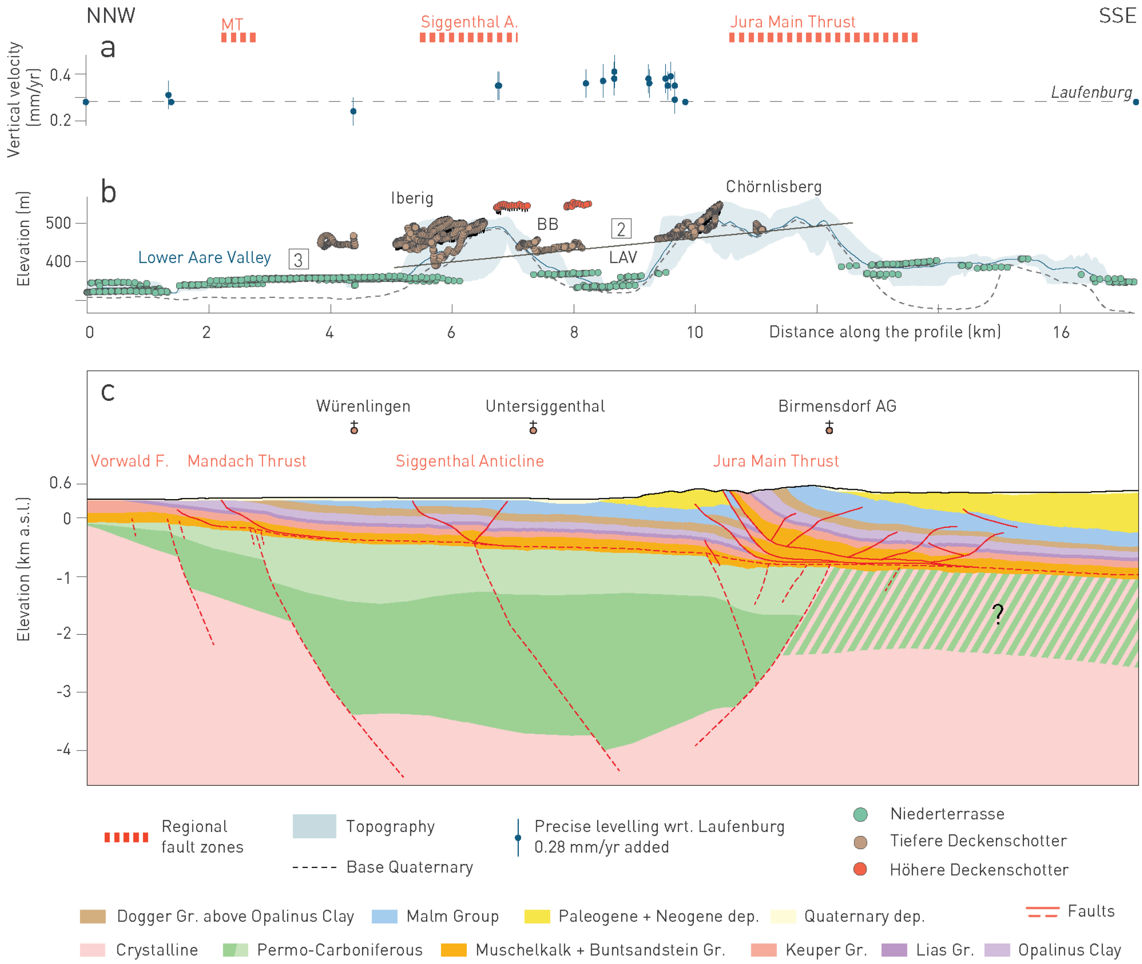

Fig. 4-11: Summary profile along the 2D seismic reflection line 11-NS-10

Synthesis profile through the Lower Aare Valley, east of JO (see Fig. 4-7 for location and Fig. 4-9 for general description). #2 indicates the location of a staircase set of Niederterrasse gravels and inclined base of Tiefere Deckenschotter (TDS). Note that Base TDS has limited quality as strain marker owing to its complex relief as projected to the profile. BB: Brugger-berg; LAV: Lower Aare Valley, MT: Mandach Thrust, Vorwald F.: Vorwald Fault. #3 shows the location of the inferred warping of Top Niederterrasse deposits.

The first anomaly (Fig. 4-8a, Fig. 4-9, Fig. 4-12; #1) constitutes a series of high 'ksn' values in the area of the Jura-Fold-and-Thrust Belt. # 1a is highlighted by an Aare segment of high 'ksn' values south of Bad Schinznach. This steep section is narrow and located in the hanging wall of the Jura Main Thrust and across the wider associated regional fault zone and associated thrusts (Fig. 4-8a).

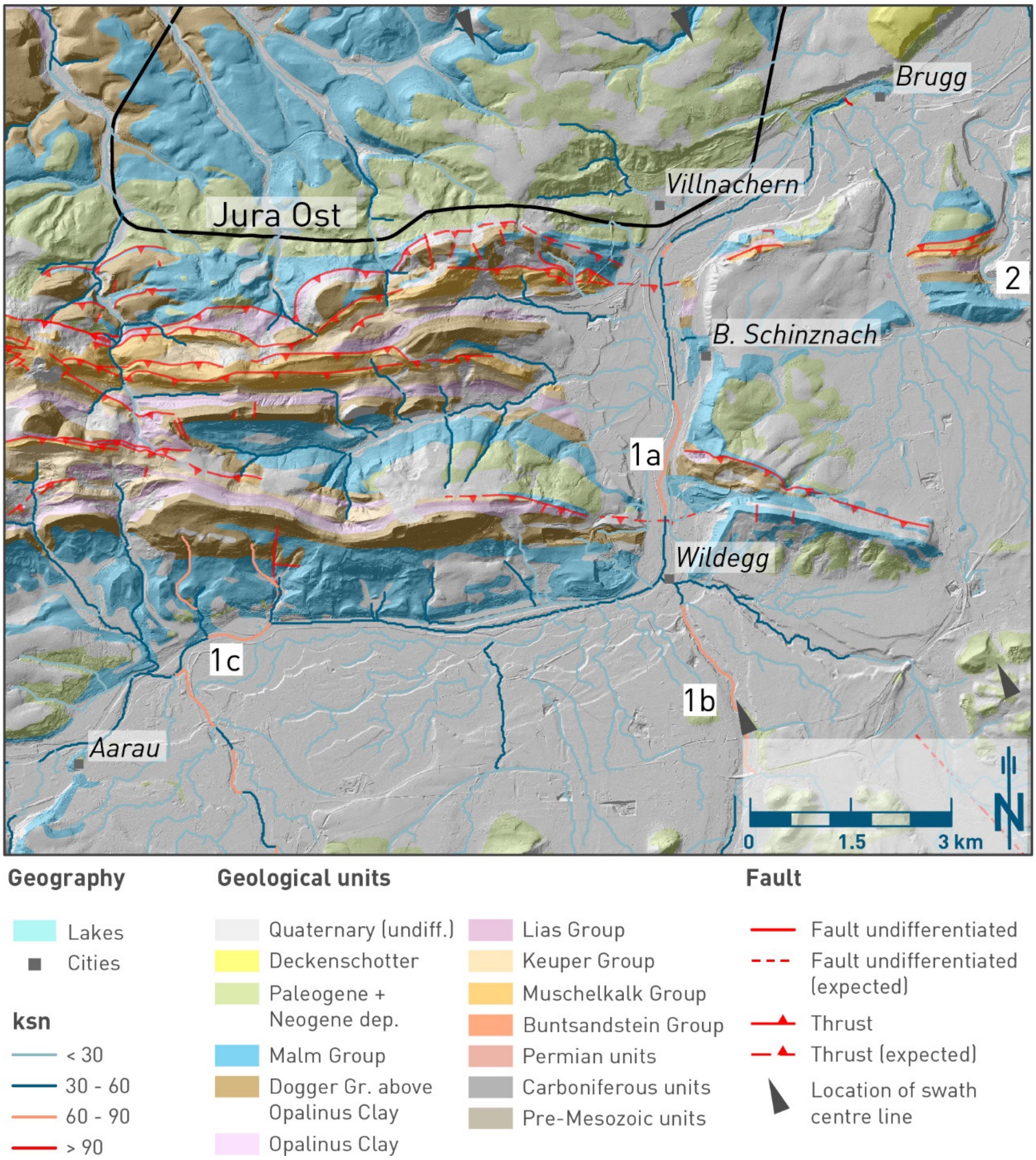

Fig. 4-12: Detailed geological map of the Lower Aare Valley and the potential geomorphic anomaly #1

Hillshade (based on 2-m swissALTI3D lidar data) is shown with the 'ksn'-based colour coded Aare River and tributaries. For location of the map see Fig. 4-8d. Geology is overlain to highlight potential influence of harder-to-erode rock types on 'ksn'. The areas depicted with high 'ksn' values are labelled #1a to #1c. For comparison, the positions of the crossing centre lines corresponding to the swath profiles shown in Fig. 4-9 (west) and Fig. 4-10 (east) are indicated by the grey triangles. See also Fraefel (2008) for comparison and their interpretation.

To the north and south of this position, the Aare Valley is wide (~ 1.5 km) and aggraded by sediments of the Niederterrasse (NT) morphostratigraphic unit. At this position, the Aare River flows locally on bedrock outcrops of steeply inclined Keuper Group, Staffelegg Formation, and Opalinus Clay, as well as Malm Group limestone and Molasse sedimentary rocks (Fig. 4-12), for the most part, however, this river is incising the > 20 m thick NT deposits (Pietsch & Jordan 2014, Beilage 19). According to those authors, this area is not marked as a historic knickzone prior to anthropogenic engineering of the river. Incision into the NT has locally formed unpaired terrace levels and a wide floodplain (see hillshade in Fig. 4-12) that provides a geomorphic marker of good quality to further investigate potential tectonic overprint.

The terraces have a simple initial morphology and can be followed over an extended area and the general age range is known (see Section 3.6.3). Along the profile (Fig. 4-9), NT surfaces are only captured within the hanging wall of the Jura Main Thrust and cross a number of associated thrusts. The NT surfaces appear undeformed. High 'ksn' sections (anomalies #1b south of Wildegg and #1c east of Aarau) constitute alluviated reaches of tributaries to the main Lower Aare River (Fig. 4-12), although a few high 'ksn' values can also be seen in bedrock channels draining the southern slopes of the Internal Jura (#1c). Different regression levels of the wide, incised Lower Aare reach are visible between Aarau and Wildegg (Fig. 4-12). Examination of the terrace levels along this reach of the Aare was also the topic of Chapter 4 of Fraefel (2008) (building on Haldimann et al. 1984). Fraefel (2008) performed a detailed analysis and concludes "…no active tectonic structure which is crossed by the Aare can reliably be inferred." (p. 114). They suggest that the Aare River *"...has been affected by a regional tilt to the north in the past 20 ka, resulting in a lateral shift in the area between Aarau and Wildegg, or possibly by a local compressional structure south of this Aare reach."* (p. 114). They find that the Höhere Deckenschotter (HDS) and Tiefere Deckenschotter (TDS) records are discontinuous and modified by loess deposition along with glacial and fluvial deposition and erosion.

However, such incision, combined with the observation that the Aare locally incises bedrock in this area, may also be caused by locally higher rock uplift rates across the Internal Jura. Although the measurements of precise levelling data need to be treated with caution (see Section 3.3), locally slightly higher vertical velocities, as seen in Fig. 4-9 across the Internal Jura (regional fault zone around Jura Main Thrust) may support this argument. Together with potential rock-type influence on #1a and partly #1c and the apparently undeformed Niederterrasse marker in this area, we interpret this anomaly as an ambiguous signal (Tab. 4-1).

The second area (Fig. 4-8b and Fig. 4-11, partly in NE corner of Fig. 4-12; #2) is located south of the "Wasserschloss", a complex joined floodplain at the confluence of the Limmat, Reuss, and Aare rivers. Here, the Reuss River exhibits a high degree of sinuosity. Today, the rivers flow exclusively on Quaternary fill (Pietsch & Jordan 2014, Beilage 19). Remnants of TDS and NT straddle the river courses and provide fair quality geomorphic markers. Although showing complex relief conditions, the TDS remnants show an overall common gradient reflecting a previous approximate south-to-north drainage (trendline in Fig. 4-11). The gradient is steeper than that of the NT, but with no distinct offset visible at this scale. NT deposits have a complex initial geometry (several unpaired cut terraces) but also continue across a larger section and appear to be undeformed. Ages are available for both TDS and NT (see Section 3.6.3). The interpretation of this anomaly is non-tectonic, probably related to complex sediment-transport dynamics within the confluence area (Tab. 4-1).

The third anomaly (Fig. 4-8, Fig. 4-11, Fig. 4-14; #3) is located within the Lower Aare Valley, between Böttstein and Stilli, in the hanging wall of the south-dipping Mandach Thrust and north of the Siggenthal Anticline. Within the profile along the Lower Aare Valley (Fig. 4-15), the surface that is built by the NT sediments appears gently warped, suggesting a tectonic influence. At the location of the Mandach Thrust, the Aare flows on bedrock of the Staffelegg Formation and Opalinus Clay. According to Pietsch & Jordan (2014), the area was marked as knickzone on maps from AD 1890, prior to engineering measures along the river. This knickzone is not visible in the 'ksn' analysis performed in this report. The Lower Aare Valley at the NT south of the Mandach Thrust, i.e. upstream of this knickzone, is up to 2.5 km wide. The terrace surface provides a fair quality geomorphic marker (limited complexity, age control, extended signal) for the analysis. Importantly, the accumulation level of the NT can be traced at a similar level and gradient upstream and downstream of the Mandach Thrust (Fig. 4-13).

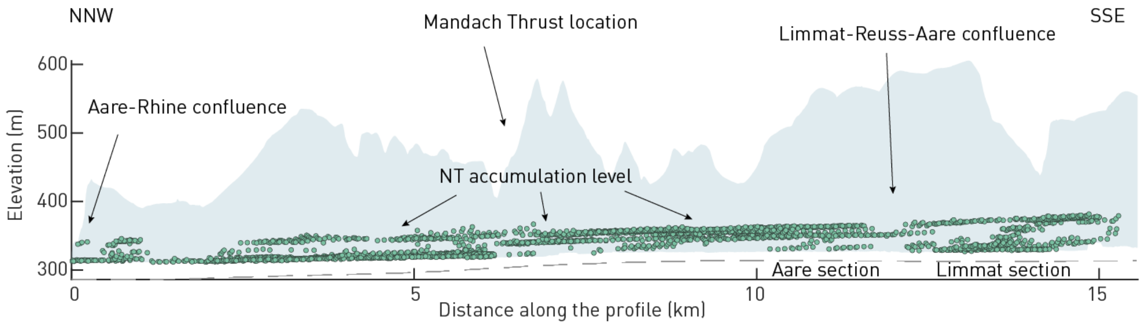

Fig. 4-13: Profile of Lower Aare Valley with focus on Niederterrasse between Rhine and Limmat confluences

Lidar-based 15-km-wide swath profile capturing the Niederterrasse (NT) accumulation and subsequently incised levels (green dots) upstream of the Aare-Rhine confluence. Blue shaded area in background constitutes minimum and maximum topography, dashed line highlights local erosion base (interpolated deepest bedrock level). The accumulation level can be traced at a similar level and gradient across the Mandach Thrust and into the Limmat valley.

At the position of anomaly #3, the Aare exhibits high lateral mobility with a general west-directed stepwise incision into the NT sediments (see arrows in Fig. 4-14).

Fig. 4-14, suggesting that oblique extraction and projection of the different terrace levels sculpted into the NT strata caused the apparent warping of the NT. To support this interpretation, a series of parallel topographic profiles was constructed across the area (Fig. 4-15, see Fig. 4-14 for location). Profiles 1 – 7 cross also HDS and TDS, profiles 6 – 10 cross the NT levels. The basis HDS in profiles 1 – 3 (Fig. 4-15) is gently inclined towards NE, seemingly undisturbed at this scale (note the different uncertainty classification highlighted in Fig. 4-14). The same trend is shown by the TDS in profiles 2 – 6, although their base has usually higher relief (compare also the colour-coded base points in Fig. 4-14). The apparent warping of the NT is best seen in profiles 7 – 9 in Fig. 4-15. However, as expected, this coincides with the superposition of different terrace levels (see arrows and Fig. 4-14), but nevertheless focused incision along this section of the Aare.

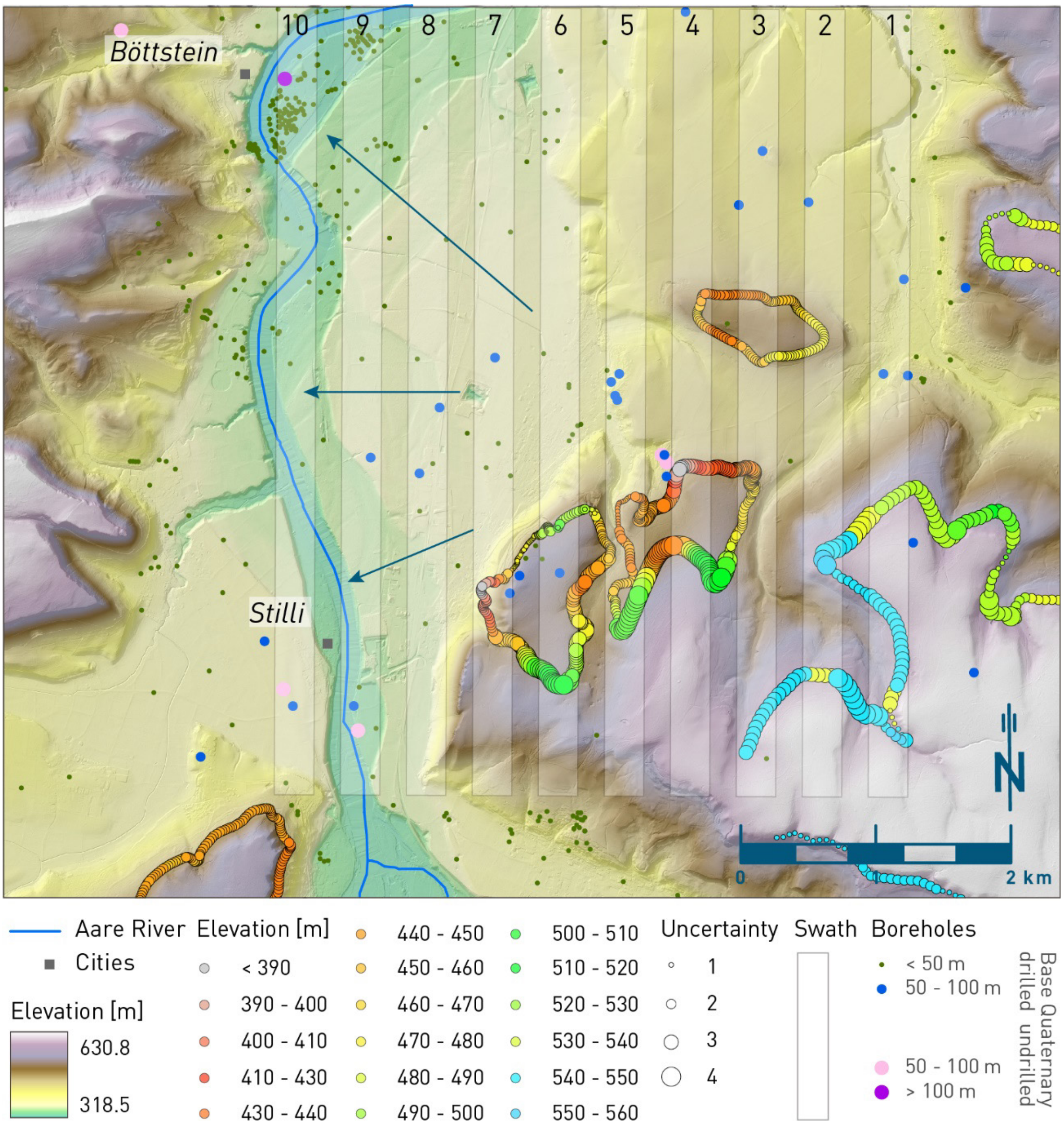

Fig. 4-14: Detailed topographic map of the Lower Aare Valley around potential geomorphic anomaly #3

Digital elevation model (DEM) and hillshade based on 2-m swissALTI3D lidar data are shown with the Aare River. See also Figure 20 in Chapter 4 of Fraefel (2008). The incised flights of terraces in the centre of the figure are visible by their elevation differences in the DEM (arrows show direction of incision and associated lowering). Also shown are extracted locations of the basis of Höhere and Tiefere Deckenschotter. The base points are colour-coded by elevation (based on the swissALTI3D lidar data). Their size is classified by uncertainty, with class 1 being the best (see Tab. 3-2 for uncertainty classification). Note the boreholes that were incorporated in the production of the bedrock model, including the base of the Deckenschotter. Numbers represent elevation of base of Quaternary below terrain, if it was drilled and the total depth of the borehole, if base of Quaternary was not reached during the drilling. The narrow, numbered rectangles correspond to the swath profiles shown in Fig. 4-15.

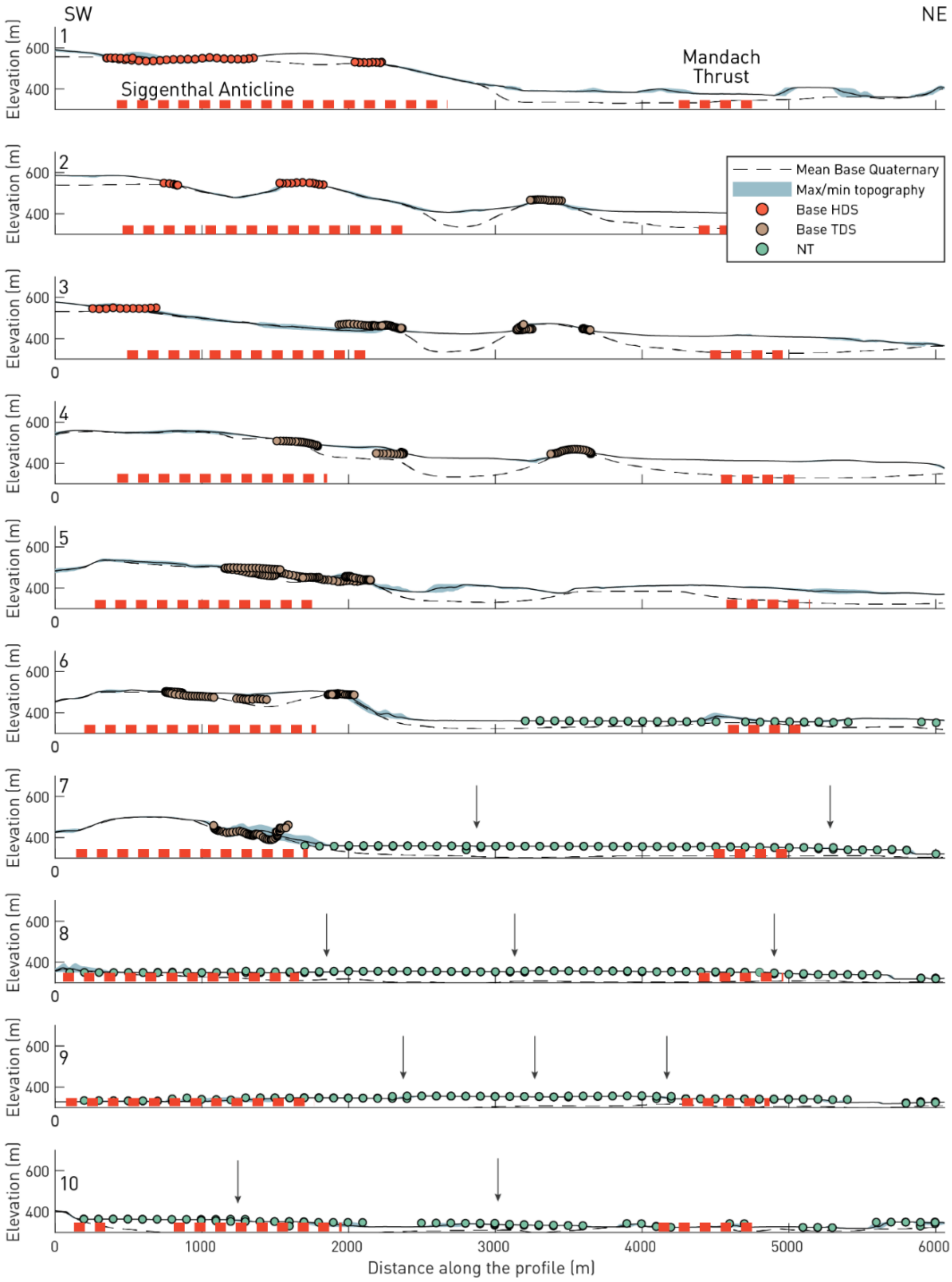

Fig. 4-15: Parallel profiles in the Lower Aare Valley

Swath profiles show topography based on swissALTI3D lidar data (50 m width), the mean Base Quaternary (Q) and Base Höhere and Tiefere Deckenschotter (HDS & TDS) (300 m width). The red dashed line shows the profile intersection with the Siggenthal Anticline and the Mandach Thrust. See Fig. 4-14 for profile locations. Profiles 7 – 10 capture the terrace surface of the Niederterrasse (NT). The apparent warping is best seen on profiles 8 and 9 and affects the area between the regional fault zones of Mandach Thrust and Siggenthal Anticline. The arrows point to areas, where projected NT data from adjacent but different terrace levels overlap at their profile location.

Together, these observations might point to complex glacial/interglacial sediment dynamics, as river planform geometry or river lateral mobility are strongly influenced by changes in sediment supply (see Nagra 2024h, Fraefel 2008). An incision pulse, caused by very low-grade tectonic deformation, with channel steepening in the vicinity of the Mandach Thrust and increased hanging wall incision upstream is considered unlikely, but cannot be excluded. A potential post-Pliocene tectonic signal was proposed for this area by Haldimann et al. (1984). We interpret this anomaly as a non-tectonic to ambiguous signal (Tab. 4-1).

Tab. 4-1: Ranking of geomorphic evidence for tectonic activity in Jura Ost

The evaluation is based on the criteria defined in Section 3.6. According to Tab. 3-3, a good marker comprises 6 points, a fair marker comprises 4 – 5 points, and a vague marker is associated with 2 – 3 points. Listed signals of deformed landforms are indicated in Fig. 4-8 to Fig. 4-14. TDS: Tiefere Deckenschotter, NT: Niederterrasse.

Signal	**Quality**	**Ranking**	**Fault association**	**# Proxies**	**Interpretation**
1			indirect	'ksn'	Ambiguous signal
2 – TDS	5	Fair	missing	Base TDS	Non-tectonic
2 – NT	4	Fair	indirect	Terrace surface	Non-tectonic
2			missing	Sinuosity	Non-tectonic
3 – NT	5	Fair	indirect	Terrace surface	Non-tectonic to ambiguous signal

4.2.2 Nördlich Lägern

4.2.2.1 Local tectonic inventory

The NL siting region is located in the External Jura. This implies that most of the tectonic evolution of this area has been associated with the formation of the Jura Fold-and-Thrust Belt. The Lägern Anticline constitutes the easternmost part of the Internal Jura.

Similar to the siting region Jura Ost, the buried Konstanz – Frick Trough strikes ENE-WSW below Nördlich Lägern (Diebold et al. 1991, Madritsch et al. 2018). However, the graben is more symmetric than in JO, and the trough base is shallower (approximately 3 km; Fig. 2-4, Fig. 4-17 and Fig. 4-18). A major fault is located south of the trough underneath the Baden – Irchel – Herdern Lineament. This fault zone delimits the siting region to the south. It is interpreted as a composite triangle zone including a series of fish-tail structures (e.g. Malz et al. 2016, Laubscher 1985). The Baden Irchel – Herdern Lineament comprises multiple thrusts and backthrusts arranged in a steep, narrow belt that involves the strata above the Middle Triassic units. The eastern continuation of the Baden – Irchel – Herdern Lineament records a change from contractional to predominantly extensional overprint (Section 4.2.1.1; Fig. 4-24).

The northern limit of the Konstanz – Frick Trough underneath Nördlich Lägern is composed of several smaller normal faults compared to the northern border beneath JO. Its expression in the Mesozoic strata consists of the southern Weiach – Glattfelden – Eglisau Lineament as well as the Siglistorf Anticline in the north (Fig. 4-16c, Fig. 4-17 and Fig. 4-18).

The Weiach – Glattfelden – Eglisau Lineament is known from seismic reflection image interpretation (Nagra 2024b, Nagra 2019b). It constitutes a highly segmented, ENE-WSW striking high-angle fault array. The main structural expression of this array is found in the Muschelkalk Group, although the northern strand is observed across the entire Mesozoic strata (Nagra 2024b, Nagra 2024i). Current 3D seismic reflection image interpretation provides sound evidence for a rooting of the Weiach – Glattfelden – Eglisau Lineament in the Konstanz – Frick Trough (Schöpfer et al. 2024, Nagra 2024b).

The Siglistorf Anticline and the faults that drove its formation represent the northernmost expression related to the Alpine contraction in the siting region Nördlich Lägern (Fig. 2-4, Fig. 4-16 and Fig. 4-17). The fault at the core of the anticline is a thrust that detaches from the Triassic evaporites. The thrust is expressed within different stratigraphic levels along strike. In the west, a 2D seismic reflection image line provides evidence for an offset of Top Malm (Fig. 4-17), whereas in the east, the faulting associated with this structure terminates within the Opalinus Clay (Fig. 4-18). The top of the Malm Group and the Paleogene-Neogene deposits form a gentle anticline above the thrust (Fig. 4-17 and Fig. 4-18).

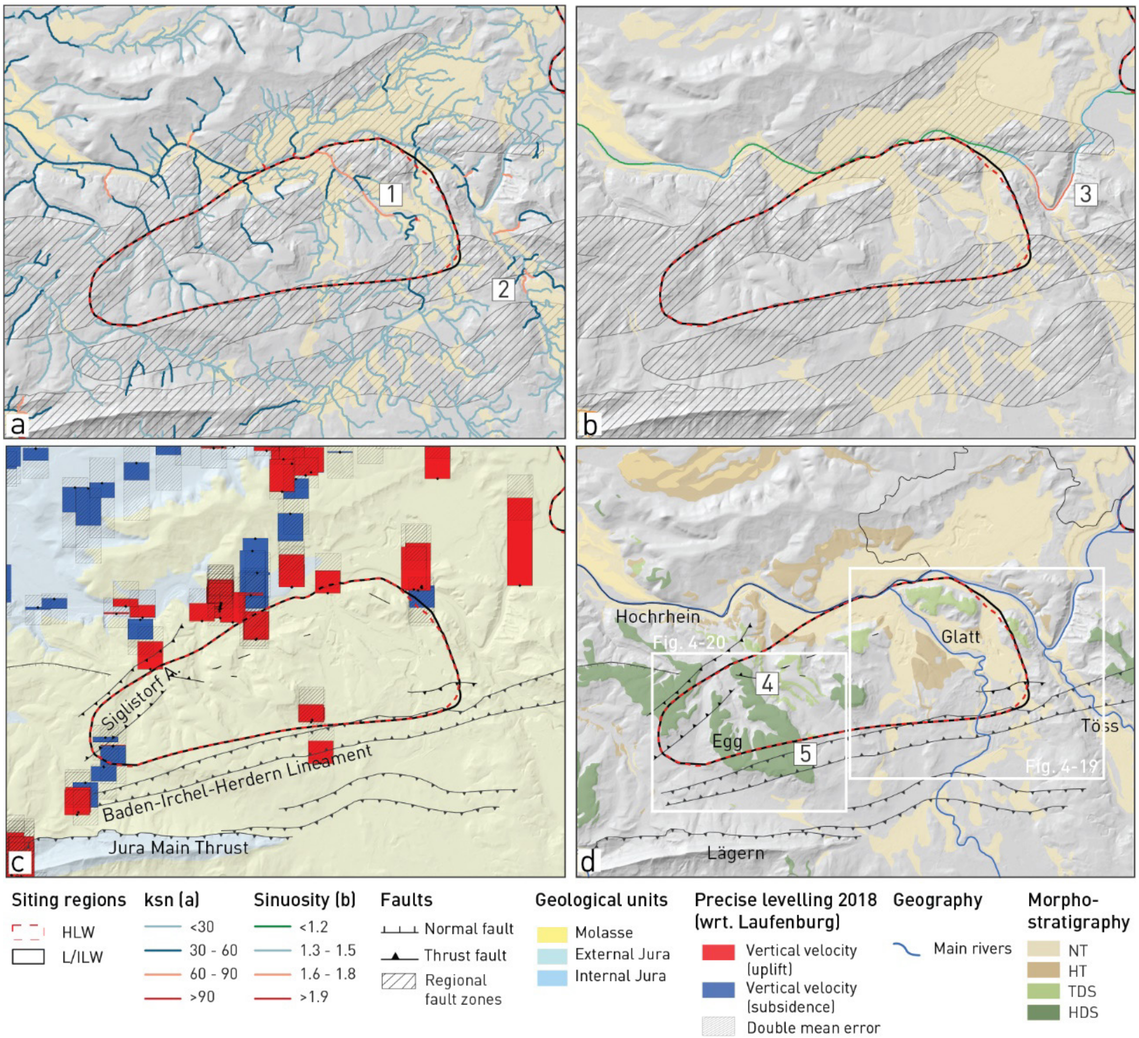

Fig. 4-16: Map compilation of river steepness and sinuosity, tectonic information and precise levelling, and Quaternary morphostratigraphic units – Nördlich Lägern

Compilation of tectonic proxy data. Selected geographic elements discussed in text or profiles are labelled. # numbers relate to anomalies, listed in Tab. 4-2. (a) Hillshade based on 2-m lidar data overlain by polygons highlighting the regional fault zones. Distribution of Niederterrasse (NT) is shown. The river network is coloured according to the channel steepness ('ksn'). #1 and #2 label steep river sections. (b) Similar to (a), but river network (main streams only) is colour-coded by sinuosity. #3 points to the highly sinuous Hochrhein section. (c) Hillshade and tectonic units with simplified faults, based on Naef & Madritsch (2014) and seismic reflection interpretation of Base Cenozoic and Top Villigen Formation (see Fig. 2-4). Vertical velocities are based on precise levelling and measured with respect to Laufenburg (orange triangle on Fig. 4-2). Only data with a good geologic quality ranking (> 8.5) are shown. (d) Quaternary morphostratigraphic units that overlay the incised bedrock and potentially provide strain marker: Höhere Deckenschotter (HDS), Tiefere Deckenschotter (TDS), Hochterasse (HT), and Niederterrasse (NT). #4 and #5 point to potential offsets in the base elevation of HDS that are shown and analysed in more detail in Fig. 4-20 and Fig. 4-21. The white rectangles outline Fig. 4-19 and Fig. 4-20. WGE: Weiach – Glattfelden – Eglisau Lineament, wrt.: with respect to.

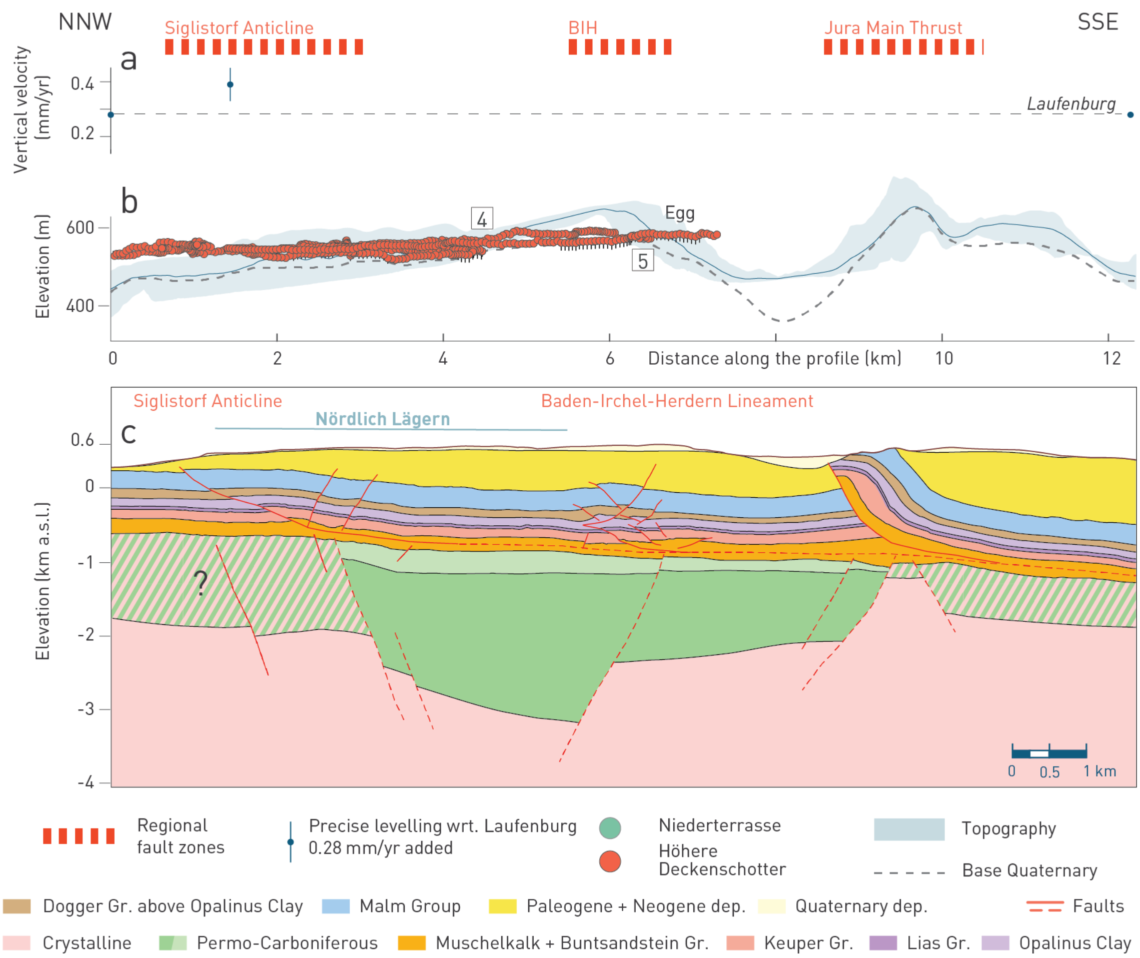

Fig. 4-17: Summary profile along the 2D seismic reflection line 91-NO-58

Synthesis profile through the NL siting region (see Fig. 4-7 for location): (a) Vertical velocity based on precise levelling. Original data were documented with respect to Laufenburg as 'zero-velocity' reference point (see triangle in Fig. 4-2). Here, the GNSS-based uplift (2024) of the Laufenburg station of ~ 0.28 mm/yr was added to each value to allow a relative comparison. The relative locations of associated regional fault zones are highlighted with the dashed red line. BIH: Baden – Irchel – Herdern Lineament. (b) Topography (min-max) based on swissALTI3D lidar data resampled to 10 m (blue swath) with base of Höhere Deckenschotter (HDS) with uncertainty (red circles), mean Base Quaternary (black dashed line). #4 and #5 indicate anomalies in Base HDS that are discussed in the text. (c) Geological profile based on 2D seismic reflection line 91-NO-58 for interpretation. The intersection with the siting region is highlighted. Green hatched zones reflect basement that could be Permo-Carboniferous deposits or crystalline basement. wrt.: with respect to.

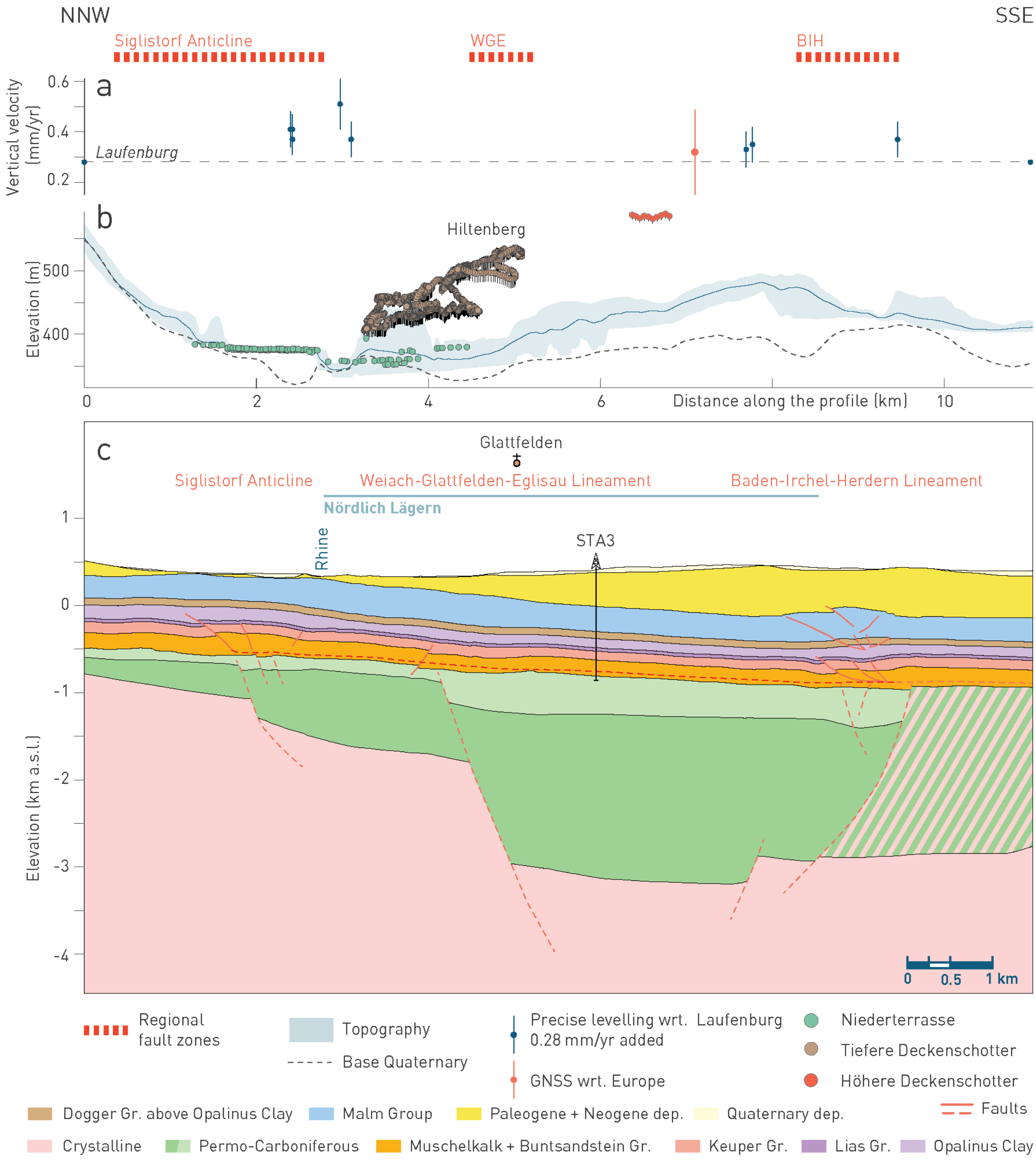

Fig. 4-18: Summary profile along the 2D seismic reflection line 11-NS-20

Synthesis profile (see Fig. 4-7 for location and Fig. 4-17 for general description), showing (top to bottom) vertical velocity based on precise levelling and GNSS, topography based on swissALTI3D lidar data resampled to 10 m (blue swath) with base of Tiefere Deckenschotter with uncertainty (brown circles), surface samples of Niederterrasse sediments (green circles), mean Base Quaternary (black dashed line), slope based on the same DEM as topography (brown) and geological profile based on 2D seismic reflection line 11-NS-20 for interpretation. Green hatched zone reflects basement that could be Permo-Carboniferous deposits or crystalline basement. WGE: Weiach – Glattfelden – Eglisau Lineament, BIH: Baden – Irchel – Herdern Lineament, wrt.: with respect to.

Seismicity of Eglisau

The earthquakes recorded beneath the town of Eglisau in Northern Switzerland exhibit distinctive characteristics that warrant scientific investigation in the context of our neotectonic assessment (Fig. 3-3, Fig. 4-2, Fig. 4-3, Fig. 4-5b). Notably, the instrumentally recorded seismicity displays a concentration of shallow hypocentres, confined within the uppermost 2 km of the Earth's crust, and potentially within the lower Mesozoic units and/or the Konstanz – Frick Trough. This anomaly is further accentuated by protracted low-level microseismic activity spanning at least two decades. Combined with historical records (Fäh et al. 2011), the seismicity data represents a series of felt earthquakes dating back to 1661 AD, with intensities reaching up to V and estimated magnitudes of M_W 3.9 for nine historical events. The most significant instrumentally recorded event associated with this cluster occurred on September 12, 1999, registering a local magnitude of M_L = 3.2 and exhibiting strike-slip kinematics. Historical as well as instrumental catalogues thus suggest persistent shallow crustal seismic activity.

The Eglisau seismicity is monitored with a locally densified microseismic monitoring network (Section 3.1). Preliminary relative relocations suggest a diffuse distribution spanning an area of at least 1 km^2 in map view, indicative of the reactivation of multiple faults rather than a single, well-established fault within the region.

4.2.2.2 Tectonic geomorphology, seismicity and geodesy

The NL siting region is characterised by low relief in the eastern part and slightly higher relief in the west. Remnants of Höhere Deckenschotter are abundant especially in the western part, where a continuous deposit can be traced across the site ("Egg"; see Fig. 4-16d). This Deckenschotter complex crosses the traces of the Baden – Irchel – Herdern Lineament in the south and the Siglistorf Anticline in the north, including parts of their potential upward-propagated fault strands (Section 3.6.1, Fig. 4-16c and d). Smaller discontinuous remnants of the Tiefere Deckenschotter (TDS) can be found in the northeastern part of NL (Fig. 4-16d). South and east of these outcrops, the siting region was repeatedly glaciated, leading to two major glacial overdeepenings and surficial glacial landforms and deposits (Nagra 2024h), see also Fig. 4-19. With exception of the Eglisau seismic activity (see Section 4.2.2.1), local seismicity is sparse (Fig. 4-16b). Precise levelling data is only discontinuous around the site (Fig. 4-16c).

The NL siting region straddles the Hochrhein and is cut in the east by the local Glatt tributary. The Töss River flows along the eastern edge of the site (Fig. 4-16d). A close-up view of the results of the 'ksn' analysis (Fig. 4-16a) reveals a few steeper channel sections: within the siting region along the Glatt River, in the vicinity of the regional fault zone polygon comprised of the Siglistorf Anticline and the Weiach – Glattfelden – Eglisau Lineament, immediately downstream of a highly sinuous section north of the moraines of the Last Glacial Maximum (LGM), along the Töss and tributary sections in the vicinity of the Baden – Irchel – Herdern Lineament (anomalies #1 and #2, respectively in Fig. 2-1a), and a few distinct smaller channels entering the Hochrhein. Because of the proximity to the regional fault zones, the area is further addressed in Fig. 4-19. The TDS occurrences located in the vicinity of the high 'ksn' values show a general gradient towards NW with an accentuation in relief close to the Hochrhein confluence. The high 'ksn' sections (especially #1) are located in alluviated reaches surrounded by the Niederterrasse. The location of the LGM terminal moraine in association with the Niederterrasse occurrences suggest a high glaciofluvial sediment pulse and subsequent postglacial fluvial adjustment. As the Glatt valley has no major contributing catchment available, the high 'ksn' might be the result of Hochrhein incision, propagating into the less efficient Glatt channel. We interpret this signal as non-tectonic.

The Töss area around the high 'ksn' values (#2) is also strongly influenced by glaciofluvial processes related to glacial retreat after LGM. We thus relate this signal to postglacial fluvial adjustment and favour a non-tectonic interpretation (Tab. 4-2).

Tab. 4-2: Ranking of geomorphic evidence for tectonic activity in Nördlich Lägern

The evaluation is based on the criteria defined in Section 3.6.3. According to Tab. 3-3, a good marker comprises 6 points, a fair marker comprises 4 – 5 points, and a vague marker is associated with 2 – 3 points. Listed signals of deformed landforms are indicated in Fig. 4-17 and Fig. 4-18.

Signal	**Quality**	**Ranking**	**Fault association**	**# Proxies**	**Interpretation**
1	-	-	missing	'ksn', Glatt	Non-tectonic
2	-	-	indirect	'ksn', Töss	Non-tectonic signal
3	-	-	missing	Sinuosity (breakthrough)	Non-tectonic
4	4	Fair	indirect	Base HDS	Ambiguous to non-tectonic signal
5	5	Fair	direct	Base HDS	Mixed signal

The high-sinuosity anomaly #3 highlights the peculiar bend of the Hochrhein between Rüdlingen and Tössegg (Fig. 4-19). This feature constitutes a breakthrough channel, either incised as response to glacial or postglacial impoundment of a present-day drainage and subsequent overspill or by ice-marginal drainage (see Nagra 2024h). We interpret this signal as non-tectonic.

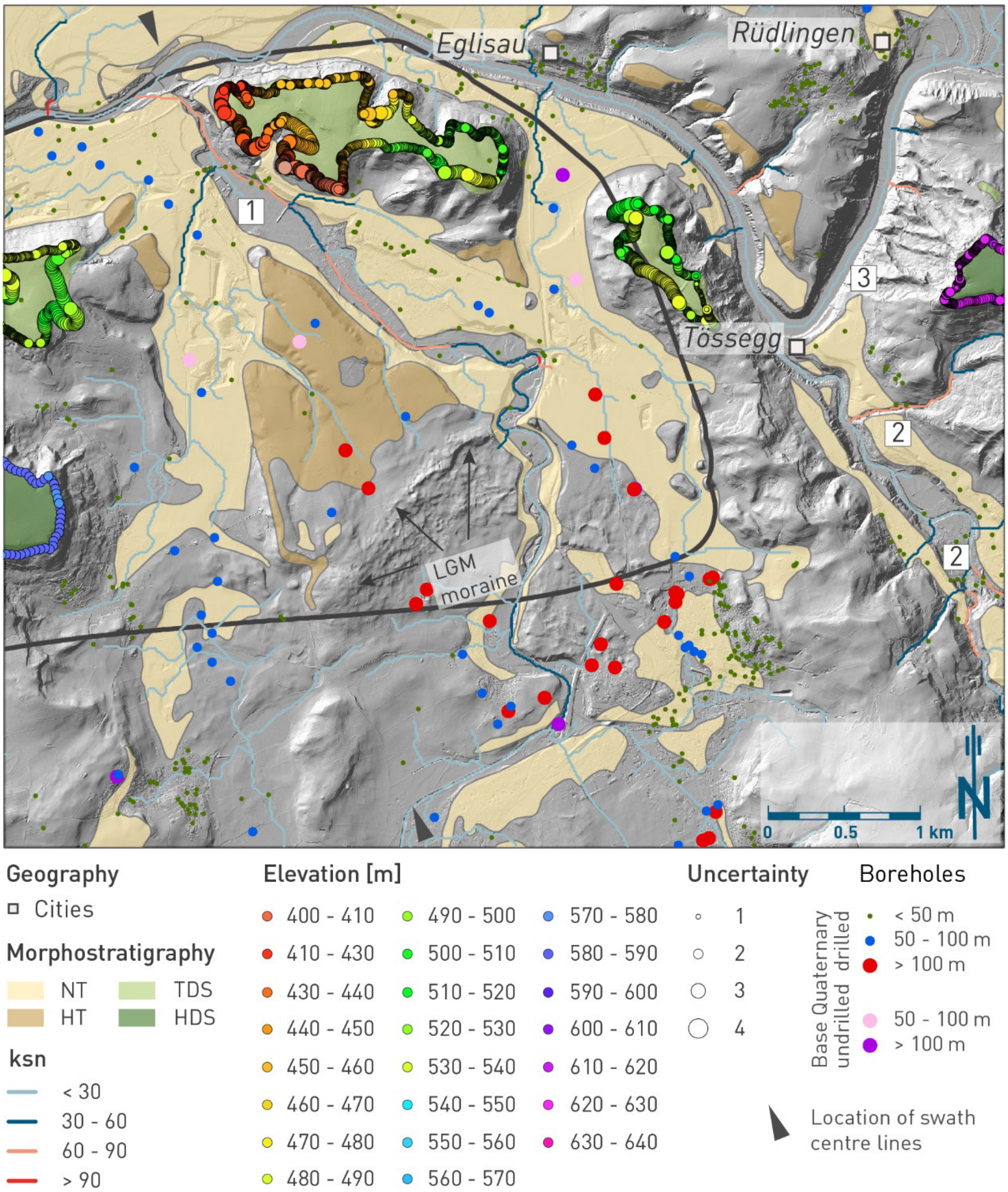

Fig. 4-19: Detailed topographic map of the area around potential geomorphic anomalies #1 – 3 in the eastern part of Nordlich Lägern

Detail map showing 'ksn' and Deckenschotter markers on a hillshade model based on 2-m lidar data. The discussed anomalies are numbered. For comparison, the position of the crossing centre line corresponding to the swath profile shown in Fig. 4-18 is indicated by the grey triangles. Note the boreholes that were incorporated in the production of the bedrock model, including the base of the Deckenschotter. Numbers represent elevation of base of Quaternary below terrain, if it was drilled and the total depth of the borehole, if base of Quaternary was not reached during the drilling. LGM: Last Glacial Maximum. NT: Niederterrasse, HT: Hochterrasse, TDS: Tiefere Deckenschotter, HDS: Höhere Deckenschotter.

Fig. 4-17 reveals a set of steps disrupting the base of the HDS deposits (#4 and 5) at the Egg location. These steps do not coincide with similar offsets in the topographic swath profile. The locations of #4 and #5 coincide with the polygon outlines of the regional fault zones encompassing the Siglistorf Anticline and the Baden – Irchel – Herdern Lineament, respectively. Considering the gentle dip of the upper "fishtail" thrusts of the Baden – Irchel – Herdern Lineament would allow also #4 to coincide with the potential surface expression of this structure (Fig. 4-16d, Fig. 4-17, Fig. 4-18). Precise levelling data are only limited to the far west of the profile and do not cross the geomorphic anomalies. The quality of the geomorphic markers depicting the anomalies differs noticeably.

Fig. 4-18 crosses the eastern part of NL. The topographic profile shows a general decrease in elevation from south to north towards the Hochrhein from where it starts to rise again. Vertical geodetic velocities (precise levelling and GNSS data) are sparse but show no gradient across the Baden – Irchel – Herdern Lineament, but instead a pronounced decrease in velocities north of the Hochrhein, which locally coincides with the approximation of the Siglistorf Anticline, is observed. The TDS sampled in the swath exhibits a complex topography and thus seems unsuitable to serve as a geomorphic marker. The area of eastern NL has a complex glacial history, including overdeepenings, as discussed above with respect to the 'ksn' anomalies.

Detailed geomorphic analysis of the HDS location "Egg"

A potential indication for Quaternary tectonic activity at this location was already suggested in Nagra (2014c) and Hammer et al. (2019). To reveal whether the apparent offsets displayed in Fig. 4-17 might be related to the Deckenschotter projection on the swath profiles and to minimise ambiguity, we visualise the samples of Base HDS in more detail (Fig. 4-20). The Egg bounding sequence of HDS provides a useful span of the Baden – Irchel – Herdern Lineament. The close-up map view is accompanied with a series of more narrow profiles, crossing the Baden – Irchel – Herdern Lineament and the Siglistorf Anticline (Fig. 4-21). Profiles were located at regular steps and arranged to cover as many Base HDS points across the area as possible. However, continuous data points to be fitted onto a single narrow swath are only available for the eastern edge of the Egg location.

Anomaly #4 is visible on profile 2 (Fig. 4-21), where the southeastern part appears slightly backtilted with respect to the northwest. A gentle tilt towards SE might also exist in profiles 4 to 6 but is no longer visible in profile 7. This morphological disturbance of Base HDS is not associated with a clear offset between the different data sections and may thus reflect a local disturbance or a gentle undulation of relief prior to Deckenschotter deposition. However, a tectonically controlled backtilt associated with the S-dipping northern thrust of the Siglistorf Anticline cannot be excluded. We interpret this anomaly as an ambiguous to non-tectonic signal.

Location #5 is visible in profile 1 (Fig. 4-21). Considering the general uncertainties of Base HDS and gently undulated palaeotopography associated with this geomorphic marker, the apparent offset at the location of anomaly #5 is small. However, this setting allows a far-field comparison of low-uncertainty markers southeast and northwest of the step. Both sections can be interpreted as a low-relief, gently inclined surface, separated by a distinct vertical step of > 10 m (see Fig. 4-22b and c). With respect to our quality ranking, this geomorphic marker has a comparably high value (5, fair quality). In association with the location of the Baden – Irchel – Herdern Lineament this allows an interpretation to suggest Quaternary tectonic activity (Tab. 4-2). Alternatively, inherited relief by early (pre-Quaternary) juxtaposition of different rock types or across the fault zone or fracturing along the fault may also play a role. Such a signal may, however, be less distinctly preserved due to the time that has elapsed and given that the Paleogene and Neogene rocks below the HDS comprise laterally heterogenic Molasse sediments. Still, erosional overprint may be possible and could either increase or decrease any potential tectonic offset. It may be considered as a weakness that this anomaly is only observed along a single profile. Here, a continuous intersection of Base HDS with the topography allows such an analysis.

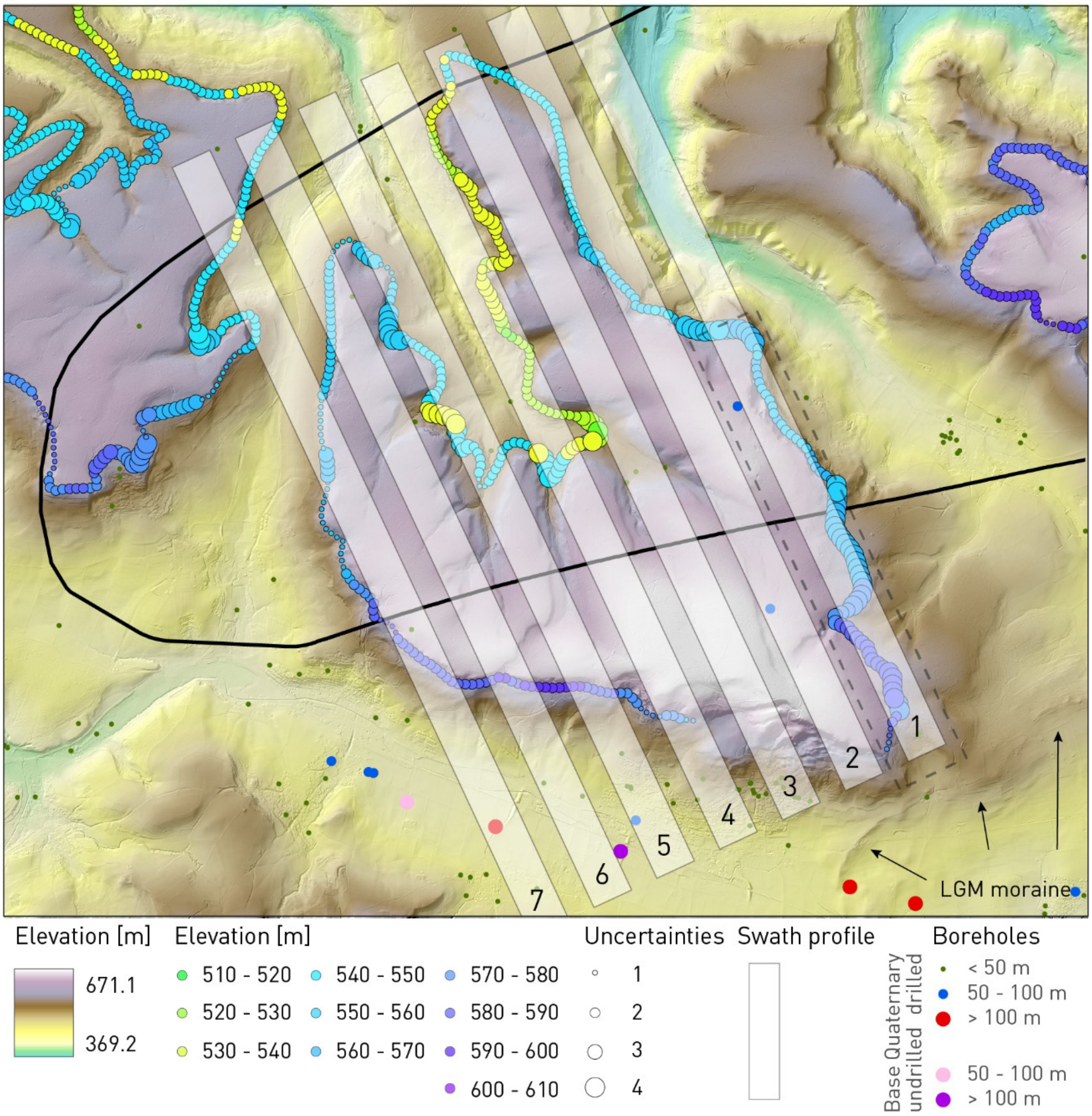

Fig. 4-20: Detailed topographic map of the "Egg" area

Digital elevation model (DEM) and hillshade based on 2-m swissALTI3D lidar data are shown. Also shown are extracted locations of the Base Höhere and Tiefere Deckenschotter (coloured points). The base points are colour-coded by elevation (based on the swissALTI3D lidar data). Their size is classified by uncertainty, with class 1 being the best (see Tab. 3-2 for uncertainty classification). Note the boreholes that were incorporated in the production of the bedrock model, including the base of the Deckenschotter. Numbers represent elevation of base of Quaternary below terrain, if it was drilled, and the total depth of the borehole, if base of Quaternary was not reached during the drilling. The narrow, numbered rectangles correspond to the 300-m wide swath profiles shown in Fig. 4-21. The dashed rectangle partly overlapping with swath 1 corresponds to the swath used for calculation of an apparent vertical slip rate (Fig. 4-22). LGM: Last Glacial Maximum.

Assuming a tectonic interpretation, we calculate an apparent fault-throw rate for potential movement along the Baden – Irchel – Herdern Lineament (Fig. 4-22). Please note that such a rate would be considered maximum, as erosional overprint or contribution cannot be separated.

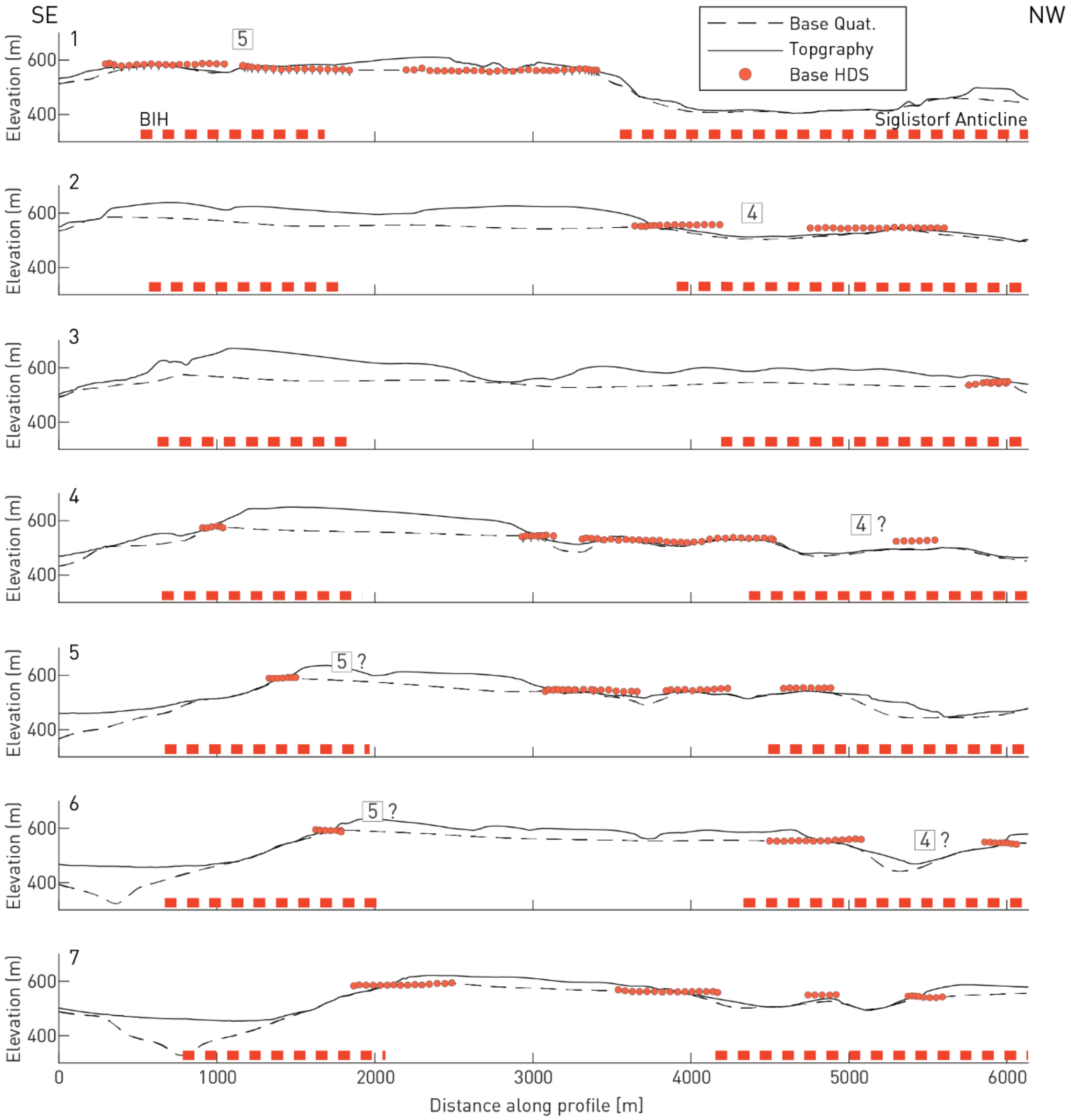

Fig. 4-21: Parallel profiles across the Baden – Irchel – Herdern Lineament at the "Egg" location

Swath profiles show topography based on swissALTI3D lidar data (50 m width), the mean Base Quaternary and Base Deckenschotter (300 m width). The bold red dashed line shows the profile intersection with the Baden – Irchel – Herdern Lineament (BIH). See Fig. 4-20 for profile location. Quat.: Quaternary, HDS: Höhere Deckenschotter. #4 and #5 refer to anomalies in the Base HDS that are discussed in the text.

Apparent vertical slip rate for tectonic activity along the Baden – Irchel – Herdern Lineament

Assuming the interpretation that the anomaly #5 (Fig. 4-17, Fig. 4-21, and Tab. 4-2), observed within the Base Deckenschotter above the Baden – Irchel – Herdern Lineament represents Quaternary tectonic activity, we estimated the maximum apparent rate of vertical offset (fault throw).

To do so, we rely on the more or less continuous profile along the eastern edge of the "Egg" Deckenschotter location (Fig. 4-22a). The undulations in Base HDS are in the order of approximately five metres. The observed offset is approximately 22 m, based on comparison of the far-field slope between hanging wall and footwall (see Fig. 4-22b). As seen in Fig. 4-22a, data closer to the scarp are subject to larger height uncertainties but data at the edges of the profile can be compared with high confidence. Height uncertainty (Fig. 4-22b) was incorporated in the apparent slip-rate calculation.

The approach used follows a Monte Carlo procedure adapted from Gold & Cowgill (2011) (see also Kleber et al. 2021). Rates were calculated by sampling from the range of height differences between hanging wall and footwall and the associated Deckenschotter uniformly distributed age range, assuming that throw has accumulated steadily since HDS deposition (Fig. 4-22c and e).

Two estimates are presented based on different assumptions: firstly, a low-confidence version that includes Base HDS measurements with their elevation uncertainty paired with the full age range of HDS, including biostratigraphy (see Section 3.6.3 and Fig. 4-22d) and secondly, a high-confidence version, where far-field height estimates of Base Quaternary measurements were paired with the youngest age estimate derived at the Egg location itself (Feusi till, 0.95 ± 0.08 Myr; see Nagra 2024h, Section 3.6.3, and Fig. 4-22f). Given the uncertainties, the mean rates are 15 m/Myr (full 2-sigma range of 7 – 33 m/Myr using the full HDS range (see Fig. 4-22d), and 19 m/Myr (full 2-sigma range of 11 – 34 m/Myr) using the local age (Fig. 4-22f).

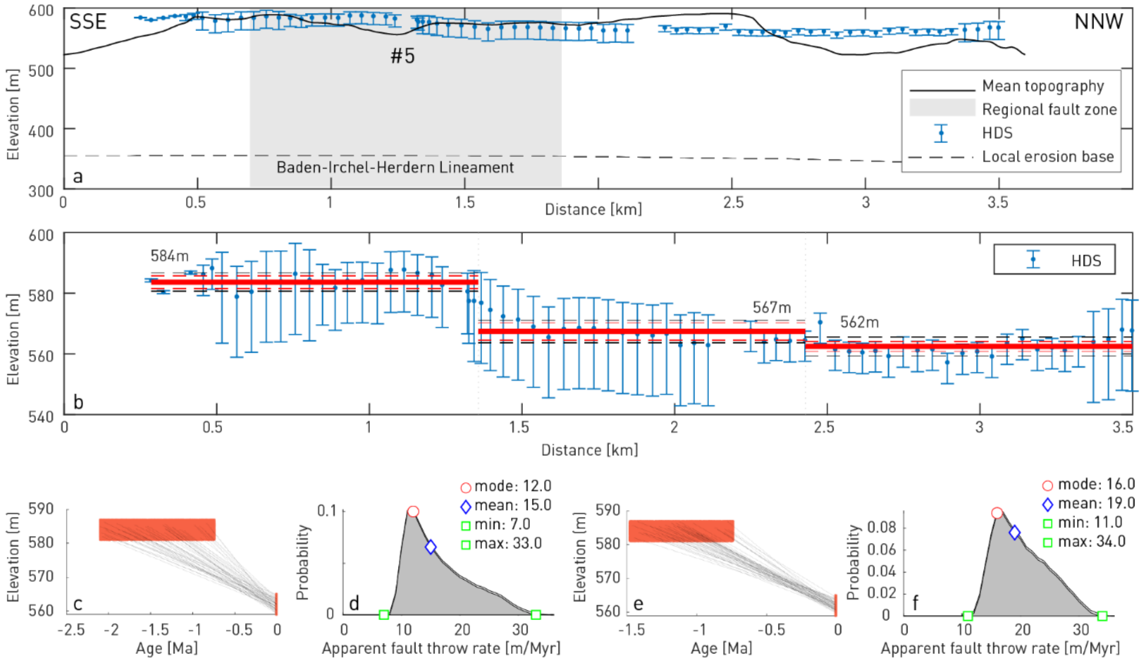

Fig. 4-22: Apparent fault throw rate at the Baden – Irchel – Herdern Lineament since HDS deposition

Plots show Monte Carlo-derived apparent fault throw rates based on the apparent offset observed in base Deckenschotter at the landmark "Egg" above the Baden – Irchel – Herdern Lineament (BIH) and Höhere Deckenschotter (HDS) ages. (a) A narrow swath profile captured the eastern edge of the Egg Deckenschotter (see dashed rectangle in Fig. 4-20 for location). Displayed are mean topography, Base Quaternary with their uncertainty marks, the outline of the regional fault zone polygon and local erosion base (LEB). The latter corresponds to the lowest fluvial incision level, highlighting that the HDS base is well preserved from present fluvial reworking. The offset, which is spatially coincident with the BIH is labelled as #5 below the profile. (b) Zoom to the geomorphic marker showing the step in Base HDS. For three sections of rather homogeneous marker elevation, the mean (red line with numbers shown), standard deviation (red dashed line) and standard error (black dashed line) were calculated.

Apparent fault-throw rates were subsequently calculated from the height difference between hanging wall and footwall samples and the Deckenschotter age, assuming that slip accumulated steadily since HDS deposition. In this example, we relied on far-field estimates of the apparent offset (22 m) using samples with lower uncertainty, skipping the central section. Samples were taken from a uniform age distribution and normal distribution of elevation. (c) Sampling using height estimates of Base Quaternary measurements were paired with the full age range of HDS, including biostratigraphy. (d) Probability density distribution (2-sigma range) of the corresponding vertical slip rate (with respect to subfigure c) shows mean rate of 15 m/Myr. (e) Sampling using the same heights, but only the youngest HDS age estimate derived at the Egg location itself (Feusi Till). (f) The mean rate shown in the associated probability density distribution is 19 m/Myr.

4.2.3 Zürich Nordost

4.2.3.1 Local tectonic inventory

The ZNO siting region is located at the southwestern border of the Hegau – Bodensee Graben (e.g. Birkhäuser et al. 2001, Nagra 2014a, Marchant et al. 2005, Müller et al. 2002, Nagra 2024c, Ibele 2015). The northeastern border of ZNO is marked by the Neuhausen Fault (Fig. 4-2 and Fig. 4-23), a normal fault with approximately 60 m offset and kinematically linked with the Middle Miocene to recent deformation of the Hegau – Bodensee Graben (Egli et al. 2017, Diehl et al. 2023, Ibele 2015). Associated with the Neuhausen Fault is the Wildensbuch Flexure (Fig. 4-25) representing a zone of highly segmented normal faults striking WNW-ESE (Roche et al. 2020).

The Konstanz – Frick Trough underlying and strongly influencing localisation of deformation in the siting regions Jura Ost and Nördlich Lägern, also occurs in the southwestern corner of Zürich Nordost (Fig. 4-24, and Fig. 4-25). The central part of ZNO is located on a crystalline horst referred to as Benken Horst (Müller et al. 2002, Birkhäuser et al. 2001).

In the recent 3D seismic reflection image interpretations, numerous high-angle faults were mapped in ZNO (Nagra 2024c). These high-angle faults are probably associated with trans-tensional formation of the Hegau – Bodensee Graben. They primarily affect the Triassic units but sporadically also affect the entire Mesozoic sedimentary sequence. Discrete high-angle faults in this setting are often associated with folds in the upper stratigraphic levels. The folds show up-ward-decreasing amplitudes as expected for buckle folds in a multi-layered mechanical stratig-raphy (e.g. Currie et al. 1962, Nagra 2024j).

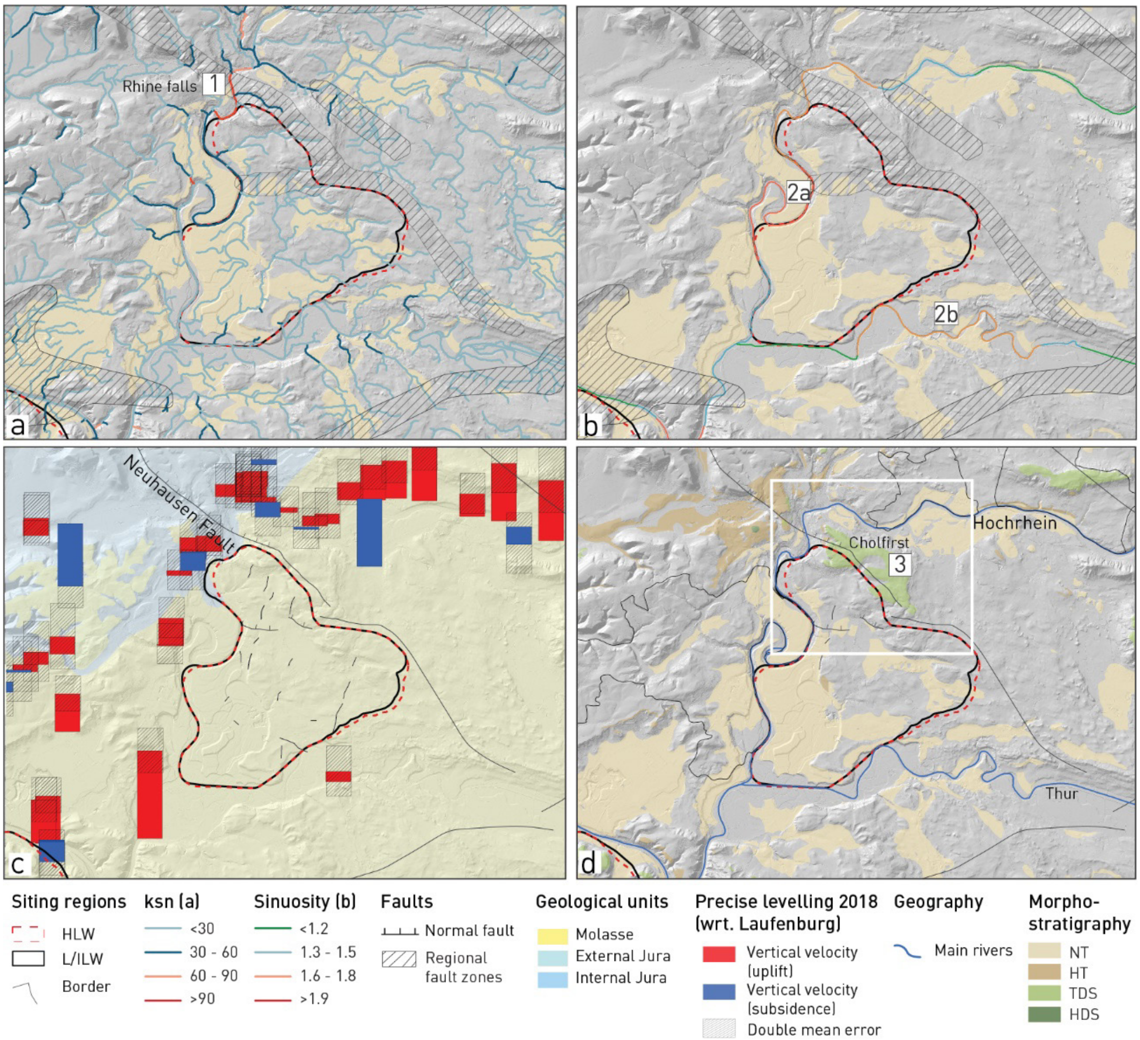

Fig. 4-23: Map compilation of river steepness and sinuosity, tectonic information and precise levelling, and Quaternary morphostratigraphic units – Zürich Nordost

Compilation of tectonic proxy data. Selected geographic elements discussed in text or profiles are labelled. #numbers relate to anomalies, listed in Tab. 4-3. (a) Hillshade based on 2-m lidar data overlain by polygons highlighting the regional fault zones. Distribution of Niederterrasse (NT) is shown. The river network is coloured according to the channel steepness ('ksn'). Anomaly #1 points to a comparably steep river section, which is widely known as the location of the Rhine Falls. (b) Similar to (a), but river network (main streams only) is colour-coded by sinuosity. # 2 point to the highly sinuous Hochrhein River section around the Rhine Falls and the Thur River, respectively. (c) Hillshade and tectonic units with simplified faults, based on Naef & Madritsch (2014) and seismic reflection interpretation of Base Cenozoic and Top Villigen Formation (see Fig. 2-4). Vertical velocities are based on precise levelling and measured with respect to Laufenburg (orange triangle on Fig. 4-2). Only data with a good geologic quality ranking (> 8.5) are shown. (d) Quaternary morphostratigraphic units that overlay the incised bedrock and potentially provide strain markers: Höhere Deckenschotter (HDS), Tiefere Deckenschotter (TDS), Hochterrasse (HT) and Niederterrasse (NT). #3 points to an apparent offset in the base of TDS deposits, which is spatially coincident with the Neuhausen Fault. This location is analysed in more detail in Fig. 4-25, Fig. 4-26, Fig. 4-27, as well as Fig. 4-28 and Fig. 4-29. See Tab. 4-3 for a summary of the anomalies. The white rectangle denotes outlines of Fig. 4-26. wrt.: with respect to.

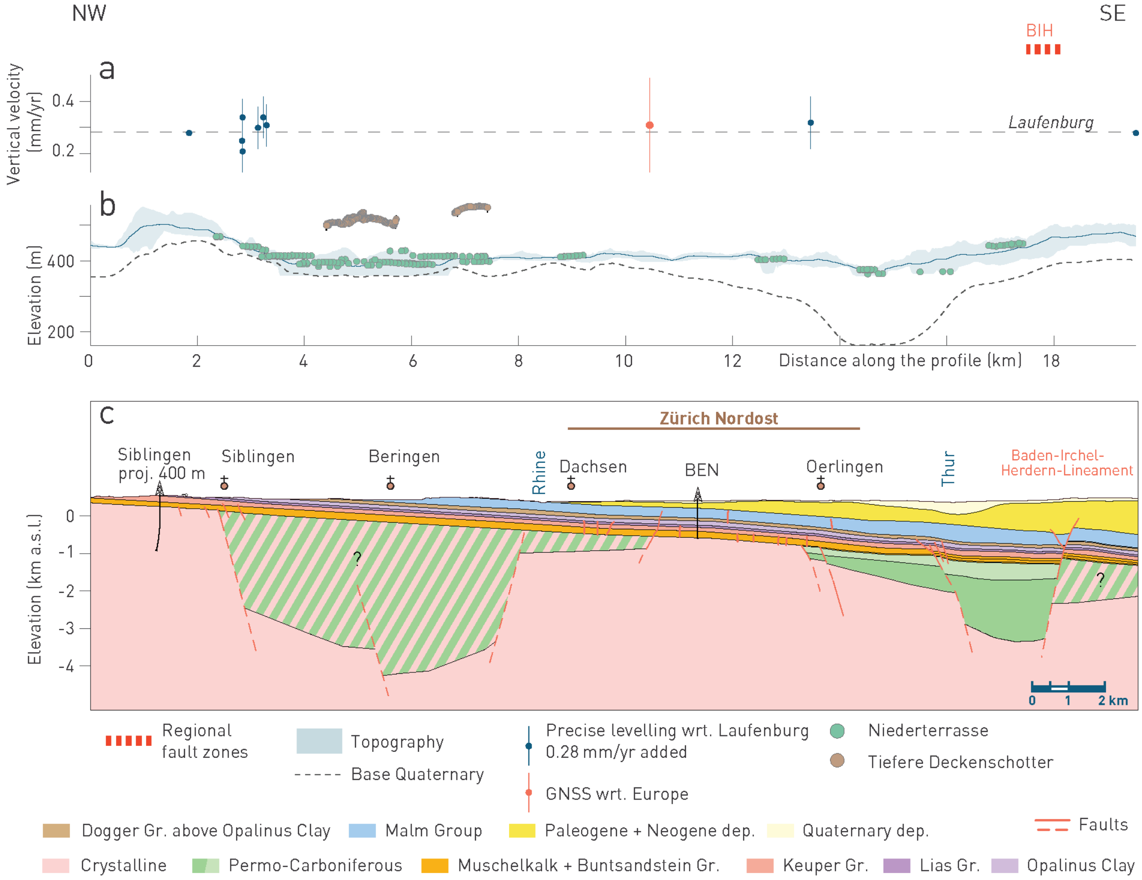

Fig. 4-24: Summary profile along the 2D seismic reflection line 91-NO-68

Synthesis profile through the ZNO siting region (see Fig. 4-7 for location): (a) Vertical velocity based on precise levelling and GNSS. Original data were documented with respect to Laufenburg as 'zero-velocity' reference point (see triangle in Fig. 4-2). Here, the GNSS-based uplift (2024) of the Laufenburg station of ~ 0.28 mm/yr was added to each value, respectively, to allow a relative comparison. BIH: Baden – Irchel – Lineament. (b) Topography (min-max) based on swissALTI3D lidar data resampled to 10 m (blue swath), samples of Base Tiefere Deckenschotter with uncertainties (brown circles), surface samples of Niederterrasse sediments (green circles) and mean Base Quaternary (black dashed line). (c) Geological profile based on 2D seismic reflection line 91-NO-68 for interpretation. The intersection with the siting region is highlighted. Green hatched zones reflect basement that could be Permo-Carboniferous deposits or crystalline basement. wrt.: with respect to.

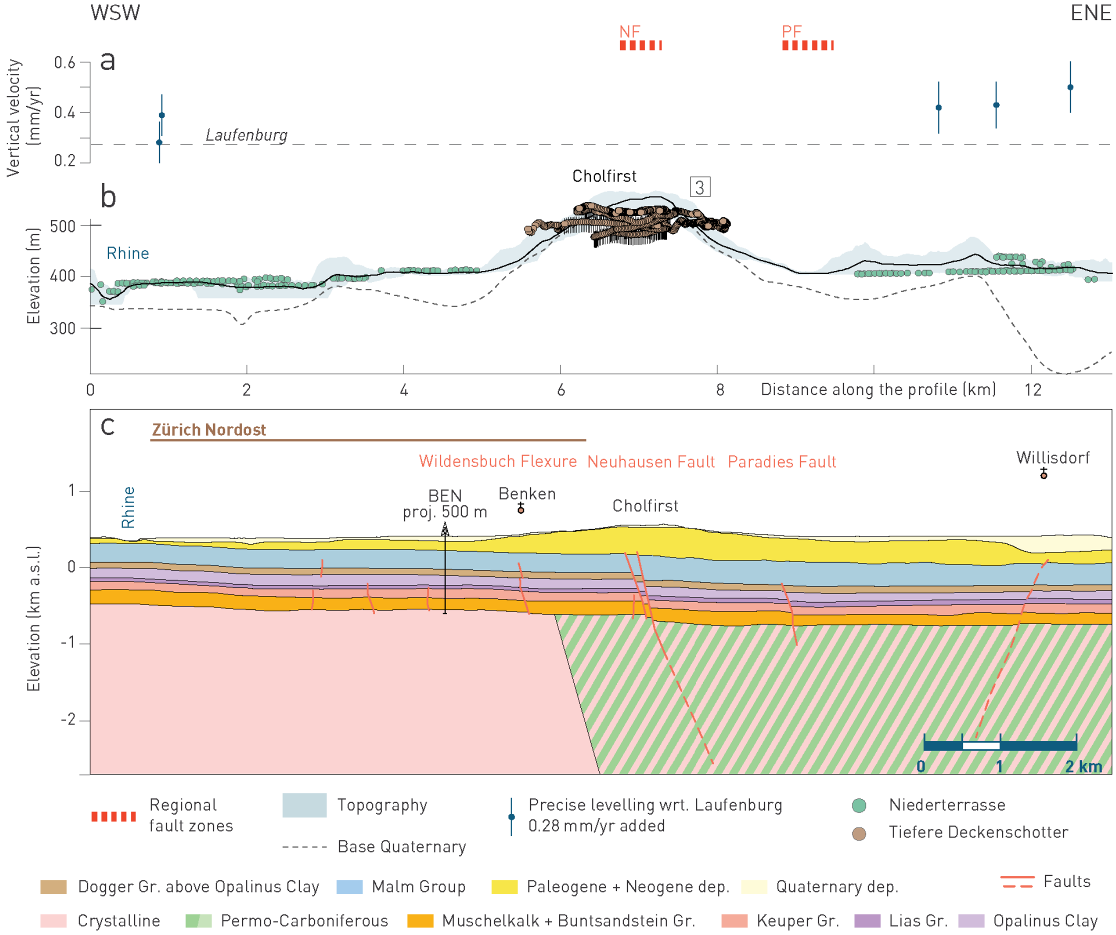

Fig. 4-25: Summary profile along the 2D seismic reflection line 91-NO-77

Synthesis profile (see Fig. 4-7 for location and Fig. 4-24 for description), showing (top to bottom) vertical velocity based on precise levelling, topography based on swissALTI3D lidar data resampled to 10 m (blue swath), samples of Base Tiefere Deckenschotter with uncertainties (brown circles), surface samples of Niederterrasse sediments (green circles), mean Base Quaternary (black dashed line), and geological profile based on 2D seismic reflection line 91-NO-77 for interpretation. Green hatched zone reflects basement that could be Permo-Carboniferous deposits or crystalline basement. NF: Neuhausen Fault, PF: Paradies Fault, wrt.: with respect to.

4.2.3.2 Tectonic geomorphology, seismicity, and geodesy

ZNO constitutes a low-relief area. It was heavily influenced by previous glaciations and the complex postglacial fluvial interactions at the Thur – Hochrhein confluence. Only the eastern edge of ZNO is bounded by a zone of higher topography, including the Cholfirst landmark (Fig. 4-23). The change in tectonic style is not only demonstrated by the overall structural setting but is also indicated by the distribution and type of seismicity, which is already influenced by the transtensional deformation associated with the Hegau – Bodensee Graben (Fig. 4-6d). ZNO is bordered to the east by the Neuhausen Fault, one of the regional fault zones, which appears to be linked with the Wildensbuch Flexure (Fig. 2-4, Section 4.2.3.1). The Hochrhein section straddling ZNO is also structurally and geomorphically complex. The Rhine Falls exhibit a prominent knickpoint. The upstream area has especially high 'ksn' values (Fig. 4-23a, Tab. 4-3, anomaly #1). This anomaly is closely linked with the glacial history and remaining transient fluvial responses and, although they are located in the vicinity of the Neuhausen Fault, are regarded as non-tectonic signal. Similarly, the two areas of high sinuosity in Fig. 4-23b, along the Hochrhein and Thur Rivers, marked as #2a and #2b are considered as non-tectonic signal related to complex postglacial fluvial adjustment (Tab. 4-3).

The profile shown in Fig. 4-24 is oriented parallel to the main regional fault zone comprising the Neuhausen Fault but crosses the Konstanz – Frick Trough and the eastern continuation of the Baden – Irchel – Herdern Lineament in its southernmost part. A limited number of observations of vertical geodetic velocities are available along the profile, which fluctuate slightly around about the same rate as the levelling reference point Laufenburg. Only shorter segments of Niederterrasse (NT) surfaces are incised by the Hochrhein and are located at the complex avulsions at the Thur – Hochrhein confluence. The drop of the mean Base Quaternary (Fig. 4-24b) is the expression of a major glacial overdeepening (Nagra 2024h).

Fig. 4-25 shows a geological and topographic profile oriented obliquely to the Wildensbuch Flexure and perpendicular to the Neuhausen Fault. A number of precise levelling measurements are located along the profile and show hardly any change but for a very slight E-W gradient in vertical velocities. The low relief at ZNO is evident in the topographic swath profile, with topography often aligned with the NT deposits and only the Cholfirst area standing out.

The NT deposits form good-quality markers, as they are extensive and of simple initial complexity, especially in the Paradies Basin, east of the location of the Paradies Fault (Fig. 4-25). The NT marker is apparently undeformed and thus not further discussed.

There is, however, a possible vertical offset of the base of the Tiefere Deckenschotter (TDS) at the approximate location of the Neuhausen Fault (#3 in Fig. 4-25 and Tab. 4-3). This marker at the location of the swath profile is of fair quality and spatially extensive. Marker distribution complexity results in a slight stacking of marker points within the perimeter of the swath profile. The distinct offset, combined with the direct fault association of the Neuhausen Fault, as well as associated seismic activity (Diehl et al. 2023) suggests a tectonic contribution for this Quaternary geomorphic marker. However, field observations also indicate the occurrence of a moraine approximately near the offset of the Base TDS (pers. communication M. Büchi). Graf (2009) described the Base TDS at the Cholfirst landmark as gently decreasing from SE to NW with a shallow channel in the southeastern part, and an elevated Molasse zone which develops into a second channel towards north. Graf (2009) describes the TDS deposits at Cholfirst as glaciofluvial gravel that were deposited in a palaeochannel draining towards WNW to NW. Such a direction is oblique to parallel with respect to the strike of the Neuhausen Fault. To better distinguish potential tectonic from erosional overprint, we present location #3 at the Cholfirst area in a detailed map (Fig. 4-26) and add a series of narrow parallel swath profiles (Fig. 4-27).

Detailed geomorphic analysis of the Neuhausen Fault at the TDS location "Cholfirst"

The Cholfirst area constitutes an isolated hilly area at the northeastern edge of the otherwise low-relief area of ZNO (Fig. 4-26). Base TDS is mapped around the elevated area and with higher uncertainty along the cuts of transverse incised channels. The northwestern half of Cholfirst is surrounded by the Hochrhein channel. The elevation distribution suggests that the elongated eastern edge is characterised by relatively stable heights (green colours) with slight decrease towards both the northwestern and southeastern ends, while the more strongly incised western part of Base TDS is associated with Base TDS points of the highest uncertainty class (4), i.e., these points are extrapolated only. The grey triangles in Fig. 4-26 mark the intersection of the centre line of the interpretative swath profile (Fig. 4-25) for comparison. Eight narrow swath profiles were constructed perpendicular and at regular intervals to the location of the Neuhausen Fault (Fig. 4-27). Due to the elongation of the Cholfirst area perpendicular to the fault strike, only a limited number of profiles contain continuous sections of Base TDS data. Visual inspection of the profiles shows fairly undisturbed markers in profiles 1 and 2 with a very gentle slope toward the NE. Similarly, profiles 5, 7, and 8, which reveal only short sections of Base TDS data, show no distinct perturbation or offset at the scale of this figure. However, in profile 3 and 4, the northeastern part is clearly at a deeper level than the southwestern part, most distinctly seen in profile 4. Interestingly, this apparent offset is in line with a hanging wall position, but not located at the inferred trace of the Neuhausen Fault. This observation may favour an erosional origin of the offset or the Neuhausen Fault may constitute an array of normal faults rather than one well-developed structure. Yet another interpretation considers a combined effect: the apparent offset may constitute a fault-line scarp, where the topographic break is preserved, but the fault scarp has been eroded parallel to the fault. Unfortunately, the Base TDS points that form the central section in profiles 3 and 4 all constitute extrapolations (uncertainty class 4) and should not be used for the interpretation. Discontinuous TDS marker sections, including larger sets with high uncertainty, discordance in the location between the apparent offset and the expected fault surface location, as well as large distances between the apparent offset markers create an ambiguity associated to this marker. We interpret this anomaly as ambiguous to mixed signal of tectonic activity.

To better understand these apparent offsets, we analysed profiles three and four in more detail and calculated an apparent fault-throw rate for potential movement along the Neuhausen Fault (Fig. 4-28 and Fig. 4-29). Please note that such a rate would be considered the maximum, as erosional overprint or contribution cannot be separated.

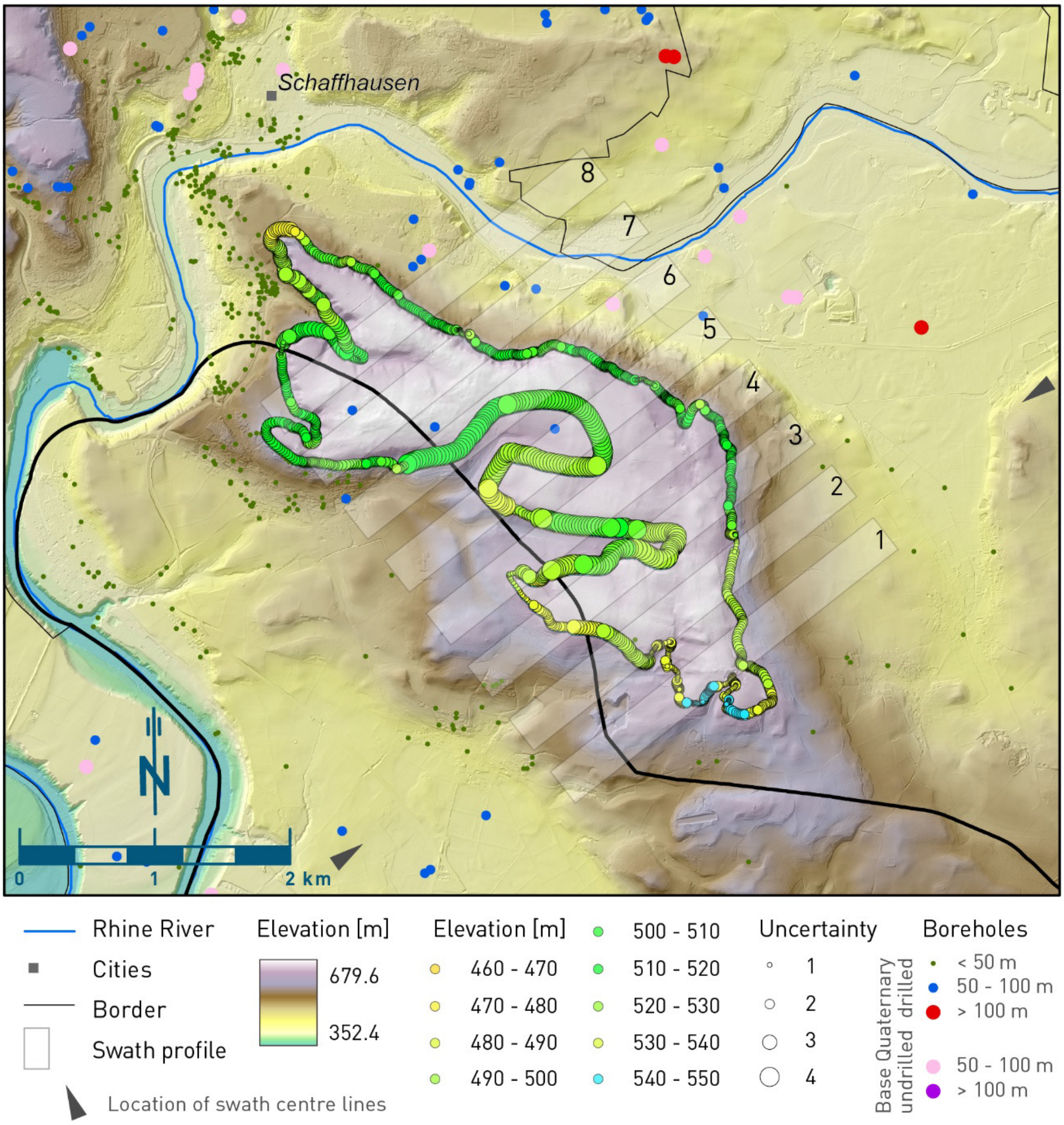

Fig. 4-26: Detailed topographic map of the Cholfirst area

Digital elevation model (DEM) and hillshade based on 2-m SwissAlti3D lidar data are shown. Also shown are extracted locations of the basis of the Tiefere Deckenschotter. The base points are colour-coded by elevation (based on the bedrock model data). Their size is classified by uncertainty, with class 1 being the best (see Tab. 3-2 for uncertainty classification). The narrow, numbered rectangles correspond to the 300-m wide swath profiles shown in Fig. 4-27. Swaths 3 and 4 correspond to the swaths used for calculation of an apparent vertical slip rate (Fig. 4-28 and Fig. 4-29). The grey triangles mark the intersection of the centre line of the interpretative swath profile (Fig. 4-25) for comparison. Note that some of the Base TDS data points in the central part are associated with the highest uncertainty class 4 – these points are extrapolated and not used for further calculations. Note the boreholes that were incorporated in the production of the bedrock model, including the base of the Deckenschotter. Numbers represent elevation of Base Quaternary below terrain, if it was drilled and the total depth of the borehole, if Base Quaternary was not reached during the drilling.

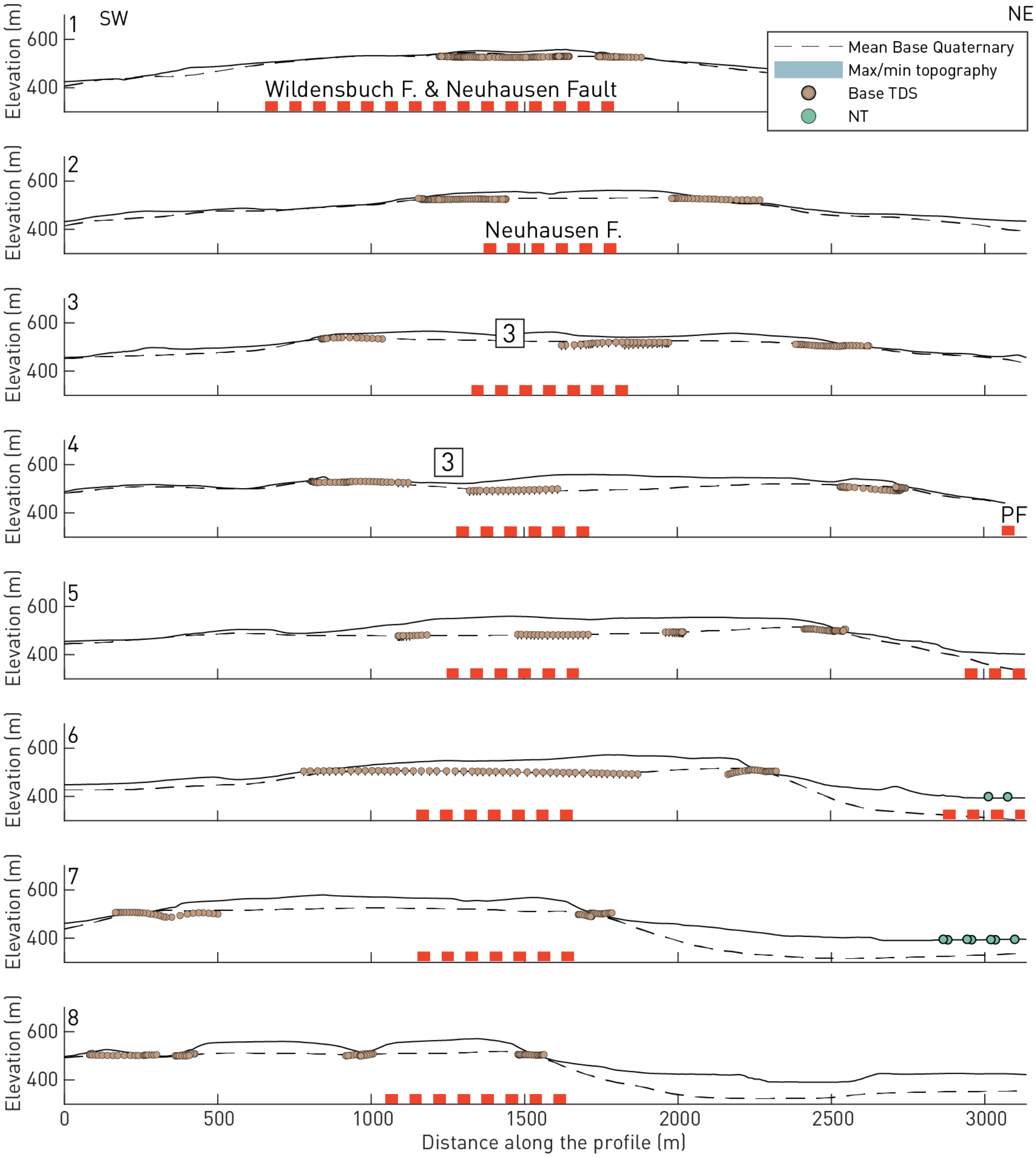

Fig. 4-27: Parallel profiles across the Neuhausen Fault at the "Cholfirst" location

Swath profiles show topography based on SwissAlti3D lidar data (50 m width), the mean Base Quaternary (Q) and Base Tiefere Deckenschotter (Base TDS; 300 m width). The red dashed line shows the profile intersection with the Neuhausen Fault and the Paradies Fault (PF). #3 indicates an anomaly in the Base TDS that is discussed in the text. See Fig. 4-26 for profile location. NT: Niederterrasse, Wildensbuch F.: Wildensbuch Flexure.

Tab. 4-3: Ranking of geomorphic evidence for tectonic activity in Zürich Nordost

The evaluation is based on the criteria defined in Section 3.6.3. According to Tab. 3-3, a good marker comprises 6 points, a fair marker comprises 4 – 5 points, and a vague marker is associated with 2 – 3 points. Listed signals of landform markers are indicated in Fig. 4-23.

Signal	Quality	Ranking	Fault association	# Proxies	Interpretation
#1	-	-	Indirect (NF)	'ksn', Rhine Falls	Non-tectonic origin
#2	-	-	missing	Sinuosity	Non-tectonic origin
#3 Cholfirst	5	fair	direct (normal faulting NF)	Seismic activity and Base Tiefere Decken-schotter TDS	Ambiguous to mixed signal of neotectonic activity

Apparent vertical slip rate for tectonic activity along the Neuhausen Fault

Assuming that anomaly #3 (Fig. 4-23, Fig. 4-27, and Tab. 4-3), observed within the Base Tiefere Deckenschotter (TDS) is at least partly associated with the Neuhausen Fault and represents Quaternary tectonic activity, we estimated a maximum apparent rate of fault throw. The procedure is similar to that outlined in Section 4.2.2.2. Along the Neuhausen Fault, a step-wise fault pattern might account for the more complex geometry. Base Quaternary (TDS) of the Cholfirst area showed class 4 quality in the apparent footwall, but the hanging wall was classified as class 2 or even class 1. We assessed two different age estimates for the TDS along two profiles (~ 3 and 4) (Fig. 4-28 and Fig. 4-29). A first apparent fault-throw rate was calculated considering only the age estimate from the Cholfirst location itself (isochron burial method of 0.83 ± 0.15 Myr, see Nagra 2024h); for the second calculation, the full range of TDS deposition in Northern Switzerland was deployed (isochron burial method between 0.68 ± 0.16 and 1.18 ± 0.09 Myr).

Two distinct offsets are visible along profile 3 (Fig. 4-28a). Excluding the central data points (class 4) from the measurements, the total apparent offset comprises a mean value of 34 m (Fig. 4-28b). Including height uncertainties, the resulting mean throw rates are 33 to 36 m/Myr for the full offset (Fig. 4-28f and d, respectively). The vertical offset calculated for profile 4 (Fig. 4-29) is approximately 26 metres high (ignoring the central section), leading to mean throw rates of 29 – 31 m/Myr.

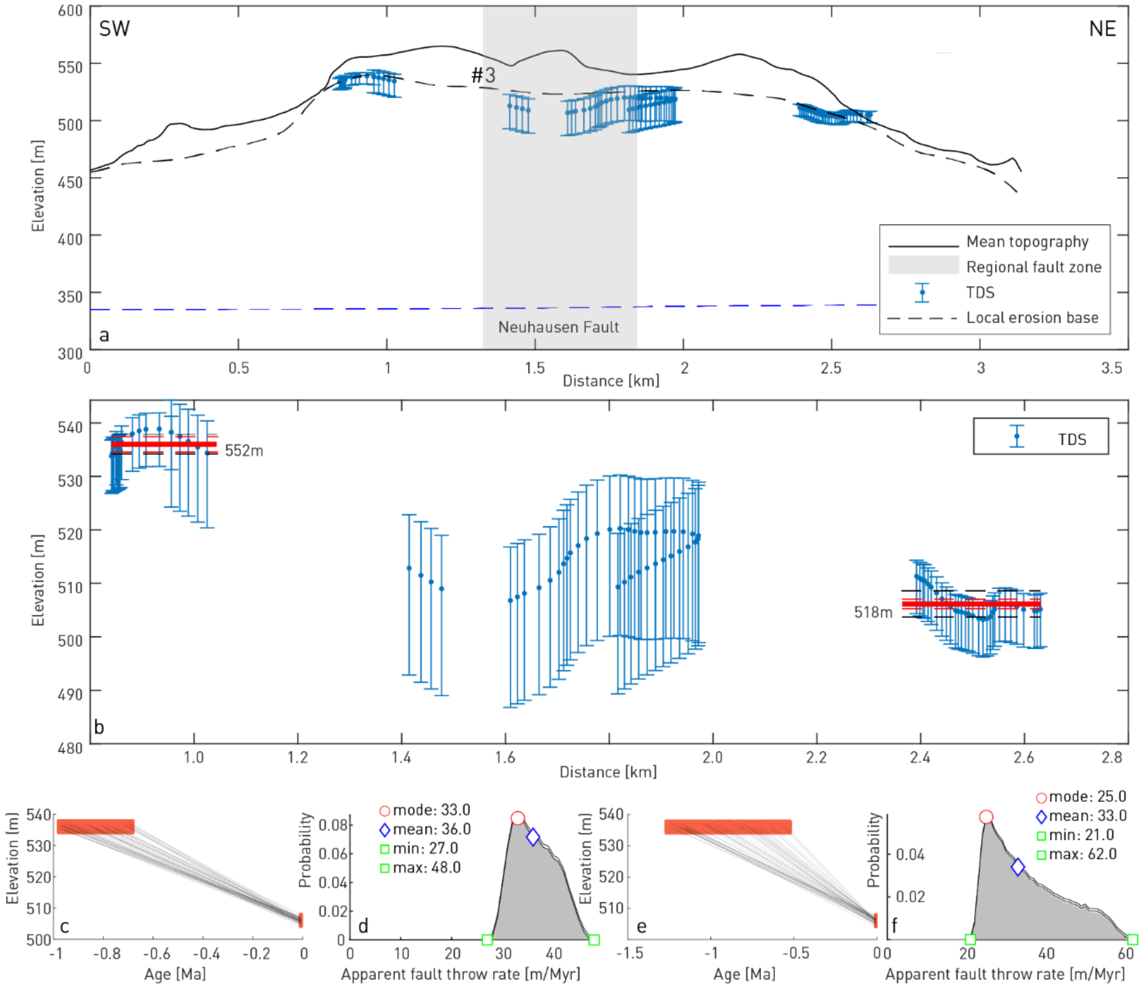

Fig. 4-28: Apparent fault throw rate of the Neuhausen Fault since TDS deposition (profile 3)

Monte Carlo-derived apparent throw rates based on the offsets observed in Base Deckenschotter at Cholfirst above the Neuhausen Fault (Fig. 4-25). (a) A narrow swath profile captured the Cholfirst Tiefere Deckenschotter (TDS; see profile 3 in Fig. 4-26 for location). Displayed are mean topography, Base Quaternary with their uncertainty marks, regional fault zone polygons, and local erosion base (LEB). The apparent offset, which may be coincident with the Neuhausen Fault is labelled as #3 below the profile. An additional offset is visible between the SW and central samples. (b) Zoom to the geomorphic marker showing the steps in the Base TDS. For three sections of rather homogeneous marker elevation, the mean (red line with numbers shown), standard deviation (red dashed line) and standard error (black dashed line) were calculated. Apparent fault-throw rates were calculated from the height difference between hanging wall and footwall samples and the Deckenschotter age, assuming that slip accumulated steadily since TDS deposition, but ignoring the high-uncertainty samples in the central section. Samples were taken from a uniform age distribution and normal distribution of elevation. In this example, two estimates of the apparent offset were calculated using the full apparent offset (34 m; c – f). Sampling and corresponding probability density distribution of apparent fault-throw rate using height estimates of Base Quaternary measurements (full apparent offset) were paired with the local TDS age derived at Cholfirst (c, d) and using the full range of TDS age estimates (e, f).

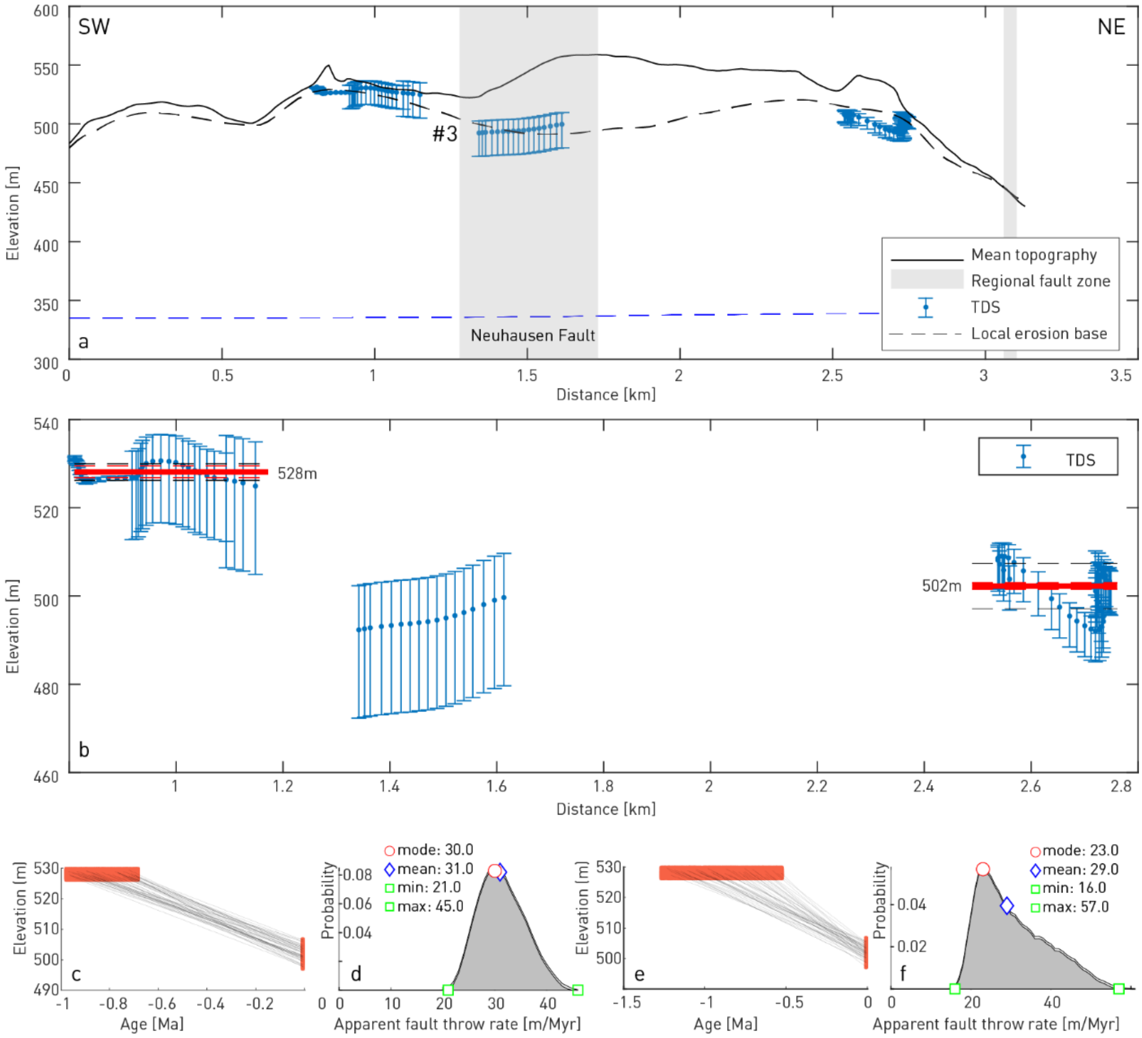

Fig. 4-29: Apparent fault throw rate of the Neuhausen Fault since TDS deposition (profile 4)

Monte Carlo-derived apparent throw rates based on the offsets observed in Base Deckenschotter at Cholfirst above the Neuhausen Fault (Fig. 4-25). General description is similar to Fig. 4-28. (a) A narrow swath profile captured the Cholfirst Tiefere Deckenschotter (TDS; see profile 4 in Fig. 4-26 for location). The apparent offset, which may be coincident with the Neuhausen Fault is labelled as #3 below the profile. (b) Zoom to the geomorphic marker. For the apparently offset sections, the mean (red line with numbers shown), standard deviation (red dashed line) and standard error (black dashed line) were calculated ignoring the high-uncertainty central section. Samples were taken from a uniform age distribution and normal distribution of elevation. Two estimates of the apparent offset were calculated using the full apparent offset (26 m; c – f). Sampling and corresponding probability density distribution of apparent fault-throw rate using height estimates of Base Quaternary measurements (full apparent offset) were paired with the local TDS age derived at Cholfirst. (c, d) and using the full range of TDS age estimates (e, f).

4.3 Discussion and conclusions with respect to neotectonic activity

Evidence for neotectonic activity in Northern Switzerland is limited. Rates of deformation are very low. Tab. 4-4 summarises the different proxies for neotectonic activity relative to their importance at prominent regional fault zones and their respective siting regions. Proxy availability is not equally distributed across the entire area, so the weighting might be biased accordingly (see Fig. 4-30 as an example of seismicity, which is influenced by the station density and temporal evolution of the seismic network). Present-day seismicity is sparse within all siting regions, with the exception of the Eglisau cluster.

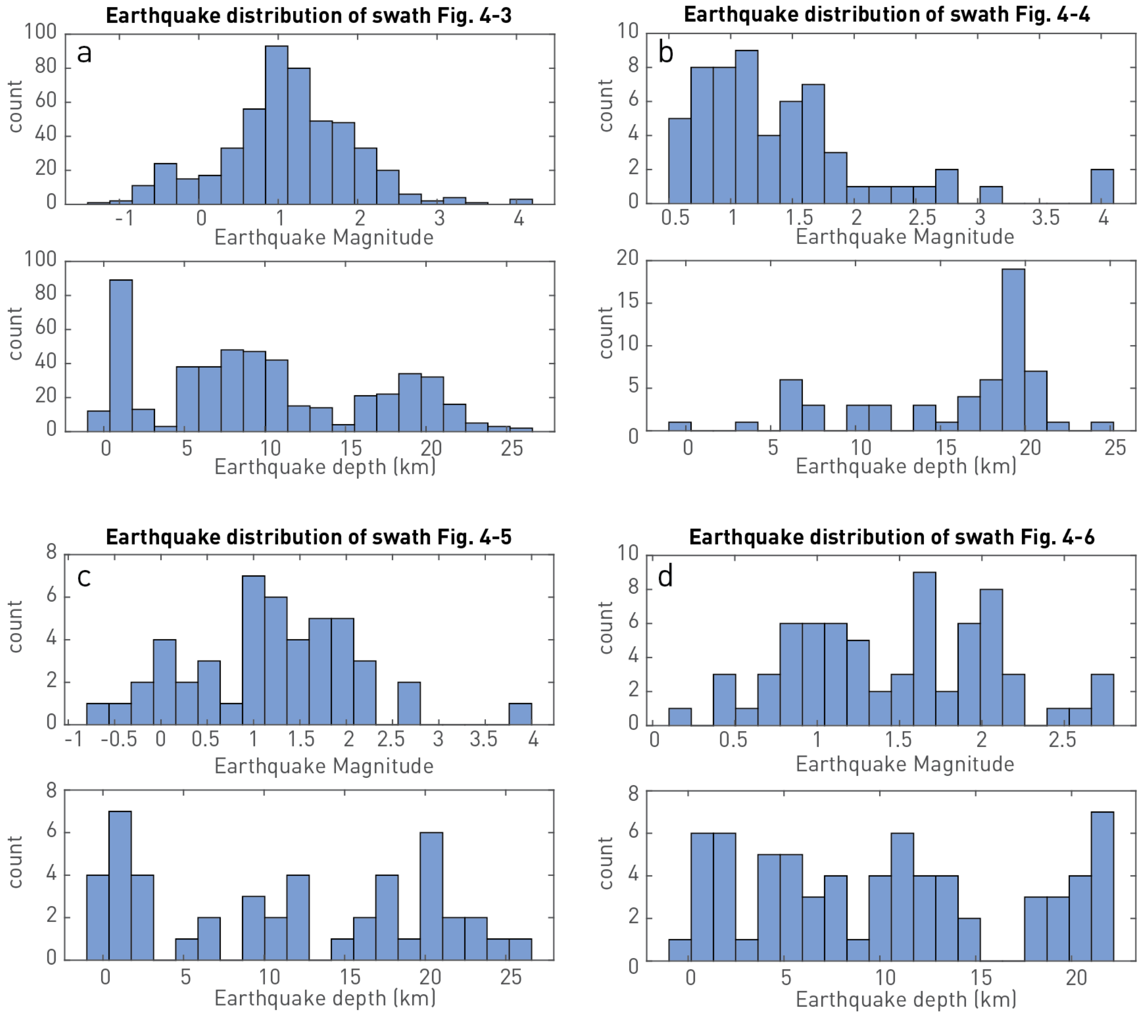

Fig. 4-30: Magnitude and depth distribution of earthquakes presented in the swath profiles

Histograms show magnitude and depth distribution for each of the swath profiles presented in Section 4.1. (a) WSW to ENE oriented swath capturing all siting regions. (b) Swath crossing JO, (c) Swath crossing NL, (d) Swath profile across ZNO. Although the magnitude of completeness is generally low in Northern Switzerland, there may still be a spatial and temporal bias (see Section 3.1 and Fig. 3-2I). The dense array of seismic stations in the vicinity of Eglisau to the northeast of NL allows the detection of smaller magnitudes (c). Please note the overall small numbers of events.

A gradient of decreasing vertical velocities from south to north is visible at the longitude of JO, less at the other siting regions. Vertical velocities from precise levelling and GNSS are widely in agreement when both are available and after applying a shift to account for the different reference systems. However, these datasets have to be interpreted with caution. Many levelling data points were only measured twice (see Section 3.3) and some GNSS antennas are mounted on high buildings. In addition, anthropogenic effects (like groundwater extraction) might influence local stations. Thus, the data can help to identify the general long wavelength deformation pattern but is not yet reliable enough to discern short-wavelength anomalies. A gradient of decreasing vertical velocities from south to north is visible at the longitude of JO and a slight gradient in NL, but less at ZNO. Within the realm of the siting regions, the majority of vertical velocities based on precise levelling are between 0.2 and 0.4 mm/yr with respect to a stable-Europe framework (i.e. after adding the GNSS-derived velocity measured at the fixpoint of Laufenburg, see Section 4.1).

The base of the Deckenschotter may provide a valuable strain marker to detect Quaternary tectonic activity, but this needs to be assessed locally for each outcrop. The Base Deckenschotter usually exhibits irregularities that may be the result of tectonic movement but could alternatively be explained by inherited palaeotopography at the time of Deckenschotter deposition. To account for this, we introduced a ranking for the marker quality (*good*, *fair*, and *vague*) and discuss potential anomalies one by one. None of the markers associated with an anomaly yielded the quality label *good*. In general, Base Höhere Deckenschotter (HDS) seems better suited than Base Tiefere Deckenschotter (TDS), because of the considerably more complex original relief of the latter.

The scrutiny of the landscape revealed little indication of tectonic deformation, and ambiguity persists. Most highlighted anomalies are classified accordingly. Only at two locations do geomorphic markers imply Quaternary tectonic activity, i.e. the anomaly #5 associated with Base HDS across the Baden – Irchel – Herdern Lineament south of NL and anomaly #3 associated with Base TDS across the Neuhausen Fault at the Cholfirst landmark east of ZNO. The possibility for the former was already acknowledged within Nagra (2014b) and Hammer et al. (2019). The inferred deformation rates on timescales of 10s kyr to Myr must be low and even then, erosional overprint cannot be excluded (Baden – Irchel – Herdern Lineament) or is even very likely (Neuhausen Fault).

Nevertheless, these two apparent offset strain markers allow the calculation of a maximum possible fault-throw rate since deposition of the respective Deckenschotter deposit, which in turn may help to ascertain their plausibility within the regional and local setting.

Assuming a pure-tectonic-scenario and incorporating the whole Baden – Irchel – Herdern Lineament, the apparent fault-throw rate at the landmark "Egg" amounts to 0.01 to 0.02 mm/yr. Such a small strain accumulation across a single regional fault zone would not yet be resolvable within the geodetic data. Approximating a 45° dip of the corresponding main fault and ignoring the complex fault geometry, the 22 m of vertical offset may translate to the same amount of shortening across the Baden – Irchel – Herdern Lineament, over one to two million years.

The potential tectonic offset of the TDS Quaternary marker in the Cholfirst area was proposed earlier and motivated shallow-geophysical investigations across the Neuhausen Fault (Section 3.4). Assuming a fully tectonic origin, the throw rate was estimated to be between approximately 0.03 and 0.035 mm/yr. The detailed analysis shows significant ambiguity with respect to Base TDS as strain marker, as some sections reveal high uncertainty. The spatial association to moraine deposits may also imply erosional reworking. The rather high Quaternary apparent vertical offsets of 26-34 m would also correspond to approximately half of the total observed offset along this fault. Nevertheless, seismicity is clearly associated with the Neuhausen Fault, so a mixed tectonic and erosional origin is a reasonable assumption, but ambiguity remains.

The offset might be the result of a mixed signal with tectonic guidance of erosion. Fault throw may guide localised fluvial or glacial incision, but the respective amounts cannot be disentangled from our results. The Neuhausen Fault in its proximity to Quaternary glaciations may also be a classic candidate for increased activity with respect to glacial isostatic adjustment.

For all regional fault zones, loading due to glacial isostatic adjustment must be considered, which means that faults may show higher activity shortly after deglaciation. Within these periods, these faults may also get reactivated in a different sense of motion than their main structural geometry suggests.

Tab. 4-4: Qualitative weighting and summary proxies for neotectonic activity

+ indicates positive indication for neotectonic activity; - the opposite. (+) at JO refers to increased incision in the Mandach Thrust hanging wall and across the JMTB, but no direct offset at the structure.

Proxy for neotectonic activity	**Mandach Thrust / Jura Fold-and-Thrust Belt (JO)**	**Baden – Irchel – Herdern Lineament (NL)**	**Neuhausen Fault (ZNO)**
Present-day seismicity	+	+	+
Precise levelling signal	+	-	-
GNSS differential horizontal velocity	-	-	-
Geomorphology	(+)	+	+
Slope breaks related to fault propagation	-	-	-
HDS/TDS baselevel offsets	-	+	+

In conclusion, the combined analysis indicates that deformation in Northern Switzerland is on-going at low rates. The geomorphic markers in Northern Switzerland are of variable quality and can only be interpreted with caution. Potential neotectonic signals are inferred and can be related to regional fault zones.

5 Possible future tectonic evolution

5.1 Introduction

Our summary of the geological history has yielded two key observations (Sections 2.2 and 4.2 and Nagra 2024i). Firstly, Northern Switzerland is a tectonically active area with low strain rates. This is indicated by different datasets (Chapters 3 and 4). Secondly, strain is preferentially localised along inherited faults, which act as zones of weakness. This phenomenon has been well-documented in scientific literature (e.g. Townend & Zoback 2000).

The future evolution of Northern Switzerland with respect to tectonic loading is anticipated to be strongly controlled by the evolution of the Alpine orogeny, as the Swiss Molasse Basin and the Jura Fold-and-Thrust Belt are part of the North Alpine Foreland and form a mechanical wedge together with the Alps. It is anticipated that N-S shortening, complemented by E-W extension will result therefrom. This could be linked to transtensional activity along the Hegau – Bodensee Graben and along the Upper Rhine Graben or buttressing effects along steeper fault segments. Furthermore, future erosion is expected to reduce overburden, consequently decreasing lithostatic stresses. Potential future ice loading and unloading during glacial – interglacial periods will further modulate the vertical stress.

From the formation of the Jura Fold-and-Thrust Belt until approximately 5 Ma, the Swiss Molasse Basin was a wedge-top basin. This means that the front of the mechanical wedge was located north of the Jura Fold-and-Thrust Belt, and thus the mechanical wedge encompassed not only the Alps but also the Swiss Molasse Basin and the Jura Fold-and-Thrust Belt. It is commonly accepted that the latest evolution of the Molasse Basin is dominated by exhumation. The amount eroded is strongly dependent on the relative position within the Swiss Molasse Basin and is widely debated. Also debated are the reason and the timing for the geodynamic change that resulted in net erosion of the Molasse Basin. Currently debated options include climatic drivers, river drainage pattern changes or mantle dynamics (e.g. Cederbom et al. 2004, Willett & Schlunegger 2010, Schlunegger & Mosar 2011, von Hagke et al. 2012, Schlunegger & Kissling 2015). Inferred timing of the initiation of predominant erosion varies between 12 and 5 Ma (Nagra 2024i).

The future evolution of the Alpine mechanical wedge offers room for interpretation. Mosar (1999) defines the present-day mechanical wedge encompassing Alps, Swiss Molasse Basin and Jura Fold-and-Thrust Belt with a weak basal décollement. von Hagke et al. (2014) provide a compilation of evidence for the critical state of the mechanical Alpine wedge, at the verge of brittle failure, internally and at its base. This includes, for instance, induced seismic activity by water reservoir impoundment (e.g. Bianchetti et al. 1992), drilling of the Gotthard Base Tunnel that triggered a series of 112 earthquakes (Husen et al. 2013) or fluid injection in a geothermal well in Basel (e.g. Häring et al. 2008).

5.2 Future deformation rate

The evaluation of a future shortening rate is based on associated observations from the past and present day. These are briefly summarised in this section. In the following, the strain rates from the geological past are revisited (Section 5.2.1) and complemented by strain rates deduced from present-day horizontal velocities (Section 5.2.2) to define the anticipated future strain rate (Section 5.3).

5.2.1 Geological past

Geometric balancing was carried out along selected 2D seismic reflection lines to assess the total shortening accumulated in relation to the thrusting and folding of the Jura Fold-and-Thrust Belt (Fig. 2-4; Jordan et al. 2015). Shortening estimates along the cross-sections were subdivided into External and Internal Jura (Tab. 5-1). Shortening estimates show an eastward decreasing shortening amount, which is typical for the eastern Jura Fold-and-Thrust Belt (Fig. 2-4).

Sampling and dating of slickenfibres related to the regional fault systems indicate the age of activity along the fault systems (Looser et al. 2021, Madritsch et al. 2024). The distribution of U-Pb ages obtained based on the detailed sampling does not permit conclusions on a typical sequence of deformation but rather indicates an oscillation of deformation between the frontal thrusts and more proximal thrusts. However, the general tectonic activity along the basal décollement of the Jura Fold-and-Thrust Belt was investigated along the Schafisheim borehole and activity was found to have started no later than 14.3 Ma ago (Looser et al. 2021). This age is used as the constraint for the initiation of shortening in both the External and the Internal Jura.

The extrapolation of the aforementioned shortening rate estimates serves the purpose of estimating the order of magnitude. Considering the 11-km long 11-NS-20 seismic reflection line and the 400 m shortening inferred from 2D geometric balancing, the total strain amounts to 0.037 m/m (Tab. 5-1). Assuming that the shortening was equally accommodated over the entire 14.3 Myr time span, the total strain converts to a strain rate of 2.6×10^{-9} yr^{-1}. This shortening rate includes shortening accommodated along the Baden – Irchel – Herdern Lineament and the Siglistorf Anticline. A recent review article on geological strain rates by Fagereng & Biggs (2019) cites 3×10^{-7} yr^{-1} as a time-averaged bulk strain rate in an orogen or 3.2×10^{-8} yr^{-1} if strain does not localise. Thus, the rates we infer for Northern Switzerland are on the low end of continental interior strain rates and are to be expected in almost any kind of tectonic setting.

The apparent fault-throw rates inferred from the detailed investigations of Quaternary deposits within Northern Switzerland (Section 4.2.2.2) are comparable with the inferred shortening rates since the initiation of the folding and thrusting within the Jura, although they are rather on the upper side of the estimations. For the Baden – Irchel – Herdern Lineament, 22 m fault throw was inferred since 1 or 2 Ma (for the simplifications of full tectonic contribution and a single, 45° dipping responsible fault). Total shortening for the Mesozoic strata since 14.3 Ma has been estimated to about 200 – 250 m (Jordan et al. 2015). Therefrom a shortening rate of ca. 14 – 17 m/Myr can be estimated, which is in a similar order of magnitude to the 15-19 m /Myr inferred from the Quaternary deposits assuming a 45° dipping fault surface.

Tab. 5-1: Shortening estimates and partitioning between internal and external domains for the eastern Jura Fold-and-Thrust Belt based on 2D geometric restoration

The 2D seismic reflection sections are arranged from east to west (Fig. 2-4). Some also serve as the basis for the local results presented in Chapter 4 (Fig. 4-7).

Profile ID	**Length**	**Shortening**		
		Total	External Jura	Internal Jura
	[m]	[m]	[m]	[m]
84-NF-65merge	31'332	400	350	50
91-NO-62	14'480	450	400	50
11-NS-20	11'008	400	400	-
91-NO-58	14'767	1'250	400	850
83-NF-31 / 82-NF-30	5'673	2'650	500	2'150
83-NF-15	23'481	3'500	250	3'250
82-NF-10	30'137	5'350	200	5'150

5.2.2 Present-day horizontal movements inferred from GNSS

Horizontal motion as measured by the Global Navigation Satellite System (GNSS) shows low to indiscernible velocity gradients in Northern Switzerland. When comparing the north and east component of the velocity vector with the north and east coordinate of the permanent stations, a decreasing trend in velocity with increasing distance from the Alps is observed. This trend is seen foremost in the north component of the velocity vector (Fig. 5-1a, c). The decreasing trend can be approximated by linear regression. No differential movements across known faults could be observed (Fig. 3-5). Therefore, the linear regression can be considered as representing the present-day bulk shortening and may be suitable for the estimation of anticipated bulk shortening in the future. Conversion of the linear regression for the NaGNet station and the surrounding permanent stations indicates strain rates in the order of $1.4 \times 10^{-9} \pm 0.8 \times 10^{-9}$ yr^{-1}or 1.4 ± 0.8 m/km/Myr (Fig. 5-1a). This estimate is subject to substantial uncertainties (inferred decreasing trend in velocity with increasing distance of the Alps is statistically not different from zero), and thus only serves for an order of magnitude estimation. The inferred strain rate agrees well with published data for Northern Switzerland also based on GNSS movements and is indicative of low rates of horizontal motion for Northern Switzerland (Sánchez et al. 2018, Houlié et al. 2018, Rabin et al. 2018, Piña-Valdés et al. 2022, Serpelloni et al. 2022). If only NaGNet stations are considered, the N-S shortening rate increases to $2.8 \times 10^{-9} \pm 0.9 \times 10^{-9}$ yr^{-1}. This inferred decreasing trend in velocity away from the Alps is statistically significantly different from zero (Person's r = -0.71).

The east component of the velocity vector is in general smaller than the north component in Northern Switzerland (Fig. 5-1c versus Fig. 5-1d). Considering only the NaGNet permanent station, the inferred trend with increasing eastern coordinate indicates E-W extension, which is approximately 1 order of magnitude smaller than the inferred N-S shortening. It should be noted that the inferred trends in the E-W velocity are statistically not different from zero.

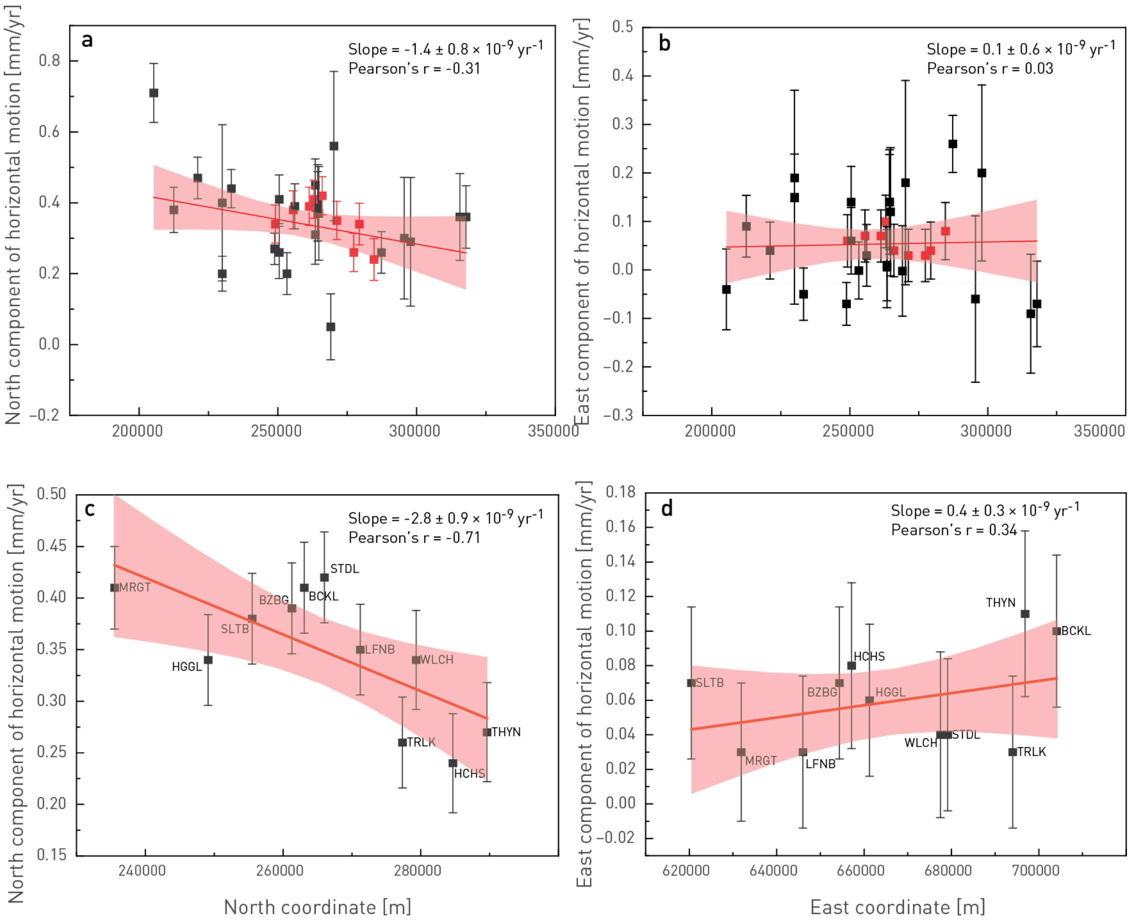

Fig. 5-1: Horizontal velocity components deduced from repeated GNSS measurements for NaGNet stations (black) and surrounding permanent stations (grey)

(a) North component of the horizontal velocity vector deduced from GNSS (Section 3.2) plotted against the north coordinate for stations in Northern Switzerland (black) and the surroundings (grey) in addition to an overall linear regression line (red) indicative for $-1.4 \times 10^{-9} \pm 0.8 \times 10^{-9}$ yr^{-1} N-S shortening. Shown are stations within a 120 km N-S and 200 km E-W rectangle centred over Northern Switzerland. (b) East component of the horizontal velocity vector deduced from GNSS plotted against the east coordinate for stations in Northern Switzerland (black) and the surroundings (grey) in addition to an overall linear regression line (red) indicative for $0.1 \times 10^{-9} \pm 0.6 \times 10^{-9}$ yr^{-1} E-W shortening. (c) North component of the horizontal velocity vector deduced from GNSS plotted against the north coordinate only for NaGNet stations in Northern Switzerland (black) in addition to a linear regression line (red) for NaGNet stations indicative for $-2.8 \times 10^{-9} \pm 0.9 \times 10^{-9}$ yr^{-1} N-S shortening. (d) East component of the horizontal velocity vector deduced from GNSS plotted against the east coordinate of the station for NaGNet stations in Northern Switzerland (black) in addition to a linear regression line (red) for NaGNet stations indicative for $0.4 \times 10^{-9} \pm 0.3 \times 10^{-9}$ yr^{-1} E-W extension. 95% confidence interval is shown as red surface. Measurements contain data recording until February 2024.

5.3 Proposed evolution

Three observations from the past tectonic evolution are considered as pivotal in inferring the possible future evolution (Nagra 2024i). **(i) The past tectonic evolution reactivated inherited faults acting as zones of weakness within the less deformed rock volume.** This is observed for example at the Mandach Thrust (Nagra 2024i). The Mandach Thrust is located above the northern graben fault of the Permo-Carboniferous Trough, which was formed by extension following the Variscan orogeny. With the inclusion of the later Mandach Thrust to the foreland of the Alps, i.e. with the northward migration of the flexural forebulge, the later Mandach Thrust was reactivated by Paleogene normal faulting, as evidenced by the downward bending of the entire Mesozoic strata (Nagra 2024a). The Miocene NW-propagation of the Alpine deformation front, resulting in the formation of the Jura Fold-and-Thrust Belt, formed the present-day Mandach Thrust (Nagra 2024a, Nagra 2019a, Bitterli-Dreher et al. 2007). It should be noted that the retrieved core material drilled within less deformed rock volume contains evidence of strain accumulation also in the rock volume in-between the regional fault zone. The accumulated strain is substantially lower than in the regional fault zones. This is exemplified in the small number of seismic-scale faults (Nagra 2024a, 2024b, 2024c).

The phenomenon that inherited faults within the crust guide subsequent strain has been previously reported in literature (e.g. Townend & Zoback 2000, Zoback et al. 2002, Kirby 1985, Handy & Brun 2004, Bürgmann & Dresen 2008, Cooke & Madden 2014, Cooke & Murphy 2004). It is mainly based on the assumption that the brittle crust is mechanically coupled to the ductile portions of the lithosphere. The lithosphere is in a critical state of failure equilibrium, meaning that any force applied to the lithosphere causes the lower crust and upper mantle to undergo ductile creep. The mechanical coupling of this to the brittle crust implies that the upper crust is progressively loaded. Three lines of evidence were reported by Townend & Zoback (2000 and references therein) for the critical state of failure along faults within the intraplate continental crust: (i) seismicity induced by small increases in fluid pressure associated with fluid injections, (ii) earthquakes triggering other earthquakes, and (iii) in-situ stress measurements in deep boreholes, which are consistently found to approximately equal those predicted using Mohr-Coulomb frictional failure theory.

(ii) **The overall geometry of the regional faults zones inferred from seismic reflection data seems suitable to allow future slip along the fault plane and thus dissipation of strain**. Gently dipping fault segments are more prone to reactivation under thrusting, whereas steeper fault segments will preferentially accommodate strike-slip movements and normal faulting.

(iii) **Strain rates inferred both for the formation of the Jura Fold-and-Thrust Belt and deduced from the recent GNSS measurements are low**. This implies that the anticipated total strain over the considered temporal and spatial scale of the deep geological repository is limited. Shortening rates between 1 and 2.8 m/km/Myr are anticipated across NL within the next one million years.

Based on the aforementioned considerations, we formulate the most likely tectonic evolution for the next one Myr with ongoing tectonic loading resulting in N-S shortening and subordinate E-W extension across the siting regions. In addition to the tectonic loading influencing the stress state, ice (un)loading and erosion are likely to affect the vertical component of the future stress tensor and thus potentially impact fault reactivation. The predominant part of the anticipated strain will be dissipated along inherited regional fault zones. The rock volume in between these is likely to experience very limited amounts of strain.

6 Conclusions

Geodynamic framework of Northern Switzerland

- In a European geodynamic context, Northern Switzerland is a low-strain area within the continental interior.
- The neotectonic setting of Northern Switzerland is influenced by the Alpine orogeny in the south, low-rate deformation within the Upper Rhine Graben and Hegau – Bodensee Graben and subordinate tectonic activity in the Internal Jura. Tectonic deformation rates in Northern Switzerland are low.
- Alpine buoyancy forces, foremost associated with glacial isostatic adjustment, contribute to the observed low uplift rates which decrease towards the foreland.

Indications for neotectonic activity in Northern Switzerland

- Present-day earthquakes occur mainly within the Upper Rhine Graben and the Hegau – Bodensee Graben. Elsewhere they are sparse, with magnitudes typically below 4. A notable, persistent, shallow, very low-magnitude cluster is currently active at Eglisau, NE of the Nördlich Lägern siting region.
- The geomorphic markers in Northern Switzerland are of variable quality and can only be interpreted with caution. When, however, potential signals are visible, they can be related to regional fault zones (Baden – Irchel – Herdern Lineament and Neuhausen Fault).
- Horizontal motion based on geodetic measurements of permanent stations indicates small but ongoing movement with a decreasing velocity with increasing distance from the Alps. Current velocities in Northern Switzerland measured with respect to a stable-Europe framework are in the order of 0.4 mm/yr. Inferred future homogeneous shortening is in the order 1.0 – 2.8 m/km/Myr. It is probable that this shortening will be accommodated largely by fault slip along existing faults in the observed structural inventory.
- Past N-S shortening associated with the formation of the Jura-Fold-and-Thrust Belt amounts to approximately 400 m across the Nördlich Lägern siting region. Inferred shortening rates are ca. 0.03 mm/yr assuming a formation after 14.3 Ma.

Anticipated future strain accomodation

- Geological records indicate that inherited faults are zones of mechanical weakness in a more competent rock volume. This anisotropy is likely to localise strain in the form of fault slip. Several fault reactivations are documented for Northern Switzerland.
- Regional fault zones may experience higher activity shortly after deglaciation. Because glacial isostatic adjustment includes temporal stress perturbations, the faults may be reactivated with a different sense of motion or different faults may be reactivated at different times. Glacial isostatic adjustment will act as non-tectonic modulator on pre-stressed, tectonically loaded faults.
- Future strain is anticipated to predominantly localise along inherited faults known from seismic characterisation. Only a subordinate portion may deform the rock volume in between inherited faults (deformation behaviour of the Opalinus Clay within a strong mechanical layering and the deduced typical fault architecture of mechanically less competent rocks are discussed in Nagra 2024i).

- The overall low strain rates, summed over the period of one million years, only allow small faults in length and offset to develop (associated scaling relationships are discussed in Nagra 2024f).
- Neotectonic deformation together with the seismicity indicate that future tectonic activity along faults, especially along the regional fault zones, is not excluded. Positioning long-term safety-relevant repository elements outside these zones will minimise any neotectonic effects.

7 References

Altamimi, Z. (2018): EUREF Technical Note 1: Relationship and Transformation between the International and the European Terrestrial Reference Systems. November 16, 2017.

Altamimi, Z., Rebischung, P., Métivier, L. & Collilieux, X. (2016): ITRF2014: A new release of the International Terrestrial Reference Frame modeling nonlinear station motions. JGR Solid Earth 121/8, 6109-6131. DOI: 10.1002/2016JB013098.

Becker, A. (2000): Der Faltenjura: geologischer Rahmen, Bau und Entwicklung seit dem Miozän. Jahresberichte und Mitteilungen des Oberrheinischen Geologischen Vereins. Neue Folge 82, 317-336. DOI: 10.1127/jmogv/82/2000/317.

Bianchetti, G., Roth, P., Vuataz, F.-D. & Vergain, J. (1992): Deep groundwater circulation in the Alps: Relations between water infiltration, induced seismicity and thermal springs. The case of Val d'Illiez, Wallis, Switzerland. Eclogae Geologicae Helvetiae 85/2, 291-305.

Birkhäuser, P., Roth, P., Meier, B. & Naef, H. (2001): 3-D Seismik: Räumliche Erkundung des mesozoischen Sedimentschichten im Zürcher Weinland. Nagra Technischer Bericht NTB 00-03.

Bitterli-Dreher, P., Graf, H.R., Naef, H., Diebold, P., Matousek, F., Burger, H. & Pauli-Gabi, T. (2007): Geologischer Atlas der Schweiz. Blatt 1070 Baden mit Erläuterungen. Bundesamt für Landestopografie swisstopo.

Bonnet, C., Malavieille, J. & Mosar, J. (2007): Interactions between tectonics, erosion, and sedimentation during the recent evolution of the Alpine orogen: Analogue modeling insights. Tectonics 26/6, 2006TC002048. DOI: 10.1029/2006TC002048.

Brandes, C., Steffen, H., Steffen, R. & Wu, P. (2015): Intraplate seismicity in northern Central Europe is induced by the last glaciation. Geology 43/7, 611-614. DOI: 10.1130/G36710.1.

Brockmann, E., Grünig, S., Ineichen, D. & Schaer, S.: Monitoring the Automated GPS Network of Switzerland AGNES. *In:* Torres, Hornik (Hg.) 2006 – Report on the Symposium.

Burbank, D.W. & Anderson, R.S. (2001): Tectonic Geomorphology. Blackwell Science, Malden.

Bürgmann, R. & Dresen, G. (2008): Rheology of the Lower Crust and Upper Mantle: Evidence from Rock Mechanics, Geodesy, and Field Observations. Annual Review of Earth and Planetary Sciences 36/1, 531-567. DOI: 10.1146/annurev.earth.36.031207.124326.

Burnett, A.W. & Schumm, S.A. (1983): Alluvial-river response to neotectonic deformation in louisiana and Mississippi. Science 222/4619, 49-50. DOI: 10.1126/science.222.4619.49.

Buxtorf, A. (1916): Prognose und Befunde beim Hauensteinbasis- und Grenchenbergtunnel und die Bedeutung der letzteren für die Geologie des Juragebirges. Verhandlungen der Naturforschenden Gesellschaft in Basel 27, 184-254.

Cavinato, G.P. & Celles, P.G. de (1999): Extensional basins in the tectonically bimodal central Apennines fold-thrust belt, Italy: Response to corner flow above a subducting slab in retrograde motion. Geology 27/10, 955-958. DOI: 10.1130/0091-7613(1999)027<0955:EBITTB>2.3.CO;2.

Cederbom, C.E., Sinclair, H.D., Schlunegger, F. & Rahn, M.K. (2004): Climate-induced rebound and exhumation of the European Alps. Geology 32/8, 709-712. DOI: 10.1130/G20491.1.

Champagnac, J.-D., Schlunegger, F., Norton, K., Blanckenburg, F. von, Abbühl, L.M. & Schwab, M. (2009): Erosion-driven uplift of the modern Central Alps. Tectonophysics 474/1-2, 236-249. DOI: 10.1016/j.tecto.2009.02.024.

Chapron, E., Simonneau, A., Ledoux, G., Arnaud, F., Lajeunesse, P. & Albéric, P. (2016): French Alpine Foreland Holocene Paleoseismicity Revealed by Coeval Mass Wasting Deposits in Glacial Lakes 41, 341-349. DOI: 10.1007/978-3-319-20979-1_34.

Cooke, M.L. & Madden, E.H. (2014): Is the Earth Lazy? A review of work minimization in fault evolution. Journal of Structural Geology 66, 334-346. DOI: 10.1016/j.jsg.2014.05.004.

Cooke, M.L. & Murphy, S. (2004): Assessing the work budget and efficiency of fault systems using mechanical models. Journal of Geophysical Research: Solid Earth 109/B10, 2004JB002968. DOI: 10.1029/2004JB002968.

Craig, T.J., Calais, E., Fleitout, L., Bollinger, L. & Scotti, O. (2016): Evidence for the release of long-term tectonic strain stored in continental interiors through intraplate earthquakes. Geophysical Research Letters 43/13, 6826-6836. DOI: 10.1002/2016GL069359.

Craig, T.J., Calais, E., Fleitout, L., Bollinger, L. & Scotti, O. (2023): Time-variable strain and stress rates induced by Holocene glacial isostatic adjustment in continental interiors. Tectonophysics 854, 229815. DOI: 10.1016/j.tecto.2023.229815.

Currie, J.B., Patnode, H.W. & Trump, R.P. (1962): Development of Folds in Sedimentary Strata. Geological Society of America Bulletin 73/6, 655. DOI: 10.1130/0016-7606(1962)73[655:DOFISS]2.0.CO;2.

DeMets, C., Gordon, R.G., Argus, D.F. & Stein, S. (1990): Current plate motions. Geophysical Journal International 101/2, 425-478. DOI: 10.1111/j.1365-246X.1990.tb06579.x.

Diebold, P., Bitterli-Brunner, P. & Naef, H. (2006): Blatt 1069/1049 Frick-Laufenburg mit Erläuterungen. Bundesamt für Landestopografie swisstopo.

Diebold, P., Naef, H. & Amman, M. (1991): Zur Tektonik der Zentralen Nordschweiz: Interpretation aufgrund regionaler Seismik, Oberflächengeologie und Tiefbohrungen. Textband. Nagra Technischer Bericht NTB 90-04.

Diehl, T., Clinton, J., Cauzzi, C., Kraft, T., Kästli, P., Deichmann, N., Massin, F., Grigoli, F., Molinari, I., Böse, M., Hobiger, M., Haslinger, F., Fäh, D. & Wiemer, S. (2021a): Earthquakes in Switzerland and surrounding regions during 2017 and 2018. Swiss Journal of Geosciences 114/1. DOI: 10.1186/s00015-020-00382-2.

Diehl, T., Kissling, E., Herwegh, M. & Schmid, S.M. (2021b): Improving Absolute Hypocenter Accuracy With 3D Pg and Sg Body-Wave Inversion Procedures and Application to Earthquakes in the Central Alps Region. Journal of Geophysical Research: Solid Earth 126/12, e2021JB022155. DOI: 10.1029/2021JB022155.

Diehl, T., Madritsch, H., Schnellmann, M., Spillmann, T., Brockmann, E. & Wiemer, S. (2023): Seismotectonic evidence for present-day transtensional reactivation of the slowly deforming Hegau-Bodensee Graben in the northern foreland of the Central Alps. Tectonophysics 846, 229659. DOI: 10.1016/j.tecto.2022.229659.

Egli, D., Mosar, J., Ibele, T. & Madritsch, H. (2017): The role of precursory structures on Tertiary deformation in the Black Forest – Hegau region. International Journal of Earth Sciences (Geologische Rundschau) 106/7, 2297-2318. DOI: 10.1007/s00531-016-1427-8.

Fagereng, Å. & Biggs, J. (2019): New perspectives on 'geological strain rates' calculated from both naturally deformed and actively deforming rocks. Journal of Structural Geology 125, 100-110. DOI: 10.1016/j.jsg.2018.10.004.

Fäh, D., Giardini, D., Kästli, P., Deichmann, N., Gisler, M., Schwarz-Zanetti, G., Alvarez-Rubio, S., Sellami, S., Edwards, B., Allmann, B., Bethmann, F., Wössner, J., Gassner-Stamm, G., Fritsche, S. & Eberhard, D. (2011): ECOS-09 Earthquake Catalogue of Switzerland. Report and Database. Public catalogue. Report SED/RISK/R/001/20110417. Release 2011, 17.4.2011. Swiss Seismological Service, ETH Zürich.

Fraefel, M. (2008): Geomorphic response to neotectonic activity in the Jura Mountains and in the southern Upper Rhine Graben. Doctoral Thesis, University of Basel, Faculty of Science.

Gaar, D., Graf, H.R. & Preusser, F. (2019): New chronological constraints on the timing of Late Pleistocene glacier advances in northern Switzerland. E&G Quaternary Science Journal 68/1, 53-73. DOI: 10.5194/egqsj-68-53-2019.

Gegg, L., Deplazes, G., Keller, L., Madritsch, H., Spillmann, T., Anselmetti, F.S. & Buechi, M.W. (2021): 3D morphology of a glacially overdeepened trough controlled by underlying bedrock geology. Geomorphology 394, 107950.

Giamboni, M., Ustaszewski, K., Schmid, S.M., Schumacher, M.E. & Wetzel, A. (2004): Plio-Pleistocene transpressional reactivation of Paleozoic and Paleogene structures in the Rhine-Bresse transform zone (northern Switzerland and eastern France). International Journal of Earth Sciences (Geologische Rundschau) 93/2, 207-223. DOI: 10.1007/s00531-003-0375-2.

Gold, R.D. & Cowgill, E. (2011): Deriving fault-slip histories to test for secular variation in slip, with examples from the Kunlun and Awatere faults. Earth and Planetary Science Letters 301/1-2, 52-64. DOI: 10.1016/j.epsl.2010.10.011.

Graf, H.R. (2009): Stratigraphie und Morphogenese von frühpleistozänen Ablagerungen zwischen Bodensee und Klettgau. Eiszeitalter und Gegenwart. Quaternary Science Journal 58/1, 12-53. DOI: 10.3285/eg.58.1.02.

Graf, H.R. & Burkhalter, R. (2016): Quaternary deposits: concept for a stratigraphic classification and nomenclature—an example from northern Switzerland. Swiss Journal of Geosciences 109/2, 137-147. DOI: 10.1007/s00015-016-0222-7.

Grollimund, B., Zoback, M.D. & D. Zoback, M. (2001): Did deglaciation trigger intraplate seismicity in the New Madrid seismic zone? Geology 29/2, 175-178. DOI: 10.1130/0091-7613(2001)029<0175:DDTISI>2.0.CO;2.

Grosset, J., Mazzotti, S. & Vernant, P. (2023): Glacial-isostatic-adjustment strain rate–stress paradox in the Western Alps and impact on active faults and seismicity. Solid Earth 14/10, 1067-1081. DOI: 10.5194/se-14-1067-2023.

Gubler, E., Schneider, D., Bundesamt, f.L. & Kellerhals, P. (1984): Bestimmung von rezenten Bewegungen der Erdkruste mit geodätischen Methoden. Nagra Technischer Bericht NTB 84-17.

Haldimann, P., Naef, H. & Schmassmann, H.-J. (1984): Fluviatile Erosions- und Akkumulationsformen als Indizien jungpleistozäner und holozäner Bewegungen in der Nordschweiz und angrenzenden Gebieten. Nagra Technischer Bericht NTB 84-16.

Hammer, P., Ibele, T., Naef, H. & Madritsch, H. (2019): Geomorphologische Analyse der Basis der Höheren Deckenschotter im Gebiet Nördlich Lägern. Nagra Arbeitsbericht NAB 15-57.

Handy, M.R. & Brun, J.-P. (2004): Seismicity, structure and strength of the continental lithosphere. Earth and Planetary Science Letters 223/3-4, 427-441. DOI: 10.1016/j.epsl.2004.04.021.

Häring, M.O., Schanz, U., Ladner, F. & Dyer, B.C. (2008): Characterisation of the Basel 1 enhanced geothermal system. Geothermics 37/5, 469-495. DOI: 10.1016/j.geothermics.2008.06.002.

Heidbach, O., Rajabi, M., Cui, X., Fuchs, K., Müller, B., Reinecker, J., Reiter, K., Tingay, M., Wenzel, F., Xie, F., Ziegler, M.O., Zoback, M.-L. & Zoback, M. (2018): The World Stress Map database release 2016: Crustal stress pattern across scales. Tectonophysics 744, 484-498. DOI: 10.1016/j.tecto.2018.07.007.

Henrion, E., Masson, F., Doubre, C., Ulrich, P. & Meghraoui, M. (2020): Present-day deformation in the Upper Rhine Graben from GNSS data. Geophysical Journal International 223/1, 599-611. DOI: 10.1093/gji/ggaa320.

Hetzel, R. & Hampel, A. (2005): Slip rate variations on normal faults during glacial-interglacial changes in surface loads. Nature 435/7038, 81-84. DOI: 10.1038/nature03562.

Holbrook, J. & Schumm, S.A. (1999): Geomorphic and sedimentary response of rivers to tectonic deformation: a brief review and critique of a tool for recognizing subtle epeirogenic deformation in modern and ancient settings. Tectonophysics 305/1-3, 287-306. DOI: 10.1016/S0040-1951(99)00011-6.

Houlié, N., Woessner, J., Giardini, D. & Rothacher, M. (2018): Lithosphere strain rate and stress field orientations near the Alpine arc in Switzerland. Scientific Reports 8/1. DOI: 10.1038/s41598-018-20253-z.

Husen, S., Kissling, E. & Deschwanden, A. von (2013): Induced seismicity during the construction of the Gotthard Base Tunnel, Switzerland: hypocenter locations and source dimensions. Journal of Seismology 17/1, 63-81. DOI: 10.1007/s10950-012-9313-8.

IAEA (2015): The Contribution of Palaeoseismology to Seismic Hazard Assessment in Site Evaluation for Nuclear Installations. IAEA-TECDOC-1767. International Atomic Energy Agency IAEA, Vienna.

IAEA (2022): Seismic Hazards in Site Evaluation for Nuclear Installations. Specific Safety Guide No. SSG-9 (Rev. 1). International Atomic Energy Agency IAEA, Vienna, available online at https://www.iaea.org/publications/14665/seismic-hazards-in-site-evaluation-for-nuclear-installations.

Ibele, T. (2015): Tectonics of the Hegau and Lake Constance region: A synthesis based on existing literature. Nagra Arbeitsbericht NAB 12-23.

Johansson, J.M., Davis, J.L., Scherneck, H.-G., Milne, G.A., Vermeer, M., Mitrovica, J.X., Bennett, R.A., Jonsson, B., Elgered, G., Elósegui, P., Koivula, H., Poutanen, M., Rönnäng, B.O. & Shapiro, I.I. (2002): Continuous GPS measurements of postglacial adjustment in Fennoscandia 1. Geodetic results. Journal of Geophysical Research 107/B8. DOI: 10.1029/2001JB000400.

Johnston, A.C. (1987): Suppression of earthquakes by large continental ice sheets. Nature 330/6147, 467-469. DOI: 10.1038/330467a0.

Jordan, P. (1992): Evidence for large - scale decoupling in the Triassic evaporites of Northern Switzerland: An overview. Eclogae Geologicae Helvetiae 85/3, 677-693.

Jordan, P., Malz, A., Heuberger, S., Pietsch, J., Kley, J. & Madritsch, H. (2015): Regionale geologische Profile durch die Nordschweiz und 2D-Bilanzierung der Fernschub-deformation im östlichen Faltenjura: Arbeitsbericht zu SGT Etappe 2. Nagra Arbeitsbericht NAB 14-105.

Jordan, P. & Nüesch, R. (1989): Deformation Structures in the Muschelkalk Anhydrites of the Schafisheim Well (Jura Overthrust, Northern Switzerland). Eclogae Geologicae Helvetiae 82/2, 429-454.

Kamleitner, S., Ivy-Ochs, S., Manatschal, L., Akçar, N., Christl, M., Vockenhuber, C., Hajdas, I. & Synal, H.-A. (2023): Last Glacial Maximum glacier fluctuations on the northern Alpine foreland: Geomorphological and chronological reconstructions from the Rhine and Reuss glacier systems. Geomorphology 423, 108548. DOI: 10.1016/j.geomorph.2022.108548.

Kirby, E. & Whipple, K.X. (2012): Expression of active tectonics in erosional landscapes. Journal of Structural Geology 44, 54-75. DOI: 10.1016/j.jsg.2012.07.009.

Kirby, S.H. (1985): Rock mechanics observations pertinent to the rheology of the continental lithosphere and the localization of strain along shear zones. Tectonophysics 119/1-4, 1-27. DOI: 10.1016/0040-1951(85)90030-7.

Kleber, E.J., DeVecchio, D.E., Arrowsmith, J.R. & Rittenour, T.M. (2021): Spatiotemporal Rates of Tectonic Deformation and Landscape Evolution above a Laterally Propagating Thrust Fault: Wheeler Ridge Anticline, California, USA. Lithosphere 2021/Special 2, 3395719. DOI: 10.2113/2021/3395719.

Kock, S., Huggenberger, P., Preusser, F., Rentzel, P. & Wetzel, A. (2009): Formation and evolution of the Lower Terrace of the Rhine River in the area of Basel. Swiss Journal of Geosciences 102/2, 307-321. DOI: 10.1007/s00015-009-1325-1.

Kremer, K., Wirth, S.B., Reusch, A., Fäh, D., Bellwald, B., Anselmetti, F.S., Girardclos, S. & Strasser, M. (2017): Lake-sediment based paleoseismology: Limitations and perspectives from the Swiss Alps. Quaternary Science Reviews 168, 1-18. DOI: 10.1016/j.quascirev.2017.04.026.

Lambert, A., Courtier, N., Sasagawa, G.S., Klopping, F., Winester, D., James, T.S. & Liard, J.O. (2001): New constraints on Laurentide postglacial rebound from absolute gravity measurements. Geophysical Research Letters 28/10, 2109-2112. DOI: 10.1029/2000GL012611.

Landgraf, A., Kübler, S., Hintersberger, E. & Stein, S. (2017): Active tectonics, earthquakes and palaeoseismicity in slowly deforming continents. SP 432/1, 1-12. DOI: 10.1144/SP432.13.

Lanza, F., Diehl, T., Deichmann, N., Kraft, T., Nussbaum, C., Schefer, S. & Wiemer, S. (2022): The Saint-Ursanne earthquakes of 2000 revisited: evidence for active shallow thrust-faulting in the Jura fold-and-thrust belt. Swiss Journal of Geosciences 115/1. DOI: 10.1186/s00015-021-00400-x.

Laubscher, H.P. (1961): Die Fernschubhypothese der Jurafaltung. Eclogae Geologicae Helvetiae 54/1, 221-282.

Laubscher, H.P. (1985): The eastern Jura: Relations between thin-skinned and basement tectonics, local and regional. Nagra Technical Report NTB 85-53.

Looser, N., Madritsch, H., Guillong, M., Laurent, O., Wohlwend, S. & Bernasconi, S.M. (2021): Absolute age and temperature constraints on deformation along the basal décollement of the Jura fold-and-thrust belt from carbonate U-Pb dating and clumped isotopes. Tectonics 40/3, e2020TC006439. DOI: 10.1029/2020TC006439.

Machette, M.N. (2000): Active, capable, and potentially active faults — a paleoseismic perspective. Journal of Geodynamics 29/3-5, 387-392. DOI: 10.1016/S0264-3707(99)00060-5.

Madritsch, H., Looser, N., Schneeberger, R., Wohlwend, S., Guillong, M. & Malz, A. (2024): Reconstructing the Evolution of Foreland Fold-And-Thrust Belts Using U-Pb Calcite Dating: An Integrated Case-Study From the Easternmost Jura Mountains (Switzerland). Tectonics 43/5, e2023TC008181. DOI: 10.1029/2023TC008181.

Madritsch, H., Meier, B., Kuhn, P., Roth, P., Zingg, O., Birkhäuser, P., Heuberger, S. & Naef, H. (2013): Regionale strukturgeologische Zeitinterpretation der Nagra 2D-Seismik 2011/12. Nagra Arbeitsbericht NAB 13-10.

Madritsch, H., Naef, H., Meier, B., Franzke, H.J. & Schreurs, G. (2018): Architecture and Kinematics of the Constance-Frick Trough (Northern Switzerland): Implications for the Formation of Post-Variscan Basins in the Foreland of the Alps and Scenarios of Their Neogene Reactivation. Tectonics 37/7, 2197-2220. DOI: 10.1029/2017TC004945.

Malz, A., Madritsch, H., Jordan, P., Meier, B. & Kley, J. (2020): Along-strike variations in thin-skinned thrusting style controlled by pre-existing basement structure in the easternmost Jura Mountains (Northern Switzerland). Geological Society, London, Special Publications 490/1, 199-220. DOI: 10.1144/SP490-2019-090.

Malz, A., Madritsch, H., Meier, B. & Kley, J. (2016): An unusual triangle zone in the external northern Alpine foreland (Switzerland): Structural inheritance, kinematics and implications for the development of the adjacent Jura fold-and-thrust belt. Tectonophysics 670, 127-143. DOI: 10.1016/j.tecto.2015.12.025.

Marchant, R., Ringgenberg, Y., Stampfli, G., Birkhäuser, P., Roth, P. & Meier, B. (2005): Paleotectonic evolution of the Zürcher Weinland (northern Switzerland), based on 2D and 3D seismic data. Eclogae Geologicae Helvetiae 98/3, 345-362. DOI: 10.1007/s00015-005-1171-8.

Mazzotti, S., Jomard, H. & Masson, F. (2020): Processes and deformation rates generating seismicity in metropolitan France and conterminous Western Europe. BSGF - Earth Sciences Bulletin 191, 19. DOI: 10.1051/bsgf/2020019.

McCalpin, J.P. (ed.) (2009): Paleoseismology. 2nd ed. (International Geophysics Series, 95). Academic Press, Burlington, MA.

Mey, J., Scherler, D., Wickert, A.D., Egholm, D.L., Tesauro, M., Schildgen, T.F. & Strecker, M.R. (2016): Glacial isostatic uplift of the European Alps. Nature communications 7/1, 13382. DOI: 10.1038/ncomms13382.

Mosar, J. (1999): Present-day and future tectonic underplating in the western Swiss Alps: reconciliation of basement/wrench-faulting and décollement folding of the Jura and Molasse basin in the Alpine foreland. Earth and Planetary Science Letters 173/3, 143-155. DOI: 10.1016/S0012-821X(99)00238-1.

Muir-Wood, R. (2000): Deglaciation Seismotectonics: a principal influence on intraplate seismogenesis at high latitudes. Quaternary Science Reviews 19/14-15, 1399-1411. DOI: 10.1016/S0277-3791(00)00069-X.

Müller, W.H., Naef, H. & Graf, H.R. (2002): Geologische Entwicklung der Nordschweiz, Neotektonik und Langzeitszenarien Zürcher Weinland [mit Korrigendum]. Nagra Technischer Bericht NTB 99-08.

Naef, H. & Madritsch, H. (2014): Tektonische Karte des Nordschweizer Permokarbontrogs: Aktualisierung basierend auf 2D-Seismik und Schwere-Daten. Nagra Arbeitsbericht NAB 14-17.

Nagra (2014a): SGT Etappe 2: Vorschlag weiter zu untersuchender geologischer Standortgebiete mit zugehörigen Standortarealen für die Oberflächenanlage: Geologische Grundlagen Dossier II Sedimentologische und tektonische Verhältnisse. Nagra Technischer Bericht NTB 14-02 Dossier II.

Nagra (2014b): SGT Etappe 2: Vorschlag weiter zu untersuchender geologischer Standortgebiete mit zugehörigen Standortarealen für die Oberflächenanlage: Geologische Grundlagen Dossier III Geologische Langzeitentwicklung. Nagra Technischer Bericht NTB 14-02 Dossier III.

Nagra (2014c): SGT Etappe 2: Vorschlag weiter zu untersuchender geologischer Standortgebiete mit zugehörigen Standortarealen für die Oberflächenanlage: Geologische Grundlagen. Nagra Technischer Bericht NTB 14-02 Dossier I - VIII.

Nagra (2018a): 2D Reflection Seismic Exploration and Provisory Interpretation of Overdeepened Quaternary Valleys around the Nagra Siting Regions Zürich Nordost and Nördlich Lägern. Nagra Arbeitsbericht NAB 18-22.

Nagra (2018b): 2D Reflection Seismic Exploration and Provisory Interpretation of Overdeepened Quaternary Valleys around the Nagra Siting Regions Zürich Nordost and Nördlich Lägern. Nagra Arbeitsbericht NAB 18-22.

Nagra (2019a): Preliminary horizon and structure mapping of the Nagra 3D seismics JO-15 (Jura Ost) in time domain. Nagra Arbeitsbericht NAB 18-34.

Nagra (2019b): Preliminary horizon and structure mapping of the Nagra 3D seismics NL-16 (Nördlich Lägern) in time domain. Nagra Arbeitsbericht NAB 18-35.

Nagra (2024a): 3D Seismic Interpretation of Stratigraphic Horizons and Structures in Time Domain Jura Ost. Nagra Arbeitsbericht NAB 23-17.

Nagra (2024b): 3D Seismic Interpretation of Stratigraphic Horizons and Structures in Time Domain Nördlich Lägern. Nagra Arbeitsbericht NAB 23-18.

Nagra (2024c): 3D Seismic Interpretation of Stratigraphic Horizons and Structures in Time Domain Zürich Nordost. Nagra Arbeitsbericht NAB 23-19.

Nagra (2024d): Erdbebengefährdungsanalyse für den Standort der Brennelementverpackungsanlage. Nagra Arbeitsbericht NAB 24-22.

Nagra (2024e): Erdbebengefährdungsanalyse für den Standort der Oberflächenanlage und die Betriebsphase des geologischen Tiefenlagers. Nagra Arbeitsbericht NAB 24-21.

Nagra (2024f): Geologic Scenarios for the Evaluation of Earthquake Impact on the Deep Geological Repository. Nagra Arbeitsbericht NAB 24-28.

Nagra (2024g): Geological long-term evolution: Climate and Iceflow. Nagra Arbeitsbericht NAB 24-14.

Nagra (2024h): Geological long-term evolution: Erosion. Nagra Arbeitsbericht NAB 24-15.

Nagra (2024i): Geosynthesis of Northern Switzerland. Nagra Technischer Bericht NTB 24-17.

Nagra (2024j): In-Situ Stress Field in the Siting Regions Jura Ost, Nördlich Lägern and Zürich Nordost. Nagra Arbeitsbericht NAB 24-19.

Nocquet, J.-M. & Calais, E. (2004): Geodetic Measurements of Crustal Deformation in the Western Mediterranean and Europe. Pure and Applied Geophysics 161/3, 661-681. DOI: 10.1007/s00024-003-2468-z.

Ouchi, S. (1985): Response of alluvial rivers to slow active tectonic movement. GSA Bulletin 96/4, 504-515. DOI: 10.1130/0016-7606(1985)96<504:ROARTS>2.0.CO;2.

Pietsch, J. & Jordan, P. (2014): Digitales Höhenmodell Basis Quartär der Nordschweiz – Version 2014 und ausgewählte Auswertungen. Nagra Arbeitsbericht NAB 14-02.

Piña-Valdés, J., Socquet, A., Beauval, C., Doin, M.-P., D'Agostino, N. & Shen, Z.-K. (2022): 3D GNSS Velocity Field Sheds Light on the Deformation Mechanisms in Europe: Effects of the Vertical Crustal Motion on the Distribution of Seismicity. Journal of Geophysical Research: Solid Earth 127/6, e2021JB023451. DOI: 10.1029/2021JB023451.

Pintori, F., Serpelloni, E. & Gualandi, A. (2022): Common-mode signals and vertical velocities in the greater Alpine area from GNSS data. Solid Earth 13/10, 1541-1567. DOI: 10.5194/se-13-1541-2022.

Plenkers, K. (2014): Das neue Schwachbebennetz in der Nordschweiz: Standortsuche, Standortauswahl, realisierte Stationen. Nagra Arbeitsbericht NAB 14-56.

Preusser, F., Büschelberger, M., Kemna, H.A., Miocic, J., Mueller, D. & May, J.-H. (2021): Exploring possible links between Quaternary aggradation in the Upper Rhine Graben and the glaciation history of northern Switzerland. Int J Earth Sci (Geol Rundsch) 110/5, 1827-1846. DOI: 10.1007/s00531-021-02043-7.

Rabin, M., Sue, C., Walpersdorf, A., Sakic, P., Albaric, J. & Fores, B. (2018): Present-Day Deformations of the Jura Arc Inferred by GPS Surveying and Earthquake Focal Mechanisms. Tectonics 37/10, 3782-3804. DOI: 10.1029/2018TC005047.

Reber, R., Akçar, N., Ivy-Ochs, S., Tikhomirov, D., Burkhalter, R., Zahno, C., Lüthold, A., Kubik, P.W., Vockenhuber, C. & Schlüchter, C. (2014): Timing of retreat of the Reuss Glacier (Switzerland) at the end of the Last Glacial Maximum. Swiss Journal of Geosciences 107/2-3, 293-307. DOI: 10.1007/s00015-014-0169-5.

Roche, V., Childs, C., Madritsch, H. & Camanni, G. (2020): Layering and structural inheritance controls on fault zone structure in three dimensions: a case study from the northern Molasse Basin, Switzerland. Journal of the Geological Society 177/3, 493-508. DOI: 10.1144/jgs2019-052.

Rotstein, Y. & Schaming, M. (2011): The Upper Rhine Graben (URG) revisited: Miocene transtension and transpression account for the observed first-order structures. Tectonics 30/3, 2010TC002767. DOI: 10.1029/2010TC002767.

Sánchez, L., Völksen, C., Sokolov, A., Arenz, H. & Seitz, F. (2018): Present-day surface deformation of the Alpine region inferred from geodetic techniques. Earth System Science Data 10/3, 1503-1526. DOI: 10.5194/essd-10-1503-2018.

Schlatter, A. (2013): Rezente vertikale Oberflächenbewegungen in der Nordschweiz und in Südwestdeutschland. Kinematische Ausgleichung der Landesnivellementlinien CH/D. Nagra Arbeitsbericht NAB 12-34.

Schlunegger, F. & Kissling, E. (2015): Slab rollback orogeny in the Alps and evolution of the Swiss Molasse basin. Nature communications 6, 8605. DOI: 10.1038/ncomms9605.

Schlunegger, F. & Mosar, J. (2011): The last erosional stage of the Molasse Basin and the Alps. International Journal of Earth Sciences (Geologische Rundschau) 100/5, 1147-1162. DOI: 10.1007/s00531-010-0607-1.

Schöpfer, K., Decker, K., Nazari, F. & Madritsch, H. (2024): 3D-seismic evidence for thick-skinned tectonics in a ‘classic’ thin skinned tectonics region (external Alpine foreland, Switzerland). Terra Nova 36/3, 217-229. DOI: 10.1111/ter.12701.

Schreiner, A. (1992): Einführung in die Quartärgeologie. Schweizerbart, Stuttgart.

Schwanghart, W. & Scherler, D. (2017): Bumps in river profiles: Uncertainty assessment and smoothing using quantile regression techniques. Earth Surf. Dynam. 5/4, 821-839. DOI: 10.5194/esurf-5-821-2017.

Serpelloni, E., Cavaliere, A., Martelli, L., Pintori, F., Anderlini, L., Borghi, A., Randazzo, D., Bruni, S., Devoti, R., Perfetti, P. & Cacciaguerra, S. (2022): Surface Velocities and Strain-Rates in the Euro-Mediterranean Region From Massive GPS Data Processing. Frontiers in Earth Sciences 10, 907897. DOI: 10.3389/feart.2022.907897.

SFOE (2008): Sectoral plan for deep geological repositories. Conceptual part. Federal Department of the Environment, Transport, Energy and Communications DETEC, Bern.

Sommaruga, A. (1997): Geology of the central Jura and the molasse basin : new insight into an evaporite-based foreland fold and thrust belt. Société Neuchâteloise des Sciences Naturelles, Neuchâtel.

Steffen, R., Eaton, D.W. & Wu, P. (2012): Moment tensors, state of stress and their relation to post-glacial rebound in northeastern Canada. Geophysical Journal International 189/3, 1741-1752. DOI: 10.1111/j.1365-246X.2012.05452.x.

Steffen, R., Steffen, H., Wu, P. & Eaton, D.W. (2014): Stress and fault parameters affecting fault slip magnitude and activation time during a glacial cycle. Tectonics 33/7, 1461-1476. DOI: 10.1002/2013TC003450.

Stein, S., Liu, M., Camelbeeck, T., Merino, M., Landgraf, A., Hintersberger, E. & Kübler, S. (2017): Challenges in assessing seismic hazard in intraplate Europe. SP 432/1, 13-28. DOI: 10.1144/SP432.7.

Sternai, P., Sue, C., Husson, L., Serpelloni, E., Becker, T.W., Willett, S.D., Faccenna, C., Di Giulio, A., Spada, G., Jolivet, L., Valla, P., Petit, C., Nocquet, J.-M., Walpersdorf, A. & Castelltort, S. (2019): Present-day uplift of the European Alps: Evaluating mechanisms and models of their relative contributions. Earth-Science Reviews 190, 589-604. DOI: 10.1016/j.earscirev.2019.01.005.

Stewart, I.S. & Hancock, P.L. (1994): Neotectonics. *In:* Hancock, P.L. (ed.): Continental Deformation. 1st ed. Pergamon Press, Oxford, 370-409.

Stewart, I.S., Sauber, J. & Rose, J. (2000): Glacio-seismotectonics: ice sheets, crustal deformation and seismicity. Quaternary Science Reviews 19/14-15, 1367-1389. DOI: 10.1016/S0277-3791(00)00094-9.

Strasser, M., Monecke, K., Schnellmann, M. & Anselmetti, F.S. (2013): Lake sediments as natural seismographs: A compiled record of Late Quaternary earthquakes in Central Switzerland and its implication for Alpine deformation. Sedimentology 60/1, 319-341. DOI: 10.1111/sed.12003.

Strecker, M.R., Hilley, G.E., Blisniuk, P.M. & Reuther, C.D. (2009): Neotectonics. *In:* EOLSS (ed.): Geology – Vol. I. EOLSS Publishers.

Studer, M. & Zanini, M. (2013): Aufbau und Betrieb eines eigenständigen CORS-GNSS Netzes. Kurzbericht (für interessierte Dritte). Nagra Arbeitsbericht NAB 10-14.

swissnuclear (2013): PEGASOS Refinement Project Probabilistic Seismic Hazard Analysis for Swiss Nuclear Power Plant Sites. Volumes 1 Summary Report. swissnuclear, Olten.

Thew, N., Kälin, D., Cuenca-Bescós, G., Buechi, M.W., Penkman, K., Scheidt, S., Knipping, M., Maier, F., Urresti, I. & Deplazes, G. (2024): The Hasli Formation of the Irchel Plateau – A key record for older Early Pleistocene interglacial sediments in northern Switzerland. Quaternary Science Reviews 332, 108550. DOI: 10.1016/j.quascirev.2024.108550.

Timár, G. (2003): Controls on channel sinuosity changes: a case study of the Tisza River, the Great Hungarian Plain. Quaternary Science Reviews 22/20, 2199-2207. DOI: 10.1016/S0277-3791(03)00145-8.

Townend, J. & Zoback, M.D. (2000): How faulting keeps the crust strong. Geology 28/5, 399-402. DOI: 10.1130/0091-7613(2000)28<399:HFKTCS>2.0.CO;2.

Trifonov, V.G. (1989): An overview of neotectonic studies. International Geology Review 31/2, 111-161. DOI: 10.1080/00206818909465866.

Turcotte, D.L. & Schubert, G. (2014): Geodynamics. 3rd ed. Cambridge University Press, Cambridge.

Ustaszewski, K. & Schmid, S.M. (2007): Neotectonic activity in the Upper Rhine Graben - Jura Mountains junction (North-Western Switzerland and adjacent France). Bulletin für angewandte Geologie 12/1, 3-19.

Ustaszewski, M. & Pfiffner, O.A. (2008): Neotectonic faulting, uplift and seismicity in the central and western Swiss Alps. SP 298/1, 231-249. DOI: 10.1144/SP298.12.

von Hagke, C., Cederbom, C.E., Oncken, O., Stöckli, D.F., Rahn, M.K. & Schlunegger, F. (2012): Linking the northern Alps with their foreland: The latest exhumation history resolved by low-temperature thermochronology. Tectonics 31/5, 2011TC003078. DOI: 10.1029/2011TC003078.

von Hagke, C., Oncken, O. & Evseev, S. (2014): Critical taper analysis reveals lithological control of variations in detachment strength: An analysis of the Alpine basal detachment (Swiss Alps). Geochemistry, Geophysics, Geosystems 15/1, 176-191. DOI: 10.1002/2013GC005018.

Wallace, R.E. (1984): Patterns and timing of Late Quaternary faulting in the Great Basin Province and relation to some regional tectonic features. Journal of Geophysical Research 89/B7, 5763-5769. DOI: 10.1029/jb089ib07p05763.

Whipple, K.X. & Tucker, G.E. (1999): Dynamics of the stream-power river incision model: Implications for height limits of mountain ranges, landscape response timescales, and researech needs. Journal of Geophysical Research 104/B8, 17661–17674. DOI: 10.1029/1999JB900120.

Willett, S.D. & Schlunegger, F. (2010): The last phase of deposition in the Swiss Molasse Basin: from foredeep to negative-alpha basin. Basin Research 22/5, 623-639. DOI: 10.1111/j.1365-2117.2009.00435.x.

Wittmann, O. (1937): Deckentuff und Molasse am Höwenegg. Ein Beitrag zur Entwicklungsgeschichte des Hegauvulkans. Jahresberichte und Mitteilungen des Oberrheinischen Geologischen Vereins 26, 1-32. DOI: 10.1127/jmogv/26/1937/1.

Wobus, C., Whipple, K.X., Kirby, E., Snyder, N., Johnson, J., Spyropolou, K., Crosby, B. & Sheehan, D. (2006): Tectonics from topography: Procedures, promise, and pitfalls. *In:* Willett, S.D., Hovius, N., Brandon, M.T. & Fisher, D.M. (eds.): Tectonics, Climate, and Landscape Evolution. (Penrose conference series, 398). Geological Society of America, Boulder, Colo., 55-74.

Woolderink, H., Cohen, K.M., Kasse, C., Kleinhans, M.G. & van Balen, R.T. (2021): Patterns in river channel sinuosity of the Meuse, Roer and Rhine rivers in the Lower Rhine Embayment rift-system, are they tectonically forced? Geomorphology 375, 107550. DOI: 10.1016/j.geomorph.2020.107550.

Zoback, M.D., Townend, J. & Grollimund, B. (2002): Steady-State Failure Equilibrium and Deformation of Intraplate Lithosphere. International Geology Review 44/5, 383-401. DOI: 10.2747/0020-6814.44.5.383.